# Immune mechanisms in the pathogenesis of experimental autoimmune hepatitis

Dissertation with the aim of achieving a doctoral degree

at the Faculty of Mathematics, Informatics, and Natural Sciences

Department of Biology

of Universität Hamburg

submitted by Max Preti

July 2019

Day of oral defense: 24.01.2020

The following evaluators recommend the admission of the dissertation:

1. Prof. Dr. rer. nat. Johannes Herkel

   Medizinische Klinik und Poliklinik des Universitätsklinikum Hamburg Eppendorf

2. Prof. Dr. rer, nat. Susanne Dobler
   Institut für Zoologie des Universität Hamburg

*La morte è la curva della strada,*

*morire è solo non essere visto.*

*Se ascolto, sento i tuoi passi*

*esistere come io esisto.*

*La terra è fatta di cielo.*

*Non ha nido la menzogna.*

*Mai nessuno s'è smarrito.*

*Tutto è verità e passaggio.*

*Fernando Pessoa*

1.INTRODUCTION ..... 7
1.1.2 Thymic tolerance ..... 7
1.1.3 Peripheral tolerance ..... 8
1.1.4 Regulatory T cells ..... 9
1.1.5 tTreg vs pTreg ..... 12
1.2 EFFECTOR T CELL RESPONSE ..... 12
1.3 HEPATIC IMMUNE TOLERANCE ..... 13
1.4 AUTOIMMUNE DISEASES ..... 14
1.4.1 Autoimmune hepatitis ..... 14
1.4.3 Mouse models of AIH ..... 15
1.4.4 Effector immune response in AIH ..... 16
1.4.5 Treg in AIH ..... 17
1.5 ROLE OF ECTOPIC LYMPHOID TISSUE IN AUTOIMMUNE DISEASE ..... 17
1.6 AIMS OF THIS STUDY ..... 18
2. MATERIALS AND METHODS ..... 19
2.1 INSTRUMENTS ..... 19
2.2 MATERIALS ..... 20
2.3 BUFFERS ..... 23
2.4 MOUSE MODELS ..... 24
2.4.1 Generation of invariant chain GP (iGP) mice ..... 24
2.5 ISOLATION OF PRIMARY CELLS ..... 26
2.5.1 Isolation of splenocytes ..... 26
2.5.2 Isolation of splenic $CD25^-$ CD4 T cells ..... 27
2.5.3 Isolation of thymocytes ..... 27
2.5.4 Isolation of hepatic non-parenchymal cells ..... 28
2.6 CELL CULTURE ..... 28
2.6.1 Determination of cell numbers ..... 28
2.6.2 Cell culture medium ..... 28
2.6.3 Restimulation for intracellular cytokine production ..... 29
2.7 MULTICOLOR FLOW CYTOMETRY ..... 29
2.7.1 Determination of cell viability ..... 29
2.7.2 Tetramer staining ..... 29
2.7.3 Cell surface marker staining ..... 29

2.7.4 Intracellular staining ..... 30
2.8 IMMUNOHISTOCHEMISTRY ..... 30
2.8.1 Organ preparation ..... 30
2.8.2 Haemalum and eosin staining ..... 30
2.8.3 Sirius red staining ..... 30
2.8.4 CD4, B220, Foxp3, PNAd and CD11c staining ..... 31
2.8.5 CD4/CD8/CD11c immunofluorescence staining ..... 31
2.8.6 Modified Hepatic Activity Index (mHAI) ..... 31
2.9 AUTOANTIBODY DETECTION ..... 32
2.10 MOLECULAR BIOLOGY ..... 32
2.10.1 RNA purification ..... 32
2.10.2 cDNA synthesis ..... 33
2.10.3 Real Time PCR ..... 33
2.11 IN VIVO EXPERIMENTS ..... 33
2.11.1 In vivo enrichment of regulatory T cells ..... 33
2.11.2 $CD25^{-}CD4^{+}$ T cell transfer ..... 33
2.11.3 Statistics ..... 34
3. RESULTS ..... 35
3.1 Generation of mouse models ..... 35
3.2 Characterization of the autoreactive T cell pool in mice with conditional autoantigen expression ..... 36
3.3 Thymic and peripheral Treg frequency ..... 39
3.4 Phenotype of peripheral CD4 Smarta T cells ..... 41
3.5 Clinical monitoring of Alb-iGP_Smarta mice ..... 42
3.5.1 Increased serum transaminase levels in Alb-iGP_Smarta mice ..... 43
3.5.2 Hepatic infiltration of inflammatory cells in the livers of Alb-iGP_Smarta mice ..... 44
3.5.3 Autoantibody detection ..... 45
3.5.4 IgG quantification ..... 47
3.5.5 CD4 T cells dominate the hepatic infiltrate ..... 47
3.5.6 Ectopic lymphoid tissues (ELT)s ..... 48
3.5.7 Impaired survival of Alb-iGP_Smarta mice ..... 49
3.6 Study of the effector T cell immune response in Alb-iGP_Smarta mice ..... 52
3.6.1 Cytokine analysis ..... 52
3.7 Regulatory T cells ..... 55

3.7.1 Antigen-specific Treg ..... 56
3.7.2 Thymus-derived Treg (tTreg) versus peripheral derived Treg (pTreg) ..... 57
3.7.3 Mean fluorescence intensity (MFI) of FOXP3 ..... 58
3.7.4 In vivo short-term Treg enrichment ..... 59
3.7.5 In vivo long-term Treg enrichment ..... 61
3.7.6 IL-12 expression ..... 63
3.7.7 Cytokine production by Treg ..... 64
3.8 Inflammatory monocytes ..... 68
3.9 Macrophages ..... 69
3.10 Dendritic cells are enriched in Alb-iGP_Smarta mice in the preclinical stage ..... 70
3.10.1 Phenotype of hepatic DCs ..... 71
3.10.2 DCs are enriched in human AIH ..... 73
3.10.3 Autoantigen-presentation by DCs is required for the activation of adoptively transferred autoreactive CD4 T cells ..... 73
4. DISCUSSION ..... 76
4.1 Tolerance mechanisms in thymus and periphery ..... 76
4.2 Alb-iGP_Smarta mice as a new mouse model for AIH ..... 77
4.3 Role of ELTs in AIH development ..... 78
4.4 Effector immune response in Alb-iGP_Smarta mice ..... 79
4.5 Regulatory T cells in Alb-iGP_Smarta mice ..... 79
4.6 Pathogenic drivers of autoreactive CD4 T cell activation ..... 82
4.7 Future perspectives ..... 83
4.7.1 Pre-clinical evaluation of new therapeutic options for AIH in Alb-iGP_Smarta mice ..... 83
4.7.2 Antigen-presenting cells in AIH ..... 83
4.7.3 Treg stability and function in Alb-iGP_Smarta mice ..... 84
5. SUMMARY ..... 85
6. REFERNCES ..... 89
7. ABBREVIATIONS ..... 97
8. CONFERENCE PARTICIPATIONS ..... 99
9. PUBLICATIONS ..... 100
10. AKNOWLEDGMENTS ..... 101
11. EIDESSTATTLICHE VERSICHERUNG ..... 102

# 1.INTRODUCTION

## 1.1 MECHANISMS OF IMMUNE TOLERANCE

The human immune system is in continuous contact with foreign and self-antigens. Antigens derived from pathogenic microorganisms are recognized by B and T cells that mount an adequate immune response against the pathogen to eliminate it. However, the adaptive immune response should not be excessive and deleterious for the host. Therefore, the adaptive immune system is unresponsive to certain foreign and self-antigens, a state that is called immunological tolerance. This state of unresponsiveness is generated by clonal deletion of self-reactive lymphocytes, by rearrangement of the T cell receptor (TCR) that recognize the self-antigen or by induction of a state of anergy. A failure of these mechanisms can trigger an aberrant immune response against self-antigens, and the development of autoimmune disease. Immunological tolerance can be induced during T cell development in the thymus (central tolerance) or in maturated T cells in the periphery (peripheral tolerance) (1,2).

### 1.1.2 Thymic tolerance

T cell maturation occurs in the thymus, where self-reactive lymphocytes are eliminated in a process called negative selection. Thymic epithelial cells present self-antigens on class I and II MHC molecules to CD4 CD8 double positive T cells. T cells that bind to the presented antigens with high affinity undergo apoptosis (negative selection), whereas T cells with intermediate affinity survive and become single positive CD4 or CD8 T lymphocytes (figure 1a and b) (2,3). Some high affinity T cells do not undergo apoptosis, but instead become thymus-derived regulatory T cells (tTreg) (figure 1a). tTreg suppress autoreactive T cells that may have escaped thymic deletion (2,3). Medullary epithelial cells present tissue-restricted antigens (TRA) in order to favor negative selection of T cells that bind with very high affinity to TRA. The expression of TRA is regulated by the transcription factor autoimmune regulator (AIRE) (2,3).

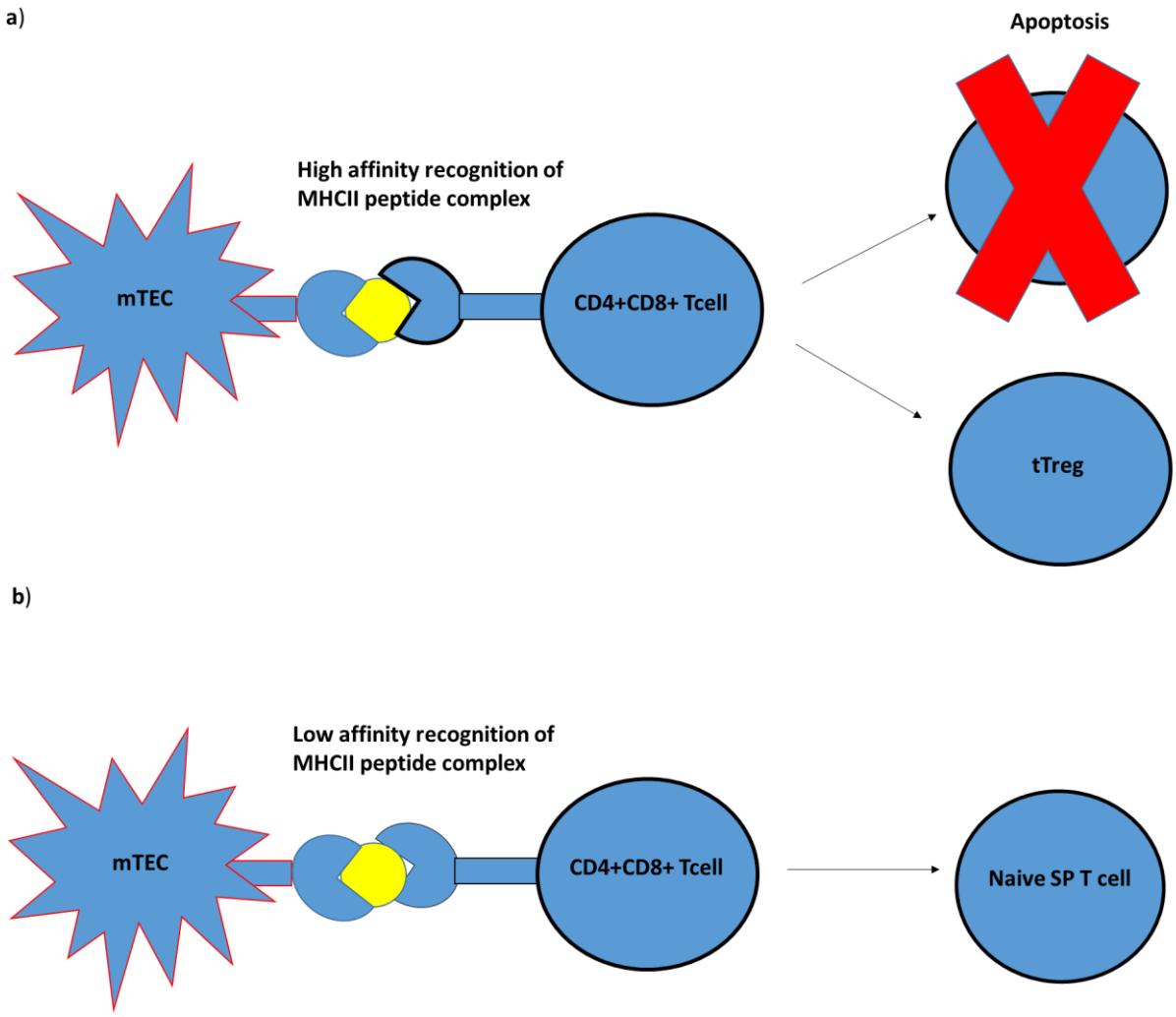


Figure 1. a) High affinity interaction between self-antigen presented on MHC molecules and TCR leads to deletion of autoreactive T cells or tTreg induction in the thymus. b) Low affinity interaction between self-antigen presented on MHC molecules and TCR leads to generation of CD4 or CD8 single positive (SP) T cells.

### 1.1.3 Peripheral tolerance

Self-reactive T cells can escape negative selection, especially when the antigen is not presented in the thymus. Peripheral tolerance mechanisms are therefore required to control the lymphocytes that encounter the antigen for the first time outside the thymus. Several mechanisms of peripheral tolerance have been described, including anergy, deletion and induction of peripheral Treg (3). T cell activation requires TCR signaling together with co-stimulation mediated by CD28 ligation, which leads to the production of interleucin-2 (IL-2). In the absence of co-stimulation, T cells become functionally inactivated/anergic upon self-

antigen encounter (figure 2). Moreover, the threshold of activation may be raised by the expression of inhibitory receptors such as programmed cell death protein (PD-1) or Cytotoxic T-Lymphocyte Antigen 4 (CTLA-4) (1-3). Tolerogenic dendritic cells can contribute to peripheral tolerance by presenting self-antigens to T cells without adequate co-stimulation necessary for T cell activation (3). Autoreactive T cells can also be deleted in the periphery by apoptosis, mediated by activation of the death receptors Fas and Bim. Finally, generation of peripherally induced Treg (pTreg) helps to suppress self-reactive T cells (figure 2)(1-3).

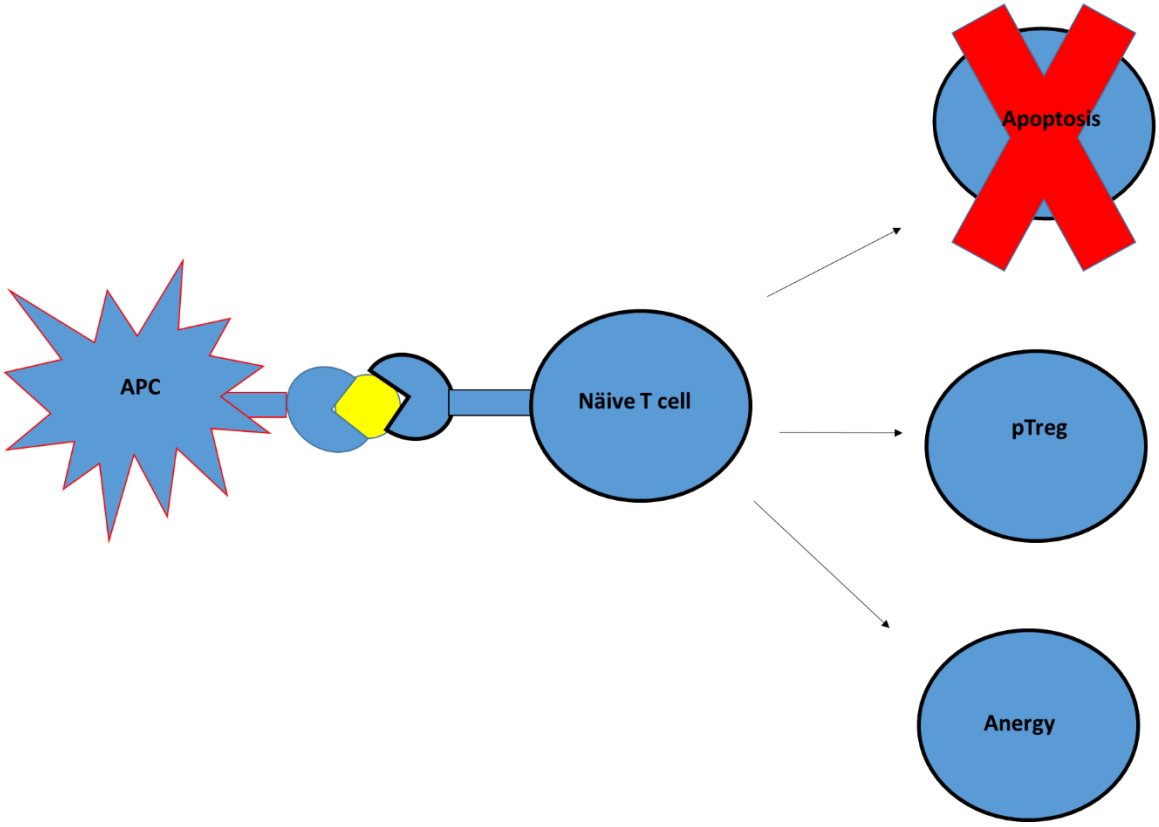


Figure 2. Mechanism of peripheral tolerance. Naive CD4 T cells undergo apoptosis, or become pTreg or become anergic.

### 1.1.4 Regulatory T cells

In 1995, a population of suppressive CD4 T cells, named regulatory T cells (Treg), was discovered. Treg cells are characterized by constitutive expression of the IL-2 receptor α-chain (IL-2Rα) (CD25) (4,5). These cells have a critical role in maintaining immune tolerance as their depletion caused various organ-specific autoimmune diseases (4,5). The generation, function and maintenance of Treg is regulated by the forkhead box protein p3 (Foxp3). Scurfy mice, which lack the Foxp3 gene, develop autoimmune lymphoproliferative disease similar to the

human syndrome X-linked neonatal diabetes mellitus, enteropathy and endocrinopathy (IPEX)(5). Treg suppress effector immune responses via different mechanisms that target T cells or antigen presenting cells. Treg produce various tolerogenic cytokines like TGF-β, IL-10 or IL-35, which suppress effector cells. Another mechanism of Treg-mediated suppression is the competition for IL-2, which can lead to Bim-mediated apoptosis of effector T cells. Treg can also produce cytotoxic molecules like perforin and granzymes, which directly kill the target cell. Moreover, Treg can block cell cycle progression of effector T cells (6) (figure 3). Recently, it has been reported that Treg can deplete peptide-MHCII from dendritic cells in an antigen-specific mechanism. (7)

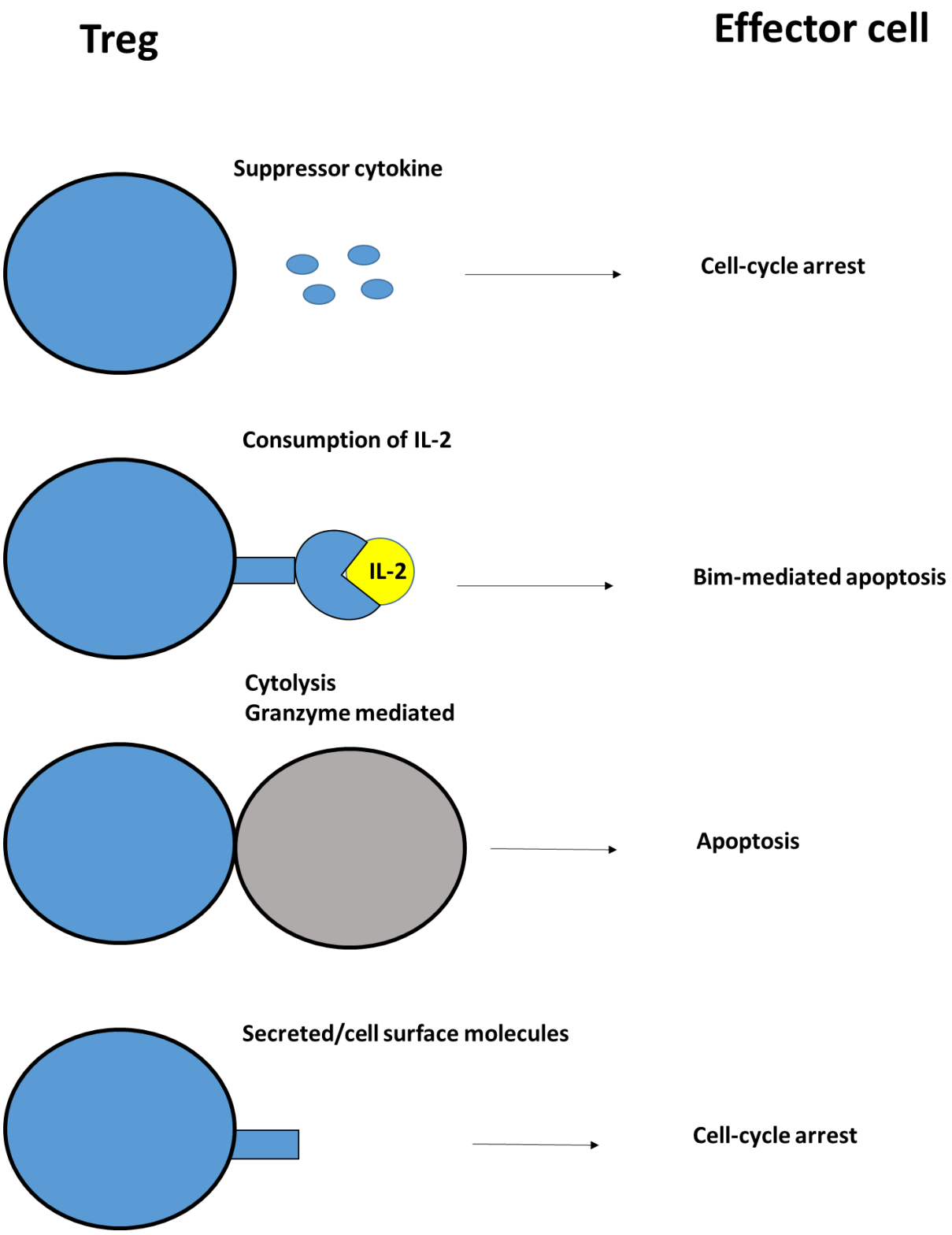


Figure 3. Different mechanisms used by Treg to exert their suppressive function. Modified from 6.

### 1.1.5 tTreg vs pTreg

Treg can be divided in two distinct populations based on their origin. Thymic induced Treg (tTreg) which originate in the thymus, and peripherally induced Treg (pTreg) which originate in the periphery. These two populations are phenotypically similar as both express FOXP3, but they have different stability and epigenetic modifications (8). tTreg are formed in the thymus upon high avidity MHCII interaction with T cell receptors (TCR). pTreg are generated from conventional CD4+ CD25- T cell in the presence of TGF-β and IL-2 (8). It has been reported that Helios and Neuropilin-1 are highly expressed on tTreg, but not on pTreg (9-11). tTreg have a pivotal role in protecting from autoimmune disease. The importance of tTreg is highlighted by the fact that newborn mice develop a polyautoimmune disease after thymectomy (12). Adoptive transfer of Treg in thymectomized mice protected from disease development (12). pTreg are generated from naive CD4+CD25- T cells in the presence of TGF-β. The importance of pTreg is highlighted by adoptive transfer experiments in a mouse model of colitis showing that pTreg are necessary for protection from diseasese development (13). The suppressive mechanisms exerted by tTreg and pTreg are similar and they act in a synergistic way.

## 1.2 EFFECTOR T CELL RESPONSE

Upon antigen stimulation and in the presence of certain cytokines, naive CD4 T cells can differentiate into diverse helper cell subtypes. The pro-inflammatory Th1 cells, which are induced by IL-12, are important for cellular immunity to intracellular pathogens by producing IFN-γ and IL-2. Th2 cells, which are induced by IL-4, are involved in humoral immunity by producing mainly the cytokines IL-4, IL-5, IL-10 and IL-13 that regulate antibody production by B cells. The combination of the cytokines IL-6, TGF-β and IL-21 drives naive CD4 T cells to differentiate into Th17 cells, which are mostly involved in the response to extracellular pathogens by controlling the activation of neutrophils. Th17 cells produce mainly IL-17 and IL-22 (14,15, figure 4). The differentiation into the various helper subsets is regulated by different transcription factors: Tbx21 drives differentiation into Th1 cells, Gata-3 drives differentiation into Th2 cells and RoRγt drives differentiation into Th17 cells (16-18).

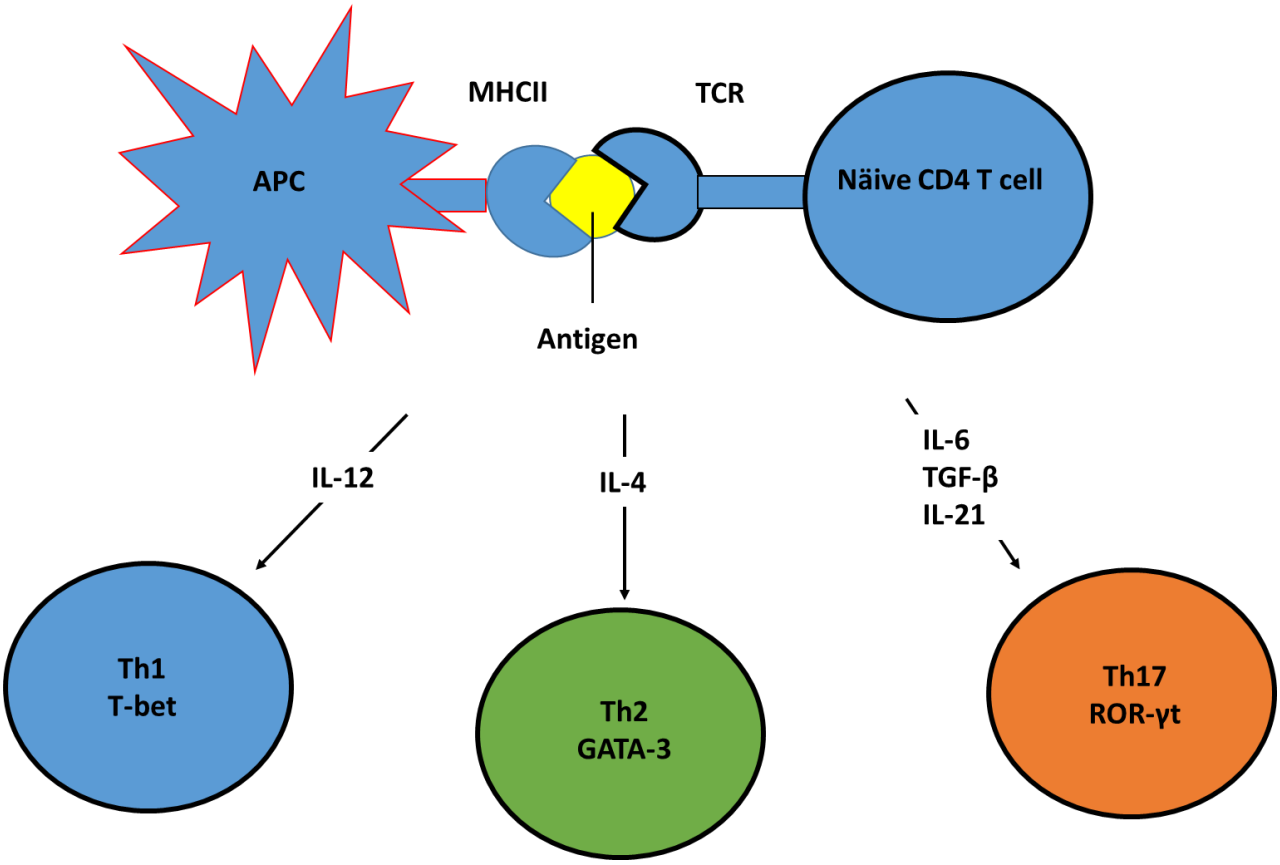


Figure 4. After antigen encounter and different cytokine milieu, naive CD4 T cell differentiate in Th1, Th2 or Th17 cells.

## 1.3 HEPATIC IMMUNE TOLERANCE

The liver has been regarded mostly as a metabolic organ. However, it is now recognized also as an immune organ often promoting immune tolerance (14). The mechanisms that lead to hepatic tolerance are similar to the mechanisms of peripheral tolerance described above. Hepatic APCs can induce formation of pTreg, produce tolerogenic cytokines such as transforming growth factor-β (TGF-β) or interleukin-10 (IL-10) that suppress effector T cell responses, and they can inhibit T cell activation via CTLA-4 and PD-1. In addition, hepatic APCs preferentially induce the expansion of Th2 cells, which produce IL-10 and IL-4, instead of Th1 (INF-γ producers) or Th17 cells (IL-17 producers) in a process called immune deviation (14). Hepatic tolerance is not only acting locally but systemically. For example, liver allografts can elicit the acceptance of otherwise rejected skin grafts derived from the same donor (14,19). However, liver immune tolerance can be broken leading to autoimmune liver diseases.

## 1.4 AUTOIMMUNE DISEASES

Autoimmune diseases result from activation of a tissue-damaging response by self-reactive lymphocytes. More than 70 different autoimmune diseases have been described, including type 1 diabetes, multiple sclerosis, rheumatoid arthritis (RA), systemic lupus erythematosus (SLE) and Sjogren's syndrome (SS). There are three main autoimmune liver diseases: primary sclerosing cholangitis (PSC), primary biliary cholangitis (PBC) and autoimmune hepatitis (AIH) (20). The causes of autoimmune diseases are not clear. Genetic predisposition as well as environmental factors may play an important role. Several data indicate that infections may be the first trigger of an autoimmune disease (21). Indeed, similarities between self and foreign antigens may cause activation of self-reactive T and B cells by the foreign peptide. This hypothesis is called molecular mimicry (21,22).

### 1.4.1 Autoimmune hepatitis

Autoimmune hepatitis (AIH) is a chronic inflammatory liver disease affecting both adults and children, with a female preponderance (23). Currently, there is no specific treatment for patients with AIH; the standard treatment is a general immunosuppression regimen with corticosteroids and azathioprine (24). Diagnostic criteria are increased serum transaminases, elevated serum immunoglobulin G or hypergammaglobulinemia, presence of autoantibodies, plasmalymphocytic periportal infiltrates with histological interphase hepatitis, and absence of viral hepatitis (25,26). The different patterns of autoantibodies enable the classification of AIH in two sub-categories. Anti-nuclear antibodies (ANA) as well as anti-smooth muscle actin antibodies (SMA) are often detected in patients with AIH type 1. AIH type 2, which affects mainly children, is characterized by the presence of anti-liver/kidney microsomal antibodies type 1 (anti-LKM1), anti-LKM3 or antibodies against liver cytosol type 1 antigen (23-26).

### 1.4.2 Pathogenesis of AIH

The etiology of AIH is not known. However, environmental triggers and genetic predisposition seem to play a role in disease pathogenesis. Up to 50% of the Caucasian patients show HLA haplotypes DRB1∗0301 and DRB1∗0401. The HLA DRB1∗1501 seems to be protective (26-28). These associations suggest a pathogenic T-cell mediated recognition of one or more hepatic

autoantigens in the context of MHCII. Several mouse models further corroborated the role of T cell in pathogenesis of AIH.

### 1.4.3 Mouse models of AIH

Several mouse models of AIH suggested a pathogenic role of T cells. In one such model, syngeneic liver homogenates (LH) and lipopolysaccharide (LPS) were injected monthly into spinal muscular atrophy mice (29,30). After 11 months, 60 to 80 % of the mice showed hepatic plasma cells and lymphocyte infiltration together with hepatocyte necrosis. The authors showed also that the disease was transferable by T lymphocytes. After cessation of the treatment, the mice gradually recovered. In another model, administration of 1.5 mg/kg of concanavalin A (Con A) intravenously to BALB/c mice led to liver damage associated with high serum transaminases, liver infiltration and necrosis (29,31). Mice lacking B and T cells were protected, as well as athymic nude mice that lack T cells. Interestingly, administration of CD4 but not CD8 monoclonal antibody protected mice from Con A induced hepatitis. Another mouse model expressing the allogeneic $K^b$ MHC class I molecule exclusively on hepatocytes was generated in which the cognate $K^b$-specific TCR was expressed as a transgene (29,32). The autoreactive CD8 T cells were not deleted in the thymus, but no sign of autoimmunity was observed. IL-2 administration was not sufficient to break tolerance. However, infection with L. monocytogenes led to autoimmune liver infiltration and elevation in serum ALT levels. Another model has been described in which ovalbumin was expressed by hepatocytes (TF-OVA) and adoptive transfer of cognate OT-1 (CD8) or OT-II (CD4) cells resulted in the priming of autoreactive T cells and development of acute hepatitis. CD8 T cells proliferated in the liver of TF-OVA mice. CD4 T cells were activated in the spleen and liver-draining lymph nodes of TF-OVA mice (29,33). However, hepatitis was only transient and disappeared after 15 days. A mouse model featuring expression of the viral protein hemagglutinin (HA) under the albumin promoter and a transgenic HA-specific TCR on CD8 T cells showed development of autoimmune hepatitis characterized by elevated serum transaminases, hepatic lesions and fibrosis (29,34). However, autoreactive CD8 T cells that accumulated in the liver were anergic and downregulated the TCR resulting in transient disease. TGF-β1 knock out mice on a BALB/c background develop strong liver inflammation and necrosis accompanied by elevated ALT levels. (29,35). One potent immune activator seems to be IL-12. Indeed, human CYP2D6 or FTCD plasmids or DNA were injected into C57/BL6 mice together with IL-12 (IL-12 was

necessary to boost the immune system) (29,36,37). After 9 months, mice developed AIH type II-like symptoms, i.e. periportal inflammation, antibodies against CYP2D6 and FTCD as well as hepatocyte necrosis. CD4 T cells dominated the infiltrates. Moreover, transient expression of IL-12 broke immunological tolerance to hepatocellular antigens and induced development of AIH due to pathogenic activation of autoreactive T cells (38). These mice showed liver infiltrates, elevated transaminases, hypergammaglobulinemia, ANA and ASMA. The important role of T cells in AIH is further confirmed by the finding that conditional depletion of the ubiquitin ligase Traf6 in murine thymic epithelial cells led to autoimmunity in the liver, with histological and immunological features of human AIH (39). In these mice, defective medullary thymic epithelial cells that normally express TRA, were not able to eliminate autoreactive T cells in the thymus. Moreover, these mice had a low frequency of tTreg, with however normal peripheral pTreg induction.

### 1.4.4 Effector immune response in AIH

CD4 T cells represent the majority of the infiltrating cells in the liver of patients with AIH (40). Upon antigen stimulation and in the presence of certain cytokines, naive CD4 T cells can differentiate into diverse helper cell subtypes. In AIH, the production of IFN-γ and IL-2 by Th1 cells lead to up-regulated expression of MHC I and II molecules by hepatocytes, and activation of macrophages to produce IL-1 and TNF-α which activate cytotoxic CD8 T cells. In addition, autoantibody production by B cells is regulated by IL-4, IL-13, IL-10-producing Th2 cells (41). These mechanisms together with complement activation lead to hepatocellular damage. Th17 cells are also expanded in AIH patients (41). Interestingly, difficult-to-treat patients with AIH responded well to treatment with the humanized chimeric anti TNF-α antibody Infliximab (42). This finding indicated that the hepatic T cells in AIH may have a Th1 inflammatory phenotype. The authors speculated that the beneficial effect of the drug was due to a pro-apoptotic effect of Infliximab on T cells, highlighting the importance of a suppressed effector T cell response in AIH.

### 1.4.5 Treg in AIH

Treg in patients with AIH were found to be present in a normal frequency and they were functional in an in vitro suppression assay (43). It was however possible that the hepatic milieu rendered Treg unable to suppress effector T cells properly (44). One other possible explanation for the failure of Treg to prevent AIH development is the generally low level of IL-2 in the liver. Treg constantly need IL-2 to survive and in AIH most of IL-2 is possibly consumed by effector cells (48). Accordingly, low dose IL-2 treatment was increasing the survival of Treg and upregulated CTLA-4 expression in patients with AIH (44,45). However, it was reported that successful expansion of Treg with IL-2 treatment did not lead to improved liver pathology in a mouse model of PSC, because the expanded Treg up-regulated IL12rb2, which impaired their immune suppressive capacity (46). Thus, increased IL-12 signalling may enable hepatic autoimmunity and explain why hepatic expression of IL-12 leads to autoimmune hepatitis in mice (38).

## 1.5 ROLE OF ECTOPIC LYMPHOID TISSUE IN AUTOIMMUNE DISEASE

Immune activation in autoimmune diseases often occurs within ectopic lymphoid tissue (ELT). ELTs are inducible structures formed in affected organs resembling the organization of lymphoid follicles with typical clusters of B and T cells (47,48). Within these structures, dendritic cells, plasma cells and high endothelial venules are also present (49). The formation of these structures is often associated with poor disease prognosis and low response to therapy. ELTs favor affinity maturation of B cells in an antigen dependent way and promote their differentiation into antibody-producing plasma cells. For example, in RA, ELTs drive the formation of high-affinity plasma cells from autoreactive B cells, which produce autoantibodies against citrullinated antigens (47,48). The mechanisms governing the formation and the maintenance of ELTs are complicated and involve many immune cell types, cytokines and chemokines. Some important cytokines and chemokines are LT-α and LT-β, which, when over-expressed, lead to the production of CXCL13 and CCL21. These chemokines foster the migration of T cells to the target organ making the development of ELTs possible (47,48). In patients with rheumatoid arthritis, anti TNF-α treatment was found to revert ELT formation, showing the importance of this cytokine in the maintenance of ELTs (50). The formation of ELTs in the liver is observed in chronic liver diseases (HBV or HCV) (51). Notably, presence of ELTs in liver cancer is associated with a poor prognosis (51,52). In autoimmune

liver diseases, the formation of ELTs is observed mainly in PSC and PBC patients (51,52). The association between the development of ELTs in the liver and AIH remains unclear.

## 1.6 AIMS OF THIS STUDY

The mechanisms that lead to a breach of hepatic immune tolerance in autoimmune liver diseases are not fully understood, and in the existing mouse models, autoimmune liver disease is often only transient due to counter-regulatory mechanisms. Autoreactive T cells are normally eliminated in the thymus or in the periphery by central and peripheral tolerance mechanisms. Autoreactive effector T cells that escape negative selection can also be suppressed by tTreg and pTreg. Thus far, it is not known how autoreactive effector T cells in autoimmune liver diseases can escape deletion and suppression. Moreover, the signals that drive the pathogenic activation of autoreactive effector cells in the tolerogenic environment of the liver are also unclear.

The overall aim of this study is to understand the immunological mechanisms underlying the breach of hepatic tolerance in autoimmune hepatitis. Specific aims are:

1) To establish a new mouse model of AIH, which is driven by CD4 T cells specifically recognizing hepatocyte antigen, and which recapitulates the main features of the human disease.

2) To elucidate the mechanisms that enable the escape of autoreactive T cells from deletional and suppressive tolerance in AIH.

3) To elucidate the mechanisms that enable the pathogenic activation of autoreactive T cells in AIH.

# 2. MATERIALS AND METHODS

## 2.1 INSTRUMENTS

| | |
|---|---|
| BZ-II Analyzer | Keyence, Neu-Isenburg |
| Centrifuge: 5417 R, 5810 R, 5920 R | Eppendorf AG, Hamburg |
| Centrifuge, Megafuge 2.0 | Heraeus Instruments GmbH, Osterode |
| $CO_2$ incubator | Sanyo Biomedica, Munich |
| Cryostat, Microm HM550 | Microm, Walldorf |
| Flow cytometer: LSR II, LSR Fortessa | BD Biosciences, Heidelberg |
| Fluorescence microscope, Biorevo BZ-9000 | Keyence, Neu-Isenburg |
| Laminar flow cabinet (BDK) | Luft und Reinraumtechnik GmbH, Sonnenbühl-Genkingen |
| Light microscope | Olympus, Hamburg |
| Luminex xMAP | Merck Millipore, Darmstadt |
| Macs MultiStand | Miltenyi Biotec, Bergisch Gladbach |
| Microtome | Slee medical, Mainz |
| Microwave | Bosch, Stuttgart |
| Neubauer chamber | Optik Labor Frischknecht, Balgach |
| Perfusion pump | Ismatech, Wertheim |
| Pipettes | Eppendorf AG, Hamburg |
| Scissors | VWR International GmbH, Darmstadt |
| Slide warmer | Stoerk Tronic, Stuttgart |
| Thermocycler ViiA 7 | Thermo Fisher Scientific, Darmstadt |
| Thermomixer Comfort | Eppendorf AG, Hamburg |
| Tissue cool plate COP 20 | Medite, Burgdorf |
| Transaminase analzyer, COBAS INTEGRA 400 PLUS | Roche Diagnostic GmbH, Mannheim |
| Tweezers | VWR International GmbH, Darmstadt |
| Vortex, GENIE 2 | Roth, Karlsruhe |

| | |
|---|---|
| Waterbath | GFL, Großburgwedel |

## 2.2 MATERIALS

| | |
|---|---|
| I-A(b) LCMV $GP_{66-77}$ APC-labelled tetramer | NIH Tetramer Core Facility, Atlanta, USA |
| 96-well cell culture plates | Sarstedt, Neumbrecht |
| Anti-APC MicroBeads | Miltenyi Biotec, Bergisch Gladbach |
| Anti-CD25 Clone PC-61.5.3 | BioXcell, West Lebanon, USA |
| Anti-FITC MicroBeads | Miltenyi Biotec, Bergisch Gladbach |
| Anti-IL-2 antibody, Clone Jes6-1A12 | BioXcell, West Lebanon, USA |
| Anti-PE MicroBeads | Miltenyi Biotec, Bergisch Gladbach |
| BD Golgi Plug | BD Pharmingen, Heidelberg |
| BD Golgi Stop | BD Pharmingen, Heidelbergn |
| Bovine serum albumin (BSA) | Sigma-Aldrich, Steinheim |
| CD4 MicroBeads | Miltenyi Biotec,Bergisch Gladbach |
| CD11c MicroBeads | Miltenyi Biotec,Bergisch Gladbach |
| Cell strainer 100µm, 40µm | greiner bio-one, Frickenhausen |
| Centrifuge tube 15ml, 50ml | greiner bio-one, Frickenhausen |
| Complete Freund´s Adjuvant (CFA) | Difco Laboratories, Detroit, USA |
| Entellan mounting medium | Merck, Darmstadt |
| Eosin | Roth, Karlsruhe |
| Fc Block, Anti mouse CD16/CD32 | eBioscinece, Frankfurt |
| Fetal calf serum | Thermo Fisher Scientific, Darmstadt |
| Fluorescent mounting medium | Dako, Hamburg |
| Haemalun | Roth, Karlsruhe |
| Hydrogen peroxide 30% | Merck, Darmstadt |
| IMDM | Thermo Fisher Scientific, Darmstadt |
| Ionomycin | Sigma-Aldrich, Steinheim |
| Isopropanol | Sigma-Adrich, Steinheim |
| KAPA PROBE FAST Universal | KAPA biosystems, Munich |
| Ketamin | aniMedica GmbH, Senden |

| | |
|---|---|
| LCMV peptide $GP_{61-80}$ (GLKGPDIYKGVYQFKSVEFD) | Panatecs, Heilbronn |
| LS-Columns | Miltenyi Biotec, Bergisch Gladbach |
| MACS Pre-separation filters | Miltenyi Biotec, Bergisch Gladbach |
| Microscope slides | Glaswarenfabrik Karl Hecht GmbH, Sondheim |
| MS-Columns | Miltenyi Biotec, Bergisch Gladbach |
| Murine IL-2 | eBioscience, Frankfurt |
| Needles, BD Microlance | BD Biosciences, Heidelberg |
| Optiprep | Sigma-Aldrich, Steinheim |
| Panserin 401 | PAN BIOTECH Gmbh, Aidenbach |
| Paraformaldeyde (PFA) 4% | Roth, Karlsruhe |
| Penicillin/streptomycin | Thermo Fisher Scientific, Darmstadt |
| Petri dish | Sarstedt, Neumbrecht |
| Phorbol 12-Myristate 13-Acetate (PMA) | Sigma Aldrich, Steinheim |
| Reaction tubes 1.5, 2ml | Sarstedt, Neumbrecht |
| Rompun 2% | Bayer Vital GmbH, Leverkusen |
| Saponin | Sigma Aldrich, Seinheim |
| Trypan blue (0,4%) | Thermo Fisher Scientific, Darmstadt |
| Xylene | O.Kindler GmbH, Freiburg |

| Kits | Company |
|---|---|
| Foxp3 staining buffer set | eBioscience, Frankfurt |
| Autoantibodies | EUROIMMUN, Lübeck |
| High Capacity cDNA Reverse Transcriptase Kit | Thermo Fisher Scientific, Darmstadt |
| In situ Cell Death Detection Kit (TUNEL) | Roche Diagnostic GmbH, Mannheim |
| MILLIPLEX MAP mouse cytokine/chemokine magnetic bead panel | Merck, Darmstadt |
| NucleoSpin® RNA isolation kit | Macherey-Nagel, Dueren |
| IgG mouse ELISA Kit | Abcam |

| Antibody (flow cytometry) | Isotype | Company |
|---|---|---|
| B220 Pe-Cy7 | Rat IgG2a,k | Biolegend |
| CD11c | Rat IgG2a,k | Biolegend |
| CD3 PE-Cy7 | Rat IgG2b,k | BD Pharmingen |
| CD4 PE-DAZZLE | Rat IgG2a,k | Biolegend |
| CD4 PE | Rat IgG2a,k | Biolegend |
| CD8 PE | Rat IgG2a,k | BD Pharmingen |
| CD19 PE | Rat IgG2a,k | Biolegend |
| CD25 PE | Rat IgG1 | Biolegend |
| CD38 APC-Cy7 | Rat IgG2a,k | Biolegend |
| CD44 PE | Rat IgG2b,k | BD Pharmingen |
| CD45 AF700 | Rat IgG2b,k | Biolegend |
| CD45.1 AF700 | Mouse IgG2a,k | Biolegend |
| CD45.2 FITC | Mouse IgG2a,k | Biolegend |
| CD69 BV785 | Armenian Hamster IgG | Biolegend |
| CD95 BV605 | Mouse IgG1,k | Biolegend |
| CD138 BV650 | Rat IgG2a,k | Biolegend |
| CXCR5 PE | Rat IgG2a,k | Biolegend |
| FOXP3 FITC | Rat IgG2a,k | eBioscience |
| GL7 PerCP-Cy5.5 | Rat IgM, k | Biolegend |
| Helios PE-Dazzle | Armenian Hamster IgG | Biolegend |
| IFN-γ AF700 | Rat IgG1,k | BD Pharmingen |
| IgG PE-Texas Red | Goat polyclonal IgG | Biolegend |
| IL-4 PE | Rat IgG1 | BD Pharmingen |
| IL-17 PE | Rat IgG1,k | Biolegend |
| IgM BV711 | Rat LOU | BD Pharmingen |
| MHC II BV421 | Mouse BALB/c IgG2a,k | BD Pharmingen |
| Neuropilin-1 PE | Rat IgG2a,k | Biolegend |
| PD-1 BV421 | Rat IgG2a,k | Biolegend |
| TNF-α BV421 | Rat IgG1,k | Biolegend |

| Antibody (histology) | Clone | Company |
|---|---|---|
| Purified rat anti-mouse B220 | RA3-6B2 | eBioscience |
| Purified rat anti-mouse CD4 | 4SM95 | eBioscience |
| Purified rat anti-mouse FOXP3 | FJK-16s | eBioscience |
| Purified rat anti-mouse follicular dendritic cell | FDC-M1 | BD Biosciences |
| Purified rabbit anti-mouse/human CD11c | Polyclonal | Thermofisher |
| Purified rat anti-mouse PNA-d | MECA-79 | eBioscience |
| CD4 AF647 | GK1.5 | Biolegend |
| CD8 PE | 53-6.7 | Biolegend |
| CD11c AF488 | N418 | Biolegend |

## 2.3 BUFFERS

### 1x PBS, pH 7.4

KCl 2.7 mM

$KH_2PO_4$ 1.5 mM

NaCl 137 mM

$Na_2HPO_4$ 6.5 mM

### 1x ACK

$NH_4Cl$ 150 mM

$KHCO_3$ 10 mM

EDTA 100 mM

### MACS-Buffer

1x PBS

0.5% BSA

2.5 mM EDTA

### Saponin

1xPBS

1%BSA

0.5% Saponin

### Sirius red 0.1%

8 g Picric Acid in 400 ml $H_2O$

+ 0.4 g Sirius Red

### 50 mM TrisHCl, pH 7.5

0.788 g Tris-HCl in 90 ml $ddH_2O$

+100 ml $ddH_20$

## 2.4 MOUSE MODELS

Animal experiments were approved by the review board of the State of Hamburg, Germany. Mice were kept under specific pathogen-free conditions with access to water and food ad libitum.

### 2.4.1 Generation of invariant chain GP (iGP) mice

The targeting vector ROSA26STOPIiMOG (53), was used to generate the targeting vector ROSA26STOPiGP by replacement of the MOG peptide encoding gene sequence with a gene sequence encoding the immunodominant GP peptide of lymphocytic choriomeningitis virus (LCMV). To that end, we generated the mutant invariant chain (iGP) by assembly PCR on the liMOG template cDNA (53), replacing the coding sequence of the MOG peptide with that of GP61-80 peptide in the correct reading-frame. This was done by amplifying two fragments of either the 5′ or the 3′ part of the invariant chain sequence using one of the two external

primers li-fwd (5′-GGATCTGACATGGTAAGTAA-3′) and li-rev (5′-CGTATAGCATACATTATACG-3′), in conjunction with one of two internal primers that were used to replace the MOG sequence by the GP sequence: (GP-fwd: 5′-CCCCGACATCTA CAAGGGCGTGTACCAGTTCAAGTCCGTGGAGTTCGACGATAACATGCTCCTTGGGCC-3′, and GP-rev: 5′-CGGACTTGAACTGGTACACGCCCTTGTAGATGTCGGGGCCGTTCAGGCCCTTCATGCGAAGGCTCTCC A-3′). The two fragments were assembled by PCR using the external primers li-fwd and li-rev to obtain one iGP minigene (886 bp) introducing one AscI restriction site to the 5’ end and one FseI restriction site to the 3’ end. The thus obtained iGP minigene was amplified after cloning into the pGEM-T Easy vector (Promega, Mannheim, Germany). The original targeting vector ROSA26STOPIiMOG, as well as the iGP minigene were restricted with AscI and FseI, followed by ligation of the two resulting gene fragments of 750 bp and 14.2 kb. The targeting vector was linearized with PvuI and electroporated into ES cells, which were cultivated as described (54). Homologous recombinants were identified by Southern blot analysis using a 700bp genomic EcoRI-PacI fragment after EcoRI digest (data not shown). Chimeras were generated from two homologous recombinant clones by injection into blastocysts. Germline transmission was confirmed by Southern blot analysis after EcoRI digest using a 1-kb SacII-XbaI fragment (probe 1; p1) from pROSA26-1. This construct was made before the project started.

The following transgenic mice with C57BL/6J background were used:

| Line | Description |
|---|---|
| Smarta | Transgenic T cell receptor specific for $GP_{61-80}$ |
| Smarta _CD45.1 | Transgenic T cell receptor specific for $GP_{61-80}$ and CD45.1 congenic |
| Alb-iGP | Alb-Cre driven conditional iGP expression and $GP_{61-80}$ presentation on MHCII by hepatocytes |
| Cdh5-iGP | Cdh5-Cre driven conditional iGP expression and $GP_{61-80}$ presentation on MHCII by endothelial cells |
| Itgax-iGP | Itgax-Cre driven conditional iGP expression |

| | |
|---|---|
| | and $GP_{61-80}$ presentation on MHCII by dendritic cells |
| Lyz2-iGP | Lyz2-Cre driven conditional iGP expression and GP61-80 presentation on MHCII by macrophages |
| CD19-iGP | CD19-Cre driven conditional iGP expression and $GP_{61-80}$ presentation on MHCII by B cells |
| Alb/Itgax-iGP | Alb-Cre and Itgax-Cre driven conditional iGP expression and $GP_{61-80}$ presentation on MHCII by hepatocytes and dendritic cells |
| Alb-iGP_Smarta | $GP_{61-80}$ presentation on MHCII by hepatocytes and transgenic T cell receptor specific for $GP_{61-80}$ |
| Cdh5-iGP_Smarta | $GP_{61-80}$ presentation on MHCII by endothelial cells and transgenic T cell receptor specific for $GP_{61-80}$ |
| Itgax-iGP_Smarta | $GP_{61-80}$ presentation on MHCII by dendritic cells and transgenic T cell receptor specific for $GP_{61-80}$ |
| Lyz2-iGP_Smarta | $GP_{61-80}$ presentation on MHCII by macrophages and transgenic T cell receptor specific for $GP_{61-80}$ |

## 2.5 ISOLATION OF PRIMARY CELLS

### 2.5.1 Isolation of splenocytes

Mice were killed by intraperitoneal injection (15 mL/kg mouse) of 12 mg/mL Ketamine + 1,6 mg/mL Xylazine, followed by cervical dislocation. The spleens were surgically removed and strained through a 100 µm cell strainer using the plunger of a syringe. Cell strainers were washed with PBS and cells were eluted into 50 ml tubes. The obtained cell suspensions were centrifuged at 400g for 5 minutes. The supernatant was discarded, and erythrocytes were lysed by resuspending the cell pellet in 1 ml of ACK buffer for 1 minute. The ACK reaction was

stopped by adding 30 ml of PBS, the resulting cell suspension was passed through a 40 µm cell strainer and subsequently centrifuged at 400g for 5 minutes. Splenocytes were resuspended in 1 ml of PBS and counted.

### 2.5.2 Isolation of splenic $CD25^-$ CD4 T cells

Splenocytes were isolated as described in 2.5.1, washed with PBS and sorted by Magnetic Activated Cell Sorting (MACS). Cells were resuspended in MACS buffer (1 ml/$10^8$ cells) and incubated with anti-CD25 PE antibody for 15 minutes at 4°C (10 µl/$10^8$ cells). After a washing step, cells were incubated with anti-PE microbeads (100 µl /$10^8$ cells) for 15 minutes at 4°C. Cells were washed again, and, meanwhile, LS columns were clamped in the magnetic stand and equilibrated with 3ml of MACS buffer. The washed cells were resuspended in 500 µl of MACS buffer and added to the column. The column was washed 3 times with 3ml MACS buffer. Magnetically labeled $CD25^+$ cells remained in the column and $CD25^-$ cells were collected in 15ml tubes. $CD25^-$ cells were incubated with anti-CD4 microbeads (10µl/$10^8$ cells) for 15 minutes at 4°C. Cells were washed again, and meanwhile, LS columns were clamped in the magnetic stand and equilibrated with 3ml of MACS buffer. The washed cells were resuspended in 500 µl of MACS buffer and added to the first column. The column was washed 3 times with 3ml MACS buffer. CD4 T cells retained by the column were subsequently eluted after removal of the column from the magnetic stand and loaded onto a second column to increase purity. The column was subsequently removed from the magnetic stand and purified cells were eluted into a 15ml tube. Purity of $CD25^-$CD4 T cells was determined by flow cytometry and was between 95-98%.

### 2.5.3 Isolation of thymocytes

Mice were sacrificed as described in 2.5.1. Thymus was surgically removed and strained through a 100 µm cell strainer using the plunger of a syringe; cells were collected in a 50 ml tube. The cell suspension was centrifuged at 400g for 5 minutes. The supernatant was discarded and thymocytes were resuspended in 1 ml of PBS.

### 2.5.4 Isolation of hepatic non-parenchymal cells

Mice were sacrificed as described in 2.5.1. The peritoneum was opened, and the portal vein exposed. A hypodermic needle was put in the portal vein and the vena cava was cut. The liver was then perfused for 30 seconds with PBS (10 ml/min), taken out and the gall bladder was removed. Using a 100 µm cell strainer, the liver was strained using the plunger of a syringe. The cell strainer was washed with PBS and cells eluted into a 50 ml tube. The cell suspension was collected and twice subjected to centrifugation at 40g for 4 minutes to discard hepatocytes that collected in the pellet. The resulting supernatant was then washed, centrifuged for 7 minutes at 400g, resuspended in 4.5 ml of PBS, mixed with 2.5 ml of Optiprep and covered with 1 ml of PBS in a 15ml tube. Cells were centrifuged for 20 minutes at 400g without break and the hepatic NPCs cumulating at the interphase were collected and subsequently washed with 50 ml PBS. The cells were then centrifuged for 7 minutes at 400g. The cell pellet was treated with 1 ml ACK buffer for 1 minute to remove residual erythrocytes. The ACK reaction was stopped by adding 30 ml of PBS, and the cell suspension was centrifuged at 400g for 5 minutes. NPCs were resuspended in 1 ml of PBS and counted.

## 2.6 CELL CULTURE

### 2.6.1 Determination of cell numbers

Cells were diluted appropriately and resuspended in a dilution of Trypan blue (1:10 in PBS) and pipetted into a Neubauer chamber. Cell number was determined by counting two of four quadrants, and dead cells colored in blue were excluded. The total cell number was calculated by using the formula:

Total cell number = counted cell number / 2 x dilution factor x volume of cell suspension x chamber factor ($10^4$)

### 2.6.2 Cell culture medium

Cells were resuspended in Panserin medium supplemented with 5% of FCS and 1% penicillin/streptomycin.

### 2.6.3 Restimulation for intracellular cytokine production

Up to $3x10^6$ cells were resuspended in 1ml Panserin medium supplemented with 5% of FCS and 1% penicillin/streptomycin. Brefeldin A (Golgi Plug, 1 µl/tube), a protein transport inhibitor, was added to the cell suspension. Alternatively, for determination of IL-4 production, monensin (Golgi Stop, 1 µl/tube), a second protein transport inhibitor was added. Cells were then stimulated by adding phorbol 12-myristate 13-acetate (PMA)/Ionomycin (50 ng/ml / 1 µg/ml) for 5 hours at 37˚C.

## 2.7 MULTICOLOR FLOW CYTOMETRY

### 2.7.1 Determination of cell viability

Cells were stained with Pacific Orange-NHS (PacO-NHS). This dye penetrates dead cells and bindsk to amine groups; therefore, dead cells can be distinguished by their high fluorescence intensity. 200 µl of 1:1000 PacO-NHS in PBS were added to the cells and incubated for 20 minutes at 4˚ C. Cells were then washed and tetramer staining was performed.

### 2.7.2 Tetramer staining

Cells were resuspended in PBS/2%FCS ($1x10^6$-$3x10^6$ cells/100 µl). 0.4 µl of APC-conjugated I-A(b) LCMV $GP_{66-77}$ tetramer was added for 1.5 hour at 37˚C. Tetramers were used to detect and quantify antigen-specific cells and consisted of 4 monomers of peptide-MHCII, which were recognized by specific TCRs. In addition, each tetramer was conjugated with a fluorochrome, which enabled flow cytometric measurement.

### 2.7.3 Cell surface marker staining

Cells were resuspended in PBS/2%FCS ($1x10^6$-$3x10^6$ cells/100µl). 1 µl of each fluorochrome-conjugated antibody was added and incubated for 10 minutes at 4˚C. Cells were washed and resuspended in PBS/2%FCS and measured immediately by flow cytometry or fixed with 1% PFA and measured the subsequent day.

### 2.7.4 Intracellular staining

Cells were stained for intracellular antigens using the FOXP3-staining buffer set (eBioscience). Cells were fixed for 30 minutes, permeabilized and incubated with 1µl of each antibody in 50 µl of permeabilization buffer for 20 minutes at 4˚C. Cells were then washed with 500 µl permeabilization buffer and resuspended in PBS.

## 2.8 IMMUNOHISTOCHEMISTRY

### 2.8.1 Organ preparation

Mice were sacrificed as described in 2.5.1. One portion each of the liver central lobe, spleen, kidney, lung, colon, and duodenum was surgically removed and put in 4% PFA for 24 hours. Samples were then processed and paraffin-embedded at the Department of Pathology at the University Medical Center Hamburg-Eppendorf. One portion of the hepatic central lobe and spleen was immerged in Tissue-Tek© O.C.T. compound and cryopreserved at -80˚C.

### 2.8.2 Haemalum and eosin staining

Formalin-fixed paraffin embedded 2 µm sections were deparaffinized in Xylene and hydrated in changes of 100%, 90%, 70% and 50% ethanol. Slides were then rinsed in distilled water. Later, slides were immerged for 10 minutes in hemalum for 10 minutes, washed with tap water for 15 minutes and put in eosin for 1-2 minutes. Sections were washed and dehydrated in changes of 50%, 70%, 90% and 100% ethanol and xylene and mounted with entellan mounting medium.

### 2.8.3 Sirius red staining

Formalin-fixed paraffin embedded 2 µm sections were deparaffinized in Xylene and hydrated in changes of 100%, 90%, 70% and 50% ethanol. Slides were then rinsed in distilled water. Section were then incubated in Sirius red solution for 1,5 hours. Finally, samples were dehydrated in ethanol, xylene and mounted with entellan mounting medium.

### 2.8.4 CD4, B220, Foxp3, PNAd and CD11c staining

Formalin-fixed paraffin embedded 2 µm sections were deparaffinized in Xylene and hydrated in changes of 100%, 90%, 70% and 50% ethanol. Slides were then rinsed in distilled water. Antigen retrieval was performed in citrate buffer for 25 minutes at 680 Watt in a microwave. Slides were cooled down at room temperature for 30 minutes. Next, 10 minutes incubation with blocking buffer was required to reduce background staining. Primary antibodies were applied at the concentration of 1:100 in Zytomed buffer and incubated overnight a 4˚C. On the next day, slides were washed with PBS and incubated with rabbit anti-rat biotin (1:200 in Zytomed buffer) for 30 minutes. After another wash in PBS, slides were incubated with anti-rabbit AP Komplex Polap Kit for 30 minutes at room temperature. Slides were washed, and the staining reaction was developed by incubating with AP Permanent Red Kit solution for 10 minutes in a dark chamber. The reaction was stopped by immersion of the slides in distilled water, followed by 2 immersions in 0.1% HCl and distilled water again. Slides were counterstained with hemalum then dehydrated and mounted with entellan mounting medium.

### 2.8.5 CD4/CD8/CD11c immunofluorescence staining

6 µm frozen sections were fixed for 10 minutes with acetone. Subsequently, the slides were washed 3 times in PBS for 3 minutes; the sections were next encircled with a hydrophobic PAP Pen (DAKO). Blocking of unspecific staining was performed with 0.1% BSA plus FcBlock (1:50) in PBS for 30 minutes at room temperature. AF647 anti mouse CD4 (1:100), and PE anti mouse CD8 (1:100) or AF488 anti mouse CD11c (1:100) were then added for 1 hour at room temperature in a dark and humid chamber. Slides were washed with PBS for 3 times, incubated with Hoechst 33258 (1:10000 in PBS) for 2 minutes. At the end, sections were washed with PBS and mounted with fluorescent mounting medium.

### 2.8.6 Modified Hepatic Activity Index (mHAI)

H/E stained paraffin sections were evaluated in a blinded fashion by a pathologist (Sören Weidemann, Department of Pathology; University Medical Centre Hamburg-Eppendorf) to assign a score according to the modified histological activity index (mHAI; *55)*. The mHAI score

determines the level of interface hepatitis (0-4), confluent necrosis (0-4), portal inflammation (0-4) and apoptotic bodies (0-4).

## 2.9 AUTOANTIBODY DETECTION

Autoantibodies were detected by indirect immunofluorescence using the TITERPLANE technique (EUROIMMUN). Briefly, onto a michrochip are loaded rat kidney, liver and stomach tissue and human Hep2 cells. Different autoantibodies bind to the specific tissue and are visualized by microscopy. Serial dilutions of mouse sera in PBS+0.01% Tween were applied into the reaction fields of a reagent tray. Subsequently, the BIOCHIP slides (EUROIMMUN) were applied on top of the reagent tray to incubate the sera with the BIOCHIP for 1 hour at room temperature. Next, the BIOCHIP was washed 3 times in PBS+TWEEN 0.01% and incubated for 30 minutes at room temperature with goat anti-mouse AF488 secondary antibody (1:500 in PBS+TWEEN 0.01%). The BIOCHIP slides were washed and mounted with fluorescent mounting medium.

## 2.10 MOLECULAR BIOLOGY

### 2.10.1 RNA purification

RNA purification from liver tissue was performed using the NucleoSpin® RNA kit (Macherey-Nagel). Liver tissue was disrupted, and cells were lysed with a solution of 350 µl of Buffer RA1 and 3.5 µl of β-mercaptoethanol. The lysate was then filtered with NucleoSpin® Filters and centrifuged (1 minute, 11000 g). The filter was discarded and 350 µl of 70% ethanol was added to the lysate which was then loaded onto a NucleoSpin® RNA Column) and centrifuged (30 seconds, 11000 g). The silica membrane was desalted by adding 350 µl of Membrane Desalting Buffer (MDB), followed by a centrifugation step (1 minute, 11000g) to dry the membrane. DNase reaction mixture was added to digest DNA and incubated for 15 minutes at room temperature. Next, the membrane was washed 3 times (250 µl of Buffer RAW2, 600 µl of Buffer RA3, 250 µl of Buffer RA3), dried and RNA eluted in 60 µl of RNase-free $H_20$.mRNA concentration was determined with nanodrop.

### 2.10.2 cDNA synthesis

High capacity cDNA Reverse Transcriptase Kit (Thermo Fisher Scientific) was used to synthesize cDNA. 6.8µl of master mix (10x Reaction Buffer, dNTPs, Random primer 10X, reverse transcriptase and RNA inhibitor,) were added to 13.2µl of RNA (0.5µg/µl) and samples were reverse transcribed in the thermocycler according to the manufacturer´s protocol. The final cDNA was diluted 1:4 in $H_20$.

### 2.10.3 Real Time PCR

KAPA PROBE FAST qPCR Master Mix (Sigma-Aldrich) containing KAPA Taq Hotstart DNA Polymerase, reaction buffer, dNTPs and $MgCl_2$ was put with the primer for *Bcl6* (Mm00477633_m1, Thermofisher), *Gata3* (Mm00484683_m1, Thermofisher), *Rorc* (Mm01261022_m1, Thermofisher), *Tbx21* (Mm00450960, Thermofisher), *Il12a* (Mm00434169_m1), *Il12b* (Mm01288989_m1), *Il12rb1* (Mm00434189_m1) and *Il12rb2* (Mm00434200_m1) in a 96-well plate. Subsequently, 4.3 µl of cDNA were added into the mix and the plate was run in the thermocycler ViiA 7.

## 2.11 IN VIVO EXPERIMENTS

### 2.11.1 In vivo enrichment of regulatory T cells

Mice were treated with repeated intraperitoneal injections of a complex of IL-2 (1 µg) and anti-IL-2 antibody (5µg), which has been described to selectively expand regulatory T cells (60-62). Mice were treated with IL2/IL-2Ab complex on three consecutive days for 4 weeks.

### 2.11.2 $CD25^-CD4^+$ T cell transfer

$10^6$ $CD25^-CD4^+$ T cells were isolated as described in 2.5.2 from Smarta_CD45.1 mice and injected intravenously into recipients of the lines Itgax-iGP, Alb-iGP or Itgax/Alb-iGP. Mice were sacrificed 7 days after cell transfer.

### 2.11.3 Statistics

All the data are shown as mean ± standard deviation. The parametric Student's t test or the non-parametric Mann-Whitney test were performed. Data were analyzed using GraphPad Prism®. For multiple comparison analyses, one way ANOVA test was performed, followed by Tukey 's post test. Survival curve was analyzed using the Mantel-Cox test. Values of $p<0.05$ (*), $p<0.01$(**), $p<0.001$(***) and $p<0.0001$(****) were considered as significant.

# 3. RESULTS

## 3.1 Generation of mouse models

We constructed a mutated invariant chain molecule (CD74) in which the CLIP peptide sequence was replaced by the LCMV GP61-80 peptide sequence, and inserted the mutated gene flanked by loxP sites into the Rosa26 gene (56), as has been done before with a similar construct (53) (figure 5). Conditional expression in hepatocytes was subsequently achieved by breeding with Alb-Cre_Smarta mice that were also transgenic for the Smarta1 T cell receptor recognizing the GP61-80 peptide (57) (figure 5). Conditional expression in dendritic cells was achieved by breeding with Itgax-Cre_Smarta mice, condtional expression in macrophages or endothelial cells was achieved by breeding with Lyz2-Cre_Smarta or Cdh5-Cre_Smarta, respectively. We thereby generated four different genetically modified mice in which MHC II molecules were conditionally loaded with a virus-derived CD4 T cell epitope in different cell types. Due to different extent of thymic deletion, these four lines manifested different degrees of abundance of the cognate CD4 T cells that specifically recognize the viral epitope. These mice present the recognized antigen by different cell types which enable us to study the different possible fates of antigen-specific CD4 T cells. These mice were further analyzed here for the development of autoimmune disease.

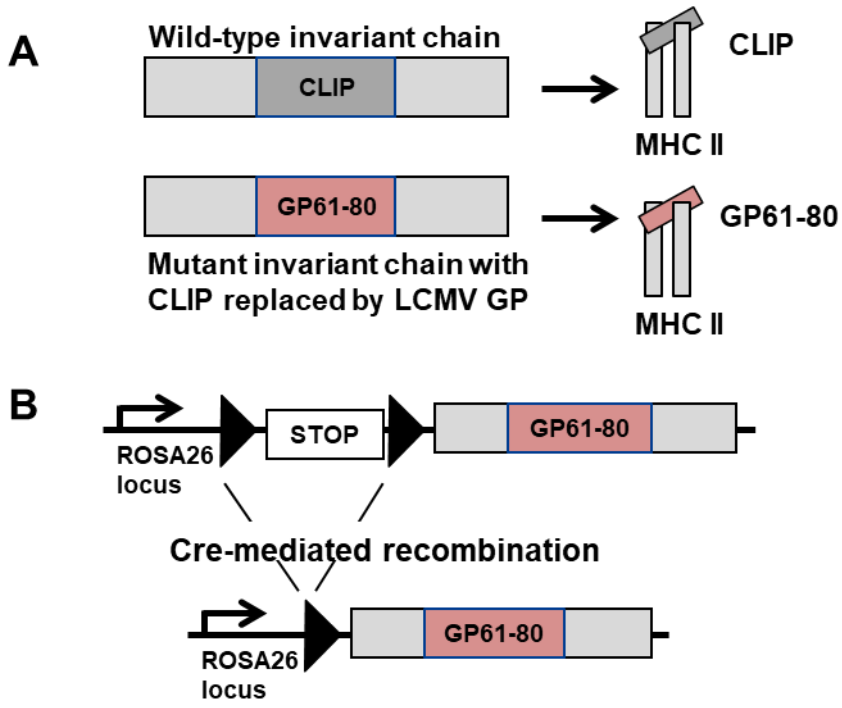


Figure 5. A) Replacement of the CLIP peptide with LCMV GP61-80 and presentation on MHCII. B) Expression of GP61-80 under the ROSA26 locus upon Cre-mediated recombination.

### 3.2 Characterization of the autoreactive T cell pool in mice with conditional autoantigen expression

To assess whether autoreactive CD4 T cells were subjected to deletion in the thymus or in the periphery, thymocytes and splenocytes of the different transgenic mouse lines that concomitantly express the autoantigen LCMV $GP_{60-80}$ and the corresponding transgenic T cell receptor were isolated and stained with LCMV $GP_{66-77}$ I-Ab specific tetramer. Autoreactive CD4 T cells in Smarta control mice, which do not express the autoantigen, were not deleted in the thymus (mean=92.6%; SD=2.084; figure 6) and in the spleen (mean=80.6%; SD=2.385; figure 6). In Itgax-iGP_Smarta mice expressing the antigen in DCs, and in Lyz2-iGP_Smarta mice expressing the antigen in monocytes/macrophages, autoreactive CD4 T cells were deleted in the thymus (mean=0.85% and 0.765%; SD=0.725 and 0.134; figure6) and not detectable in the periphery (mean=5.96% and 2.08%; SD=11.84 and 3.3; figure 6). In Cdh5-iGP_Smarta mice in which the antigen is expressed by endothelial cells, autoreactive CD4 T cells were partially deleted in the thymus (mean=13.7%; SD=24.12; figure 6). In the spleen, antigen-specific CD4 T cells were still detectable (mean=18.95%; SD=20.09; figure 6). In Alb-

iGP_Smarta mice expressing the antigen in hepatocytes, autoreactive CD4 T cells were only deleted to a small extent in the thymus (mean 73.1%; SD=6.241; figure 6) and in the periphery (mean=85.25; SD=14.48; figure 6). These mice had a significantly higher frequency of antigen-specific CD4 T cells compared to Cdh5-iGP_Smarta in thymus ($p<0.0001$) and spleen ($p<0.0001$), as well as compared to Itgax-iGP_Smarta and Lyz2-iGP_Smarta in thymus ($p<0.0001$) and periphery ($p<0.0001$).

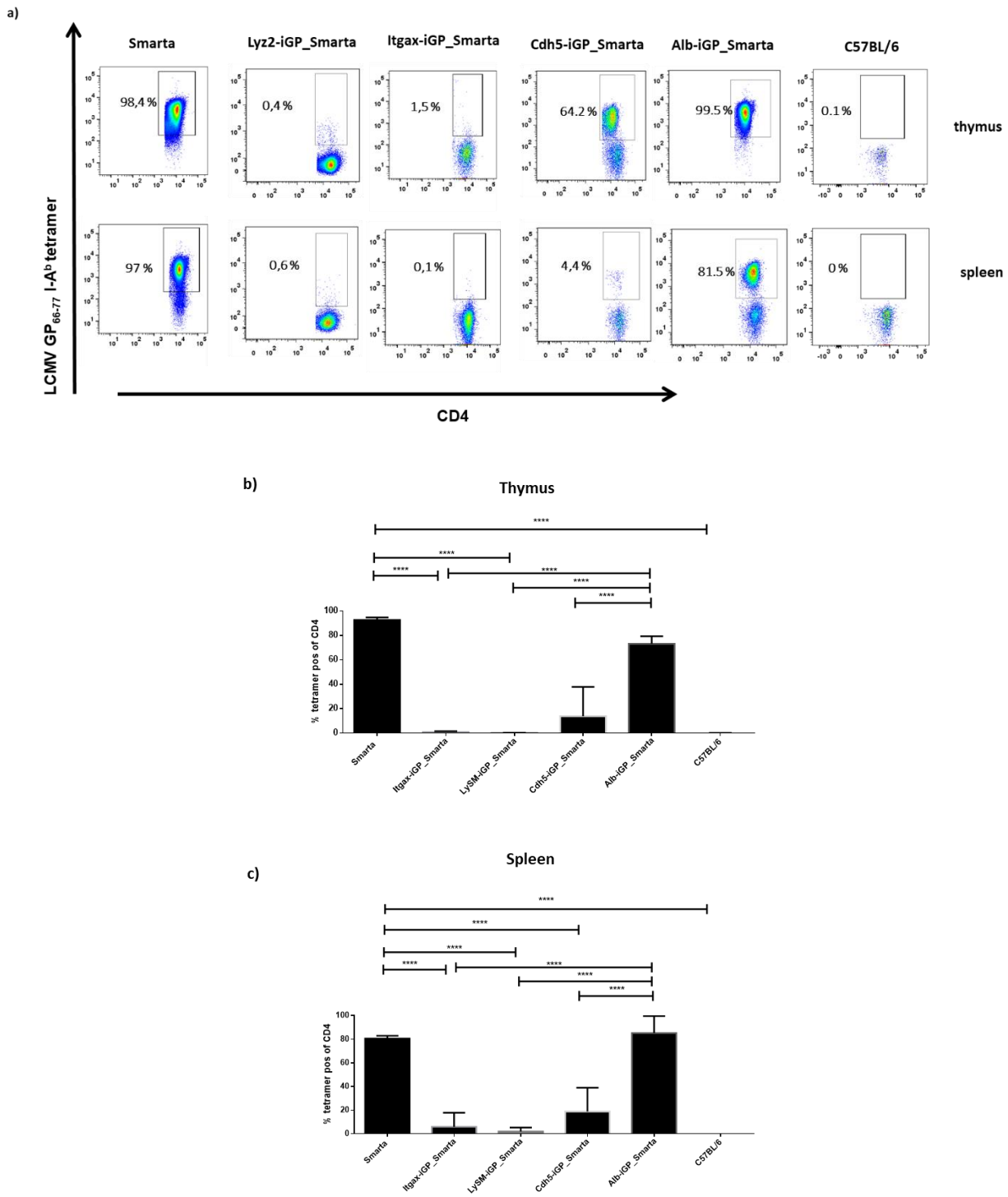


Figure 6.a) Representative dot plot showing the frequency of autoreactive $GP_{66-77}$ specific CD4 T cells in the thymus and in the spleen of the different strains with conditional autoantigen expression. Gated on viable, CD45, CD4 single positive cells. b) Quantification of autoreactive CD4 T cells in the thymus of Smarta (mean=92.6%; SD=2.084), Itgax-iGP_Smarta (mean=0.85%; SD=0.725), Lyz2-iGP_Smarta (mean=0.76%; SD=0.134), Cdh5-iGP_Smarta mice (mean=13.7%;

SD=24.12), Alb-iGP_Smarta (mean=73.1%; SD=6.241) and C57BL/6 mice (mean=0.06%; SD=0.08). N=4-15 mice per group. c) Quantification of autoreactive CD4 T cells in the spleen of Smarta (mean=80.6%; SD=2.385), Itgax-iGP_Smarta (mean=5.96%; SD=11.84), Lyz2-iGP_Smarta (mean=2.08%; SD=3.3), Cdh5-iGP_Smarta (mean=18.95%; SD=20.09), Alb-iGP_Smarta (mean=85.25%; SD=14.48) and C57BL/6 mice (mean=0%; SD=0). N=4-15 mice per group.

### 3.3 Thymic and peripheral Treg frequency

The frequency of Treg in the thymus and in the spleen of the different transgenic mouse lines was analyzed. Smarta mice, which do not express the antigen, showed no detectable Treg in the thymus (mean= 0.0%; SD=0.0) and low frequency in the periphery (mean=1.6%; SD=0.6). In Itgax-iGP_Smarta mice, where the antigen is expressed by DCs, and in Lyz2-iGP_Smarta mice, where the antigen is expressed by monocytes/macrophages, Treg were detectable in the thymus (mean=9.7% and 7.6%; SD=7.9 and 2.7; figure 7) and in the periphery (mean=14.1% and 10.7%; SD=4.8 and 2.8). In Cdh5-iGP_Smarta mice in which the antigen is expressed by endothelial cells, Treg were present in the thymus (mean=9.6%; SD=4.4; figure 7) and in the periphery (mean=15.2%; SD=7.1; figure 7). In Alb-iGP_Smarta mice that express the antigen in hepatocytes, Treg were present in a very low frequency in the thymus (mean=0.2%; SD=0.3; $p<0.0001$; figure 7), but increased in the periphery (mean=6.11%, SD=2.6, $p<0.0001$, figure 7). These data suggested that Treg may be induced in the periphery in Alb-iGP_Smarta mice.

a)

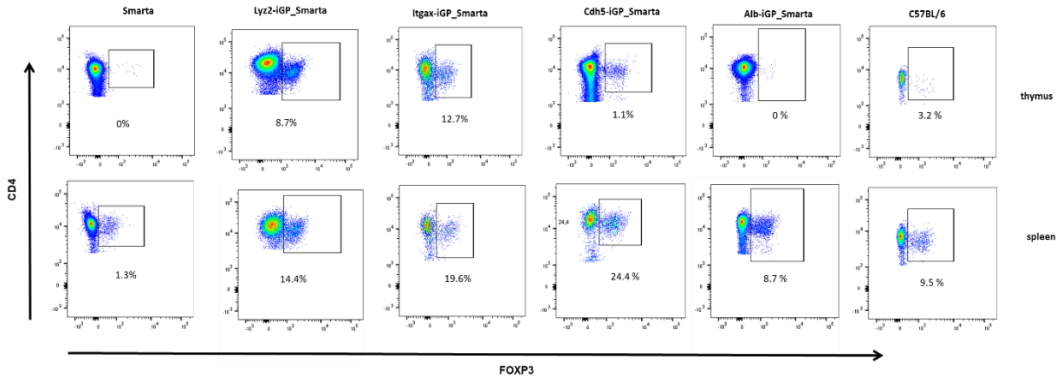


b)

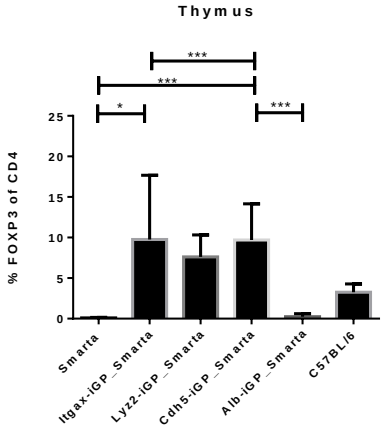


c)

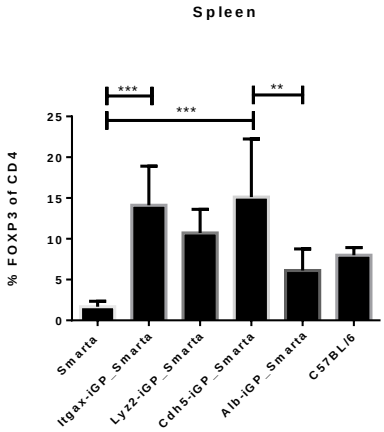


Figure 7. a) Representative dot plot showing the frequency of Treg in the thymus and in the spleen of the different strains with conditional autoantigen expression. Gated on viable, CD45,

CD4 single positive cells. b) Quantification of autoreactive CD4 T cells in the thymus of Smarta (mean=0.0, SD=0.0), Itgax-iGP_Smarta (mean=9.7, SD=7.9), Lyz2-iGP_Smarta (mean=7.6%; SD=2.7), Cdh5-iGP_Smarta mice (mean=9.6%; SD=4.4), Alb-iGP_Smarta (mean=0.2%; SD=0.3) and C57BL/6 mice (mean=3.2%; SD=1). N=4-15 mice per group. c) Quantification of Treg in the spleen of Smarta (mean=1.6%; SD=0.6), Itgax-iGP_Smarta (mean=14.1%; SD=4.8), Lyz2-iGP_Smarta (mean=10.7%; SD=2.8), Cdh5-iGP_Smarta mice (mean=15.2%; SD=7.1), Alb-iGP_Smarta (mean=6.11%; SD=2.6,) and C57BL/6 mice (mean=7.9%; SD=0.9). N=4-15 mice per group.

### 3.4 Phenotype of peripheral CD4 Smarta T cells

As the basic analysis of the T cell repertoire had revealed that, in contrast to the other strains tested, Alb-iGP_Smarta mice seemed to feature plenty of autoreactive T cells, we focused on Alb-iGP_Smarta mice in our further studies.

Splenocytes and liver NPCs of Alb-iGP_Smarta and Smarta mice were isolated and stained for the memory and homing markers CD44 and CD62L. In the spleen, Alb-iGP_Smarta mice had a higher frequency of antigen-specific $CD44^{high}CD62L^{neg}$ effector T cells compared to Smarta control mice (mean=3.9% vs 1.4%; SD=1.9 vs 0.57; p=0.0038, figure 8a), which indicated previous activation and differentiation. Correspondingly, the frequency of antigen-specific cells with a naïve $CD44^{neg}CD62L^{high}$ phenotype was slighlty higher in the spleen of Smarta controls compared with Alb-iGP_Smarta mice (mean=74.04% vs 60.52%; SD=13.8 vs 17.91; p=0.1002, figure 8c). In the liver of Alb-iGP_Smarta mice, a majority of antigen-specific CD4 T cells manifested a $CD44^{high}CD62L^{neg}$ effector phenotype, compared to Smarta controls (mean=17.98% vs 4.0%; SD=8.2 vs 2.8; p=0.0005, figure 8b). Accordingly, Smarta controls showed a higher frequency of antigen-specific CD4 T cells with a naïve $CD44^{neg}CD62L^{high}$ phenotype in the liver (mean=28.2% vs 19%, SD=10.4 vs 8.7; p=0.0483, figure 8d).

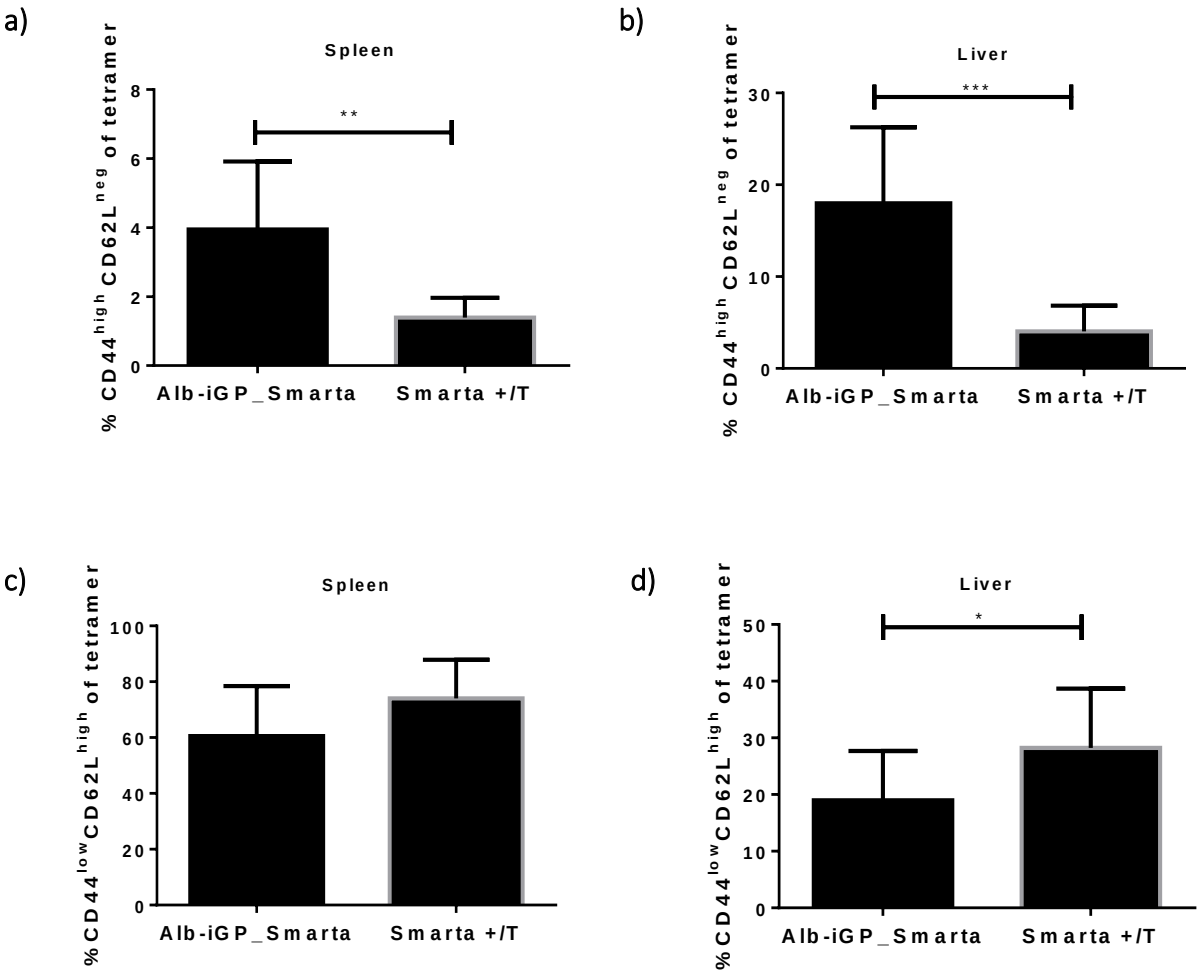


Figure 8. a) Frequency of effector $CD44^{high}CD62L^{neg}$ Smarta cells in the spleen of Alb-iGP_Smarta (mean=3.9, SD=1.9, p=0.0038) and Smarta control mice (mean=1.3, SD=0.57) b) Frequency of effector $CD44^{high}CD62L^{neg}$ antigen-specific cells in the liver of Alb-iGP_Smarta (mean=17.98, SD=8.2) and Smarta controls (mean=4.06, SD=2.8). c) Frequency of naïve $CD44^{neg}CD62L^{high}$ antigen-specific cells in the spleen of Alb-iGP_Smarta (mean=60.5, SD=17.9) and Smarta controls (mean=74.0, SD=13.8). d) Frequency of naïve $CD44^{neg}CD62L^{high}$ antigen-specific cells in the liver of Alb-iGP_Smarta (mean=18.96, SD=8.74) and Smarta controls (mean=28.2, SD=10.4). N=7-13 mice per group.

### 3.5 Clinical monitoring of Alb-iGP_Smarta mice

All the transgenic mouse lines were monitored up to 52 weeks of age to assess any clinical symptoms of autoimmune disease. As expected, Itgax-iGP_Smarta and Lyz2-iGP_Smarta mice in which the vast majority of antigen-specific T cells had been deleted in the thymus, did not

develop any signs of liver inflammation and autoimmunity (data not shown). Interestingly, Cdh5-iGP_Smarta mice did also not show any clinical sign of autoimmunity despite the remaining antigen-specific CD4 T cells in the periphery (data not shown). However, Alb-iGP_Smarta mice developed autoimmune liver inflammation resembling human AIH. These mice showed some AIH features already at 8 weeks of age but no clinical manifestations were evident (early stage). With disease progression, the symptoms became evident (late stage). Because of this reason, Alb-iGP_Smarta mice were examined in more detail.

### 3.5.1 Increased serum transaminase levels in Alb-iGP_Smarta mice

Serum ALT levels of Alb-iGP_Smarta mice in an early and late disease stage as well as ALT levels of control Alb-iGP mice were measured. At an early disease stage, Alb-iGP_Smarta mice had low ALT levels (mean=79.75 U/L; SD=19.36). However, in the late disease stage, ALT levels increased (mean=521.8 U/L; SD=639.7; figure 9) compared with early disease stage Alb-iGP_Smarta mice (p=0.0430) and Alb-iGP controls (mean=54.06 U/L; SD=16.02), indicating increased liver damage.

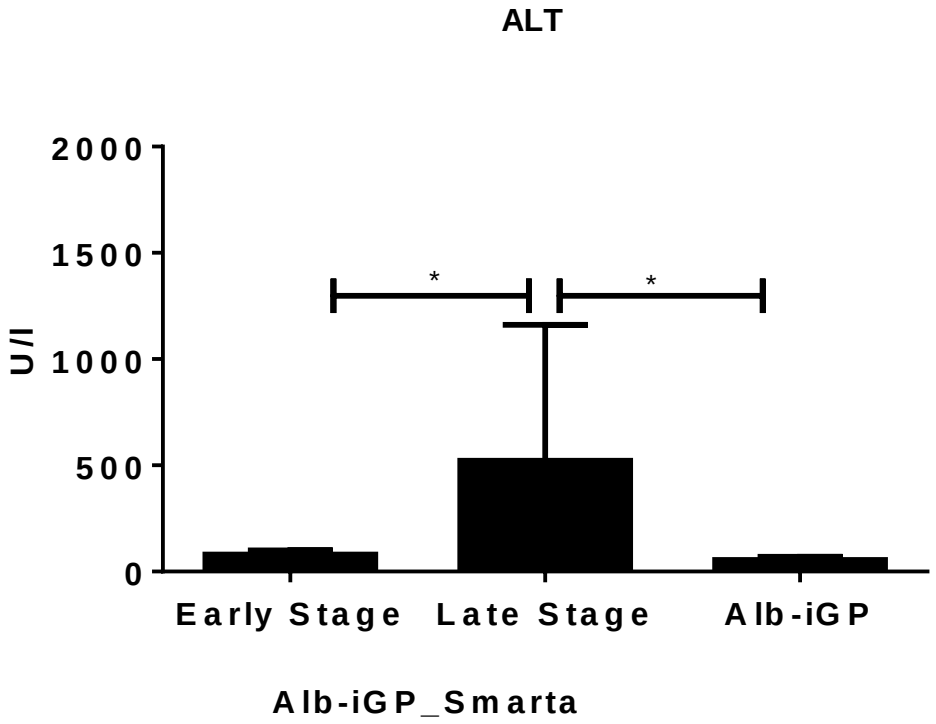


Figure 9. Serum ALT (U/L) measurement of early diseases stage (mean=79.75 U/L; SD=19.36) and late disease stage Alb-iGP_Smarta mice (mean=521.8 U/L; SD=639.7) compared to Alb-iGP control mice (f).

### 3.5.2 Hepatic infiltration of inflammatory cells in the livers of Alb-iGP_Smarta mice

, Alb-iGP_Smarta mice developed only small periportal infiltrates in the early disease stage (figure 10a). In the late stage, mice with clinical manifestations showed interphase hepatitis and portal and parenchymal infiltrates (figure 10a). Alb-iGP control mice did not develop any sign of hepatic inflammation (data not shown). H/E stained liver sections of early and late disease stage Alb-iGP_Smarta mice as well as control Alb-iGP mice were scored by a pathologist in a blinded fashion. Alb-iGP_Smarta mice showed an elevated mHAI score at an early disease stage compared to Alb-iGP controls (figure 10b). The mHAI further increased in a later disease stage, when clinical manifestations became evident, indicating the presence of liver damage including interface hepatitis, confluent necrosis, portal inflammation and apoptotic bodies ($p<0.0001$).

a) Early stage (8 weeks) Late stage (30 weeks)

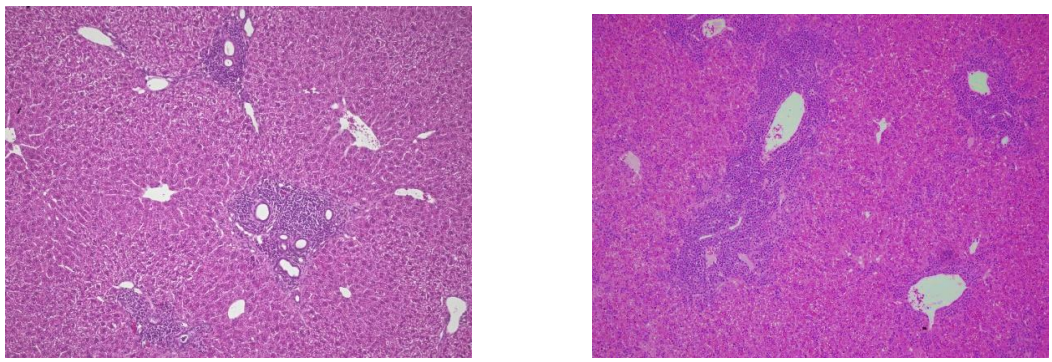

b)

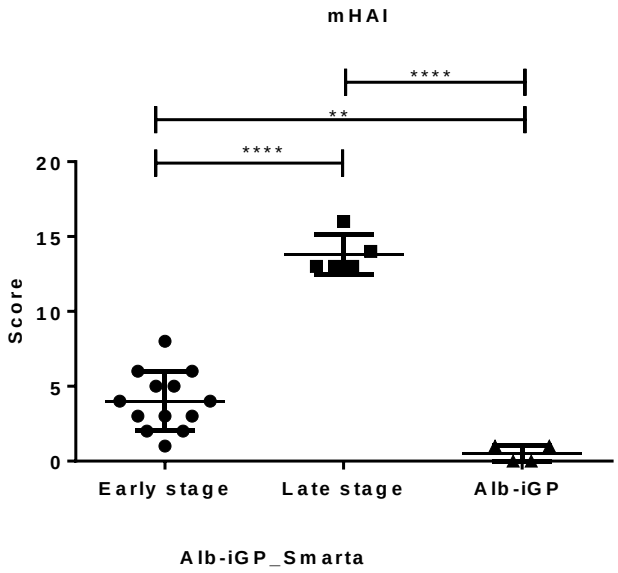


Figure 10. (a) Representative H/E staining of early and late disease stage of Alb-iGP_Smarta mice (100X magnification). (b) mHAI score of liver sections of early and late stage Alb-iGP_Smarta and Alb-iGP controls. N=4-13 mice per group.

### 3.5.3 Autoantibody detection

Antinuclear antibodies (ANA) are commonly detected in patients with autoimmune hepatitis as well as in other autoimmune diseases. The presence and the titer of autoantibodies in the sera was therefore investigated in early and late disease stage in Alb-iGP_Smarta mice and

compared with Alb-iGP controls (figure 11 a and b). In the early disease stage (8 weeks), the majority of Alb-iGP_Smarta mice developed ANAs at relevant titers (>1:80; figure 11 a and b). In the late stage (30 weeks), ANAs were still detectable at high titers. In contrast, Alb-iGP controls showed low titers (<1:40) or no ANAs.

a)

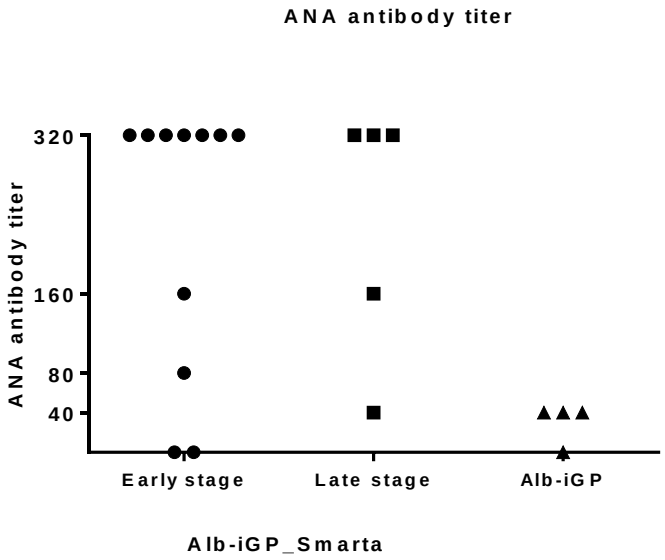


b)

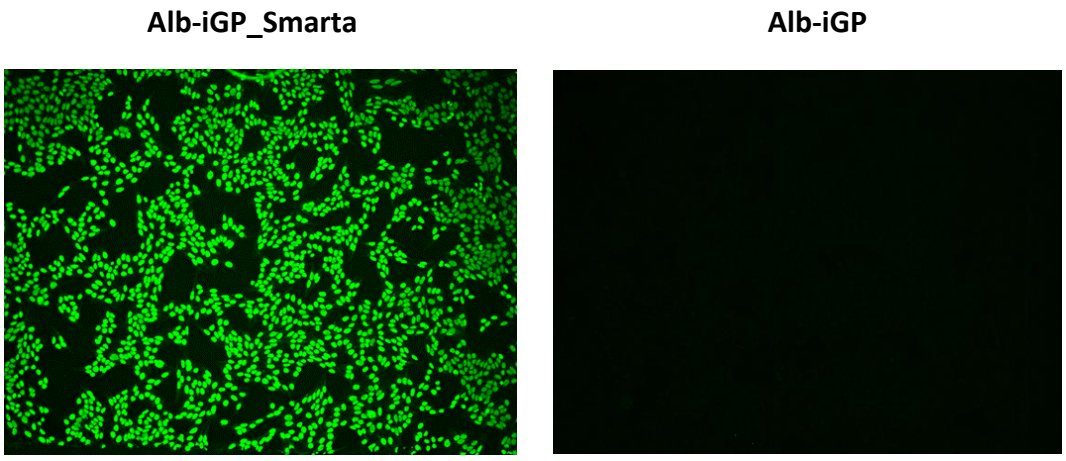


Figure 11. a) ANA titers at early (8 weeks) and late (30 weeks) disease stage in Alb-iGP_Smarta mice and Alb-iGP controls. b) Representative images of ANA detection in Alb-iGP_Smarta and Alb-iGP mice. Images were acquired at 10X magnification.

### 3.5.4 IgG quantification

IgG serum levels were measured in Alb-iGP_Smarta mice in an early and late disease stage as well as in Alb-iGP control mice. The levels of IgG were higher in Alb-iGP_Smarta mice in an early disease stage compared to Alb-iGP controls (mean=345.8 vs 143.7; SD=137.4 vs 69.14 ; p=0.0285; figure 12). With disease progression, IgG levels remained high (mean=400.4; SD=239.9; p=0.0174; figure 12).

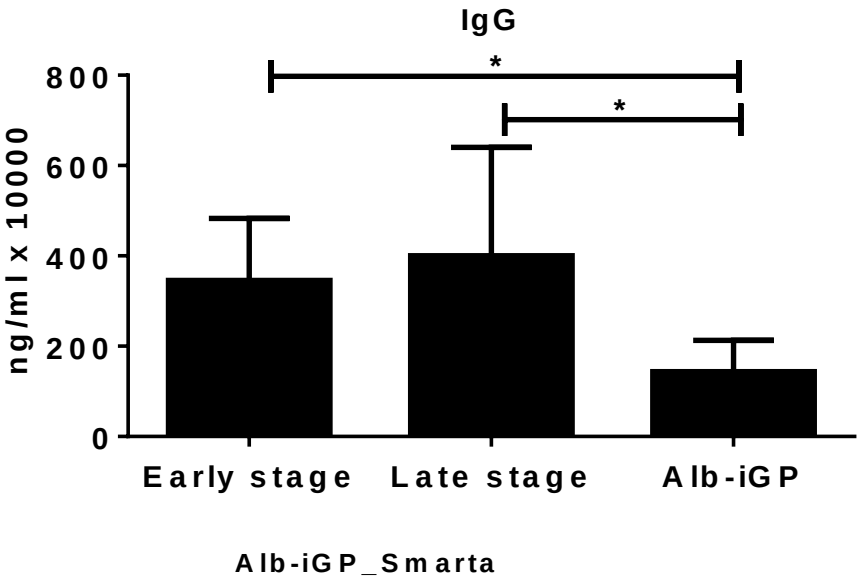


Figure 12. IgG serum levels of Alb-iGP_Smarta mice in an early (mean=345.8; SD=137) or late disease stage (mean=400.4; SD=239.9) and in Alb-iGP controls (mean=86.4; SD=10.2;). N=5-9 mice per group.

### 3.5.5 CD4 T cells dominate the hepatic infiltrate

A CD4/CD8 immunofluorescence staining was performed on liver sections of Alb-iGP_Smarta mice as well as of Alb-iGP control mice in order to characterize the composition of the hepatic inflammatory infiltrates. An increased frequency of CD8 T cells was observed in the liver of Alb-iGP_Smarta mice compared to Alb-iGP controls (figure 13). However, most of the infiltrates, notably in the periportal area, was composed of CD4 T cells, presumably the autoreactive cells.

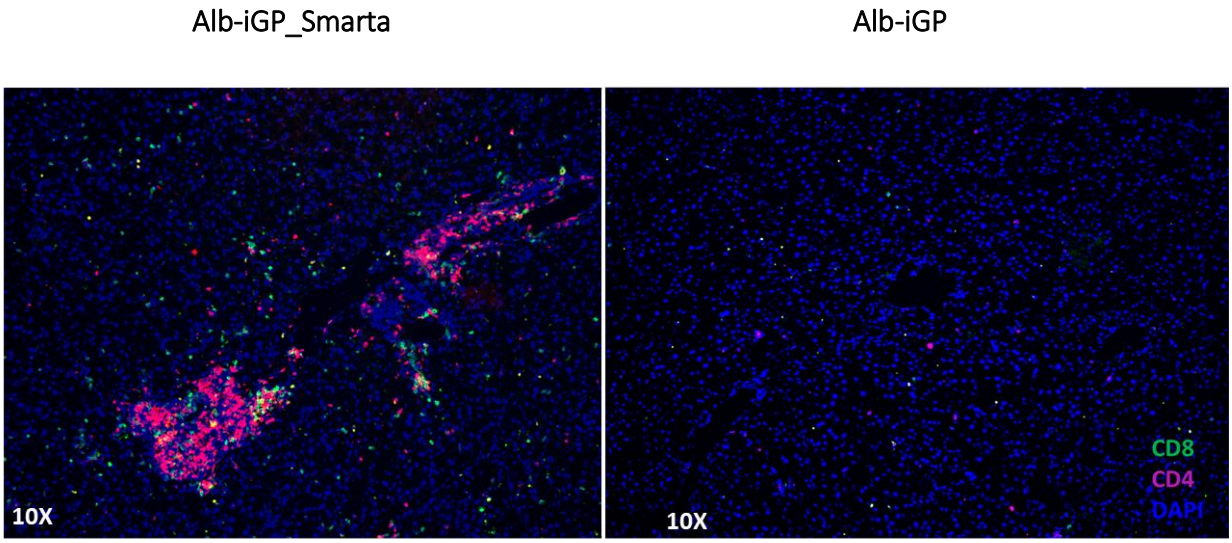


Figure 13. Representative CD8 (green) and CD4 (pink) immunofluorescence staining of liver sections. Nuclei were counterstained with Hoechst (blue).

### 3.5.6 Ectopic lymphoid tissues (ELT)s

We detected ELTs in the liver of Alb-iGP_Smarta mice, which were characterized by the segregation of CD4 T cell and B cell (B220+) zones, as well as the presence of high endothelial venules (figure 14). These structures were surrounded by collagen as indicated by sirius red staining. At 30 weeks of age, Alb-iGP_Smarta mice showed autoimmune liver inflammation dominated by CD4 T cells and B cells. At this stage, ELTs were not detectable anymore as they were merged into the large hepatic infiltrates (figure 14). ELT formation was not observed in the other strains (data not shown).

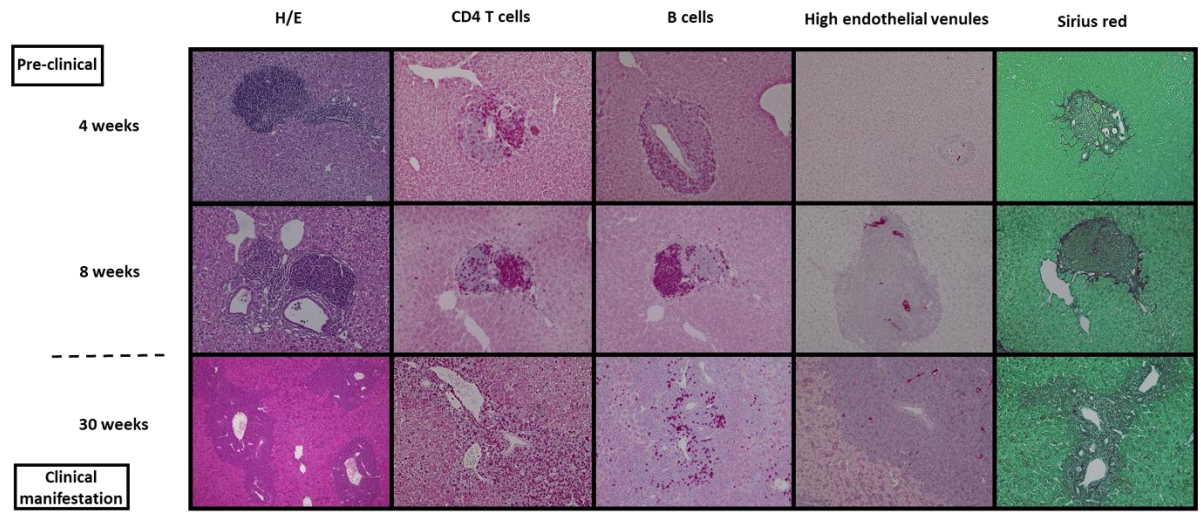


Figure 14. Representative histological pictures showing H/E, CD4, B220, PNAd and Sirius red staining of 4, 8 and 30-week old Alb-iGP_Smarta mice.

### 3.5.7 Impaired survival of Alb-iGP_Smarta mice

Alb-iGP_Smarta mice and Alb-iGP controls lacking autoreactive T cells were monitored for 52 weeks. After showing AIH symptoms, Alb-iGP_Smarta mice rapidly developed a lymphoproliferative disease, resulting in 50% mortality at 30 weeks (n=13 mice per group; $p<0.0001$; figure 15). In contrast, none of Alb-iGP control mice developed any clinical symptoms during that period.

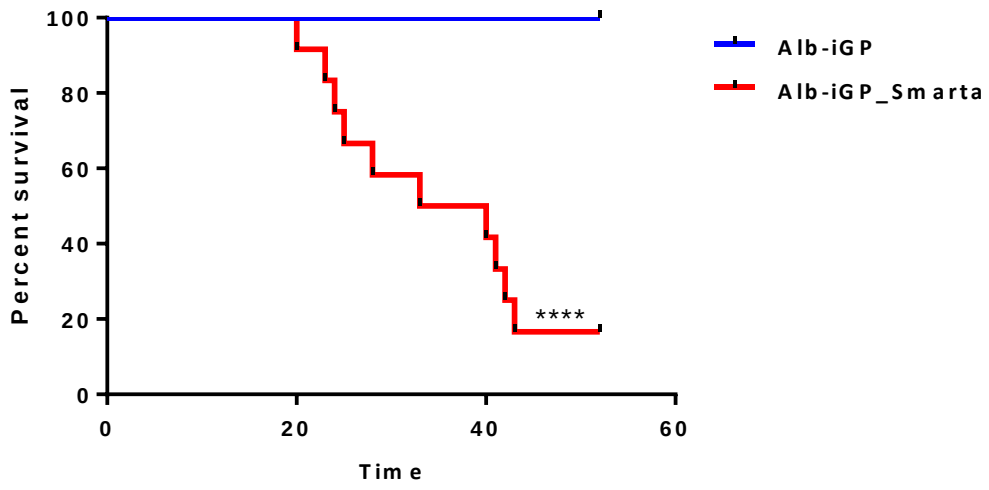


Figure 15. Survival of Alb-iGP_Smarta compared to Alb-iGP control mice. N= 13 mice per group.

The lymphoproliferative disease led to lymphoadenopathy and splenomegaly (figure 16a and b). At young age (8 weeks), no alteration in liver and spleen size as well as no signs of lymphoadenopathy were observed.

a)

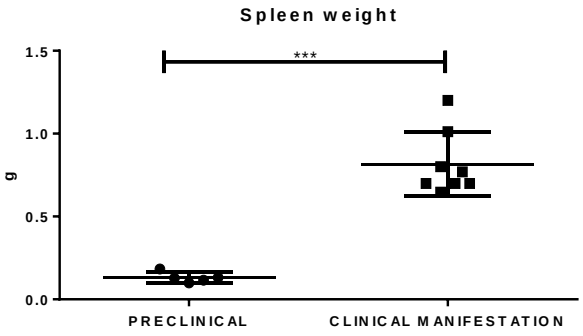


b)


Figure 16. a) Mice with clinical disease manifestation showed a significant increase in spleen weight (n=5-8 mice per group). b) Representative image showing increased size of lymph node, spleen and liver of Alb-iGP_Smarta mice compared to age- and sex-matched control Cdh5-iGP_Smarta mice.

Alb-iGP_Smarta mice with and without clinical manifestations were subjected to histological evaluation of lung, kidney, duodenum, colon and spleen to determine the cause of death. Alb-iGP_Smarta mice in a late disease stage showed massive lymphocyte infiltration in the lung and in the kidney. The spleen architecture was lost. In the ileum and colon, only small infiltrates were detected (figure 17).

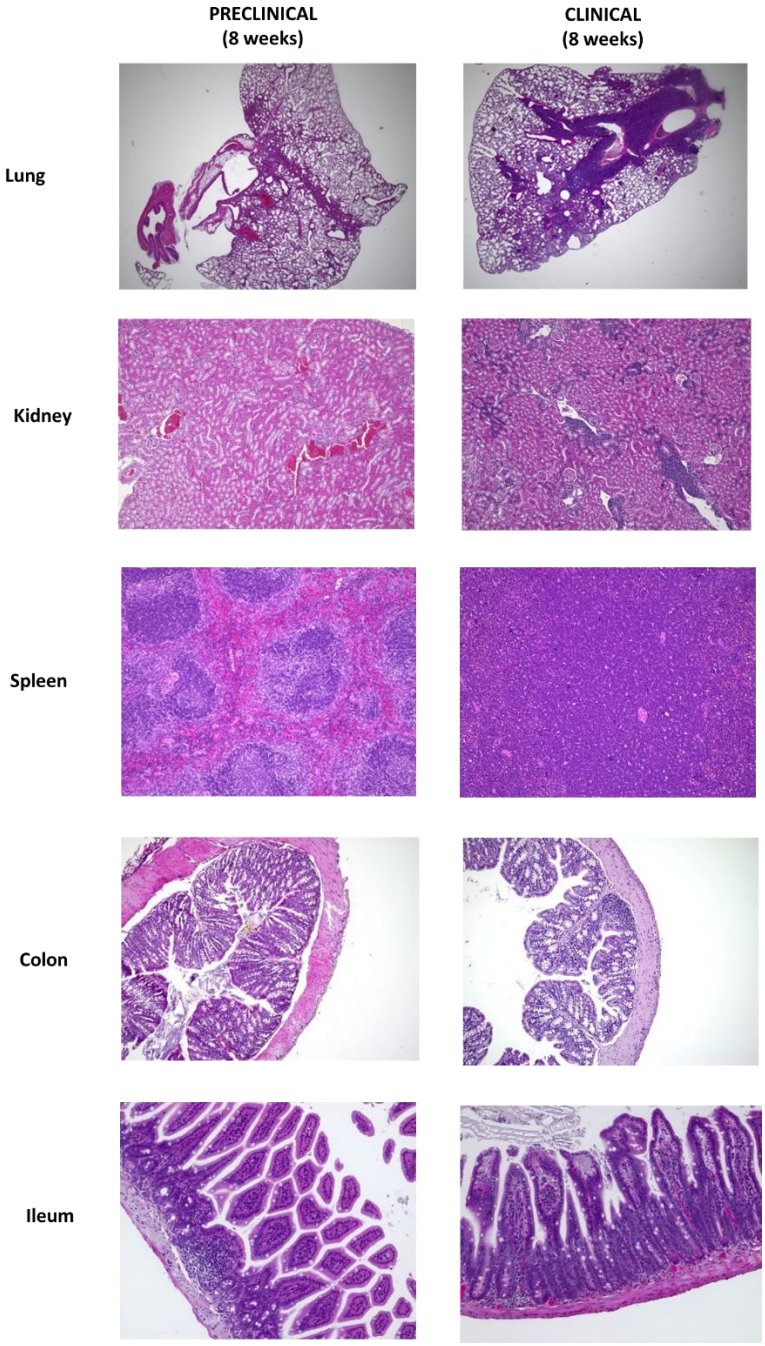


Figure 17. Representative H/E stainings of different organs of Alb-iGP_Smarta mice before and after clinical manifestation.

## 3.6 Study of the effector T cell immune response in Alb-iGP_Smarta mice

### 3.6.1 Cytokine analysis

Liver NPCs and splenocytes of 8 weeks old Alb-iGP and Alb-iGP_Smarta mice were isolated and stimulated for 5 hours in the presence of the Golgi inhibitor Golgi Stop. Subsequently, cells were stained for TNF-α, IFN-γ, IL-17 and IL-4. CD4 T cells of Alb-iGP_Smarta mice produced higher levels of IFN-γ in the spleen compared to Alb-iGP controls (mean=11.72% vs 1.96%; SD=7.27; vs. 0.61; p=0.0038; figure 18). Also in the liver of Alb-iGP_Smarta mice, CD4 T cells produced higher amounts of IFN-γ than hepatic CD4 T cells of Alb_iGP controls (mean=37.51 vs 8.58%; SD=18.81 vs. 5.34; p=0.0018; figure 18).

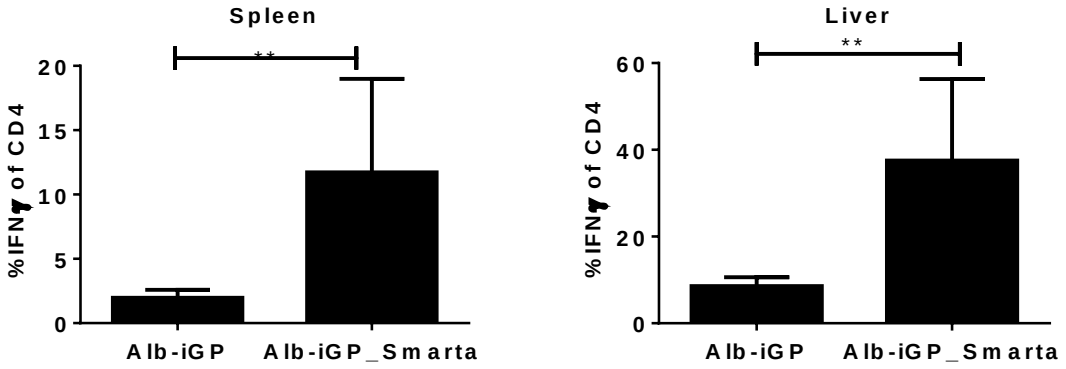


Figure 18. Frequency of IFN-γ positive CD4 T cells in the spleen (mean=11.72% vs 1.96%; SD=7.27 vs. 0.61) and in the liver (mean=37.51 vs 8.58%; SD=18.81 vs. 5.34) of Alb-iGP and Alb-iGP_Smarta mice. N=7-8 mice per group.

CD4 T cells of Alb-iGP and Alb-iGP_Smarta mice produced comparable and very high levels of TNF-α in the spleen (mean=48.64% vs. 42.14%; SD=14.61 vs. 10.28; p=0.3317; figure 19) as well as in the liver (mean=46.39% vs. 58.1%; SD=14.43 and 15.16; p=0.1411; figure 19).

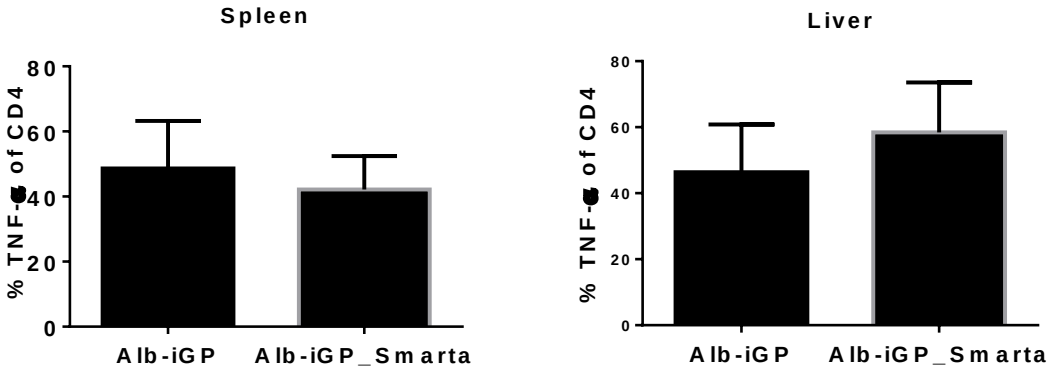


Figure 19. Frequency of TNF-α positive CD4 T cells in the spleen (mean=48.64% vs. 42.14%; SD=14.61 vs. 10.28) and in the liver of Alb-iGP and Alb-iGP_Smarta mice (mean=46.39% vs. 58.1%; SD=14.43 and 15.16). N=7-8 mice per group.

Interestingly, IFN-γ and TNF-α double positive CD4 T cells were increased in Alb-iGP_Smarta mice in the spleen (mean=12.86% vs 2.27%; SD=5.38 vs. 0.69; p=0.0002) and in the liver (mean=30.7% vs. 8.2%; SD=15.97 vs. 6.1; p=0.0039; figure 20).

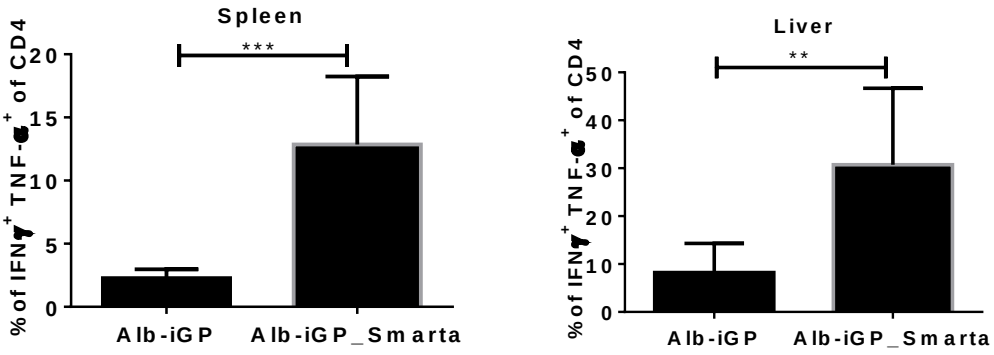


Figure 20. Frequency of IFN-γ and TNF-α double positive CD4 T cells in Alb-iGP_Smarta mice and Alb-iGP controls in the spleen (mean=12.86% vs 2.27%; SD=5.38 vs. 0.69) and in the liver (mean=30.7% vs. 8.2%; SD=15.97 vs. 6.1). N=7-8 mice per group.

The production of IL-17 by CD4 T cells was also evaluated. IL-17 production in CD4 T cells was higher in the spleen of Alb-iGP_Smarta mice compared to Alb-iGP controls (mean=7.1% vs. 1.0%; SD=3.7 vs. 0.68; p=0.0009; figure 21). In the liver, Alb-iGP_Smarta CD4 T cells produced also higher amounts of IL-17 compared to Alb-iGP control mice (mean=14.8% vs.2.2%; SD=6.74 vs. 0.86; p=0.0003; figure 21).

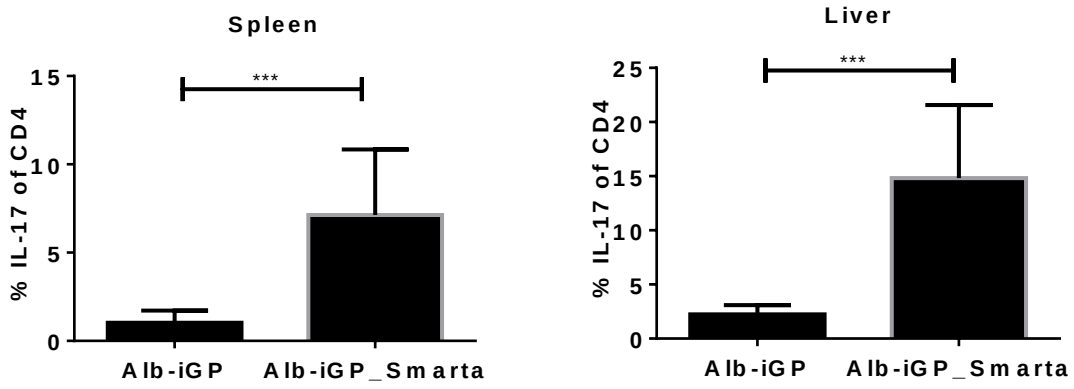


Figure 21. Frequency of IL-17 producing CD4 T cells in the spleen (mean= 1.0% vs. 7.1% SD=0.68 vs. 3.7) and in the liver (mean=2.2% vs. 14.8%; SD= 0.86 vs. 6.74) of Alb-iGP_Smarta and Alb-iGP control mice. N=7-8 mice per group.

The production of the Th2 cytokine IL-4 was evaluated. The level of IL-4 was low in the spleen of both Alb-iGP_Smarta and Alb-iGP control mice (mean=1.77; SD=0.70 vs. mean=20.2; SD=0.44; p=0.8571; figure 22). In the liver, the level of IL- 4 was also low and comparable between the two lines (mean=3.47; SD= 1.26 vs. mean=5.45; SD=1.42; p=0.2286; figure 22).

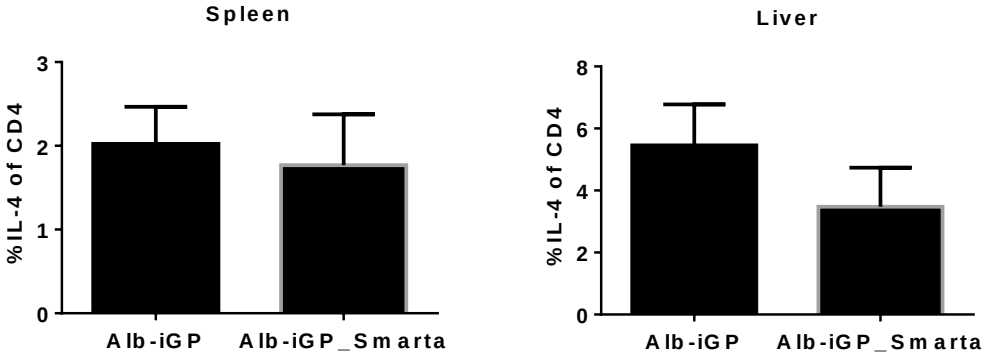


Figure 22. IL-4 production of CD4 T cells in the spleen (mean=1.77; SD=0.70 vs. mean=20.2; SD=0.44) and in the liver (mean=3.47; SD= 1.26 vs. mean=5.45; SD=1.42) of Alb-iGP_Smarta mice compared to Alb-iGP controls. N=3-4 mice per group.

Taken together, these data suggest that Alb-iGP_Smarta mice, even at the preclinical stage, show a Th1-dominated effector response.

### 3.7 Regulatory T cells

CD4 FOXP3 regulatory T cells were analyzed in the spleen and liver of Alb-iGP_Smarta mice before and after development of clinical disease symptoms. At an early disease stage, Alb-iGP_Smarta mice had detectable levels of regulatory T cells in the spleen (mean=6.11; SD=2.63; figure 2 and 23 a) and c) as well as in the liver (mean=6.36; SD=1.61), and nearly 50% were antigen-specific as indicated by tetramer staining (figure 23 a). However, in the late disease stage, FOXP3+ regulatory T cells were not detectable any longer in the spleen (mean=0.71, SD=2.63, p=0.0016, figure 23 a) and c) as well as in the liver (mean=0.28, SD=0.54, p=0.0079, figure 23). These data suggest that the loss of Treg may be important in disease progression of Alb-iGP_Smarta mice.

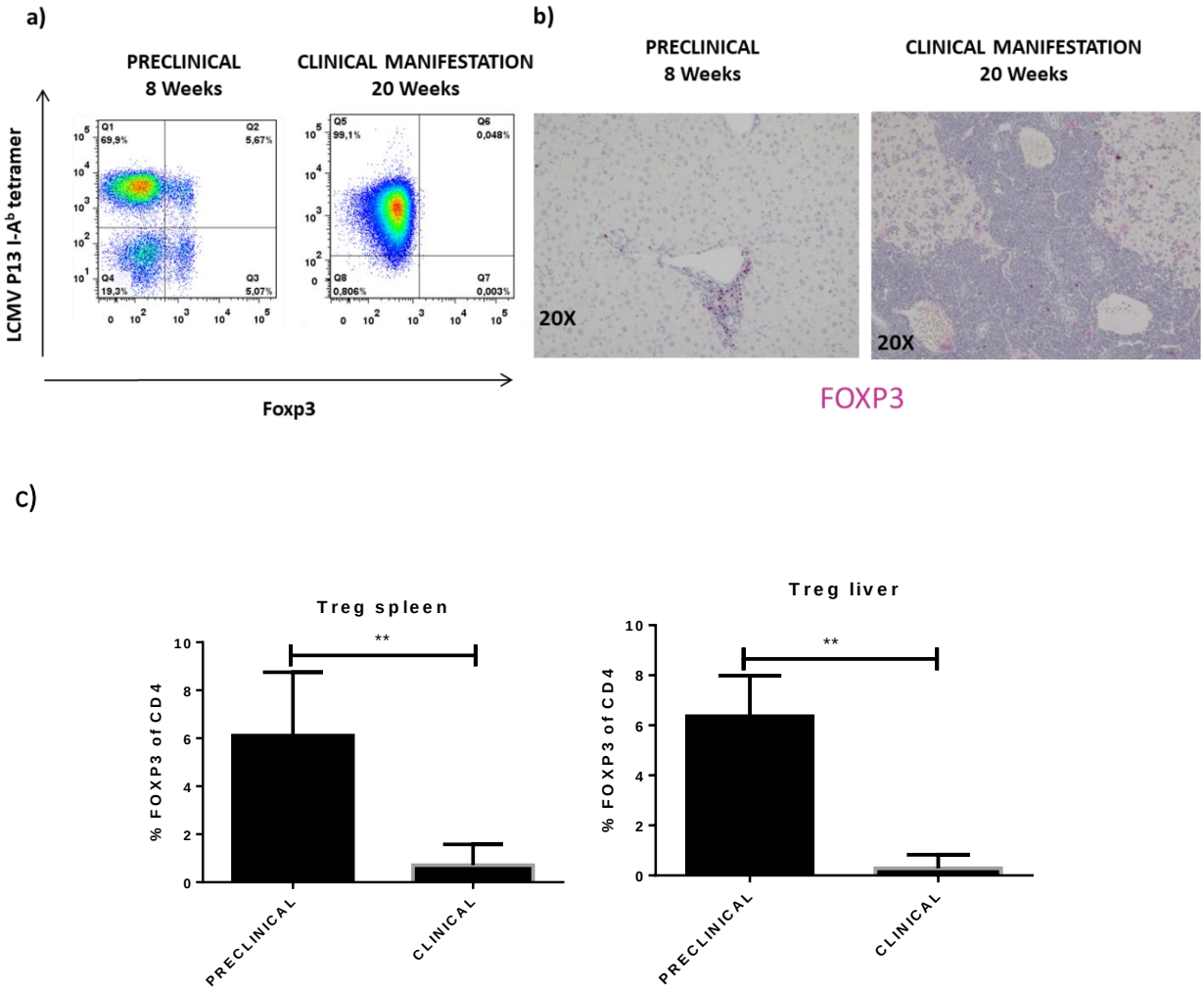


Figure 23. a) Representative dot plot showing splenic FOXP3+ Treg frequency in Alb-iGP_Smarta mice with and without clinical manifestations. b) Representative immunohistochemical staining of FOXP3 in Alb-iGP_Smarta mice at an early and late disease stage. c) Frequency of Treg in the

spleen of Alb-iGP_Smarta mice with (mean=0.714%, SD=0.86) and without (mean=6.11, SD= 2.63) clinical manifestations (left); frequency of Treg in the liver of Alb-iGP_Smarta with (mean=0.710, SD=0.86) and without (mean=6.36, SD=1.61) clinical manifestations (right). N=5-8 mice per group.

### 3.7.1 Antigen-specific Treg

$GP_{66-77}$ specific Treg frequency was analyzed in Alb-iGP_Smarta and compared to Cdh5-iGP_Smarta mice expressing the autoantigen peptide in endothelial cells. These lines both had detectable levels of potentially pathogenic autoreactive CD4 T cells (figure 1). However, whereas Alb-iGP_Smarta mice developed severe autoimmune disease over time (figure 4), Cdh5-iGP_Smarta mice did not show any symptoms, although autoreactive $GP_{66-77}$ specific T cells were present in the periphery (figure 1). This might be explained by the much higher antigen-specific Treg numbers in Cdh5-iGP_Smarta mice (mean=39.5%; SD=24.25) as compared to Alb-iGP_Smarta in the periphery (mean=4.55%; SD=1.61; p=0.0009, figure 24).

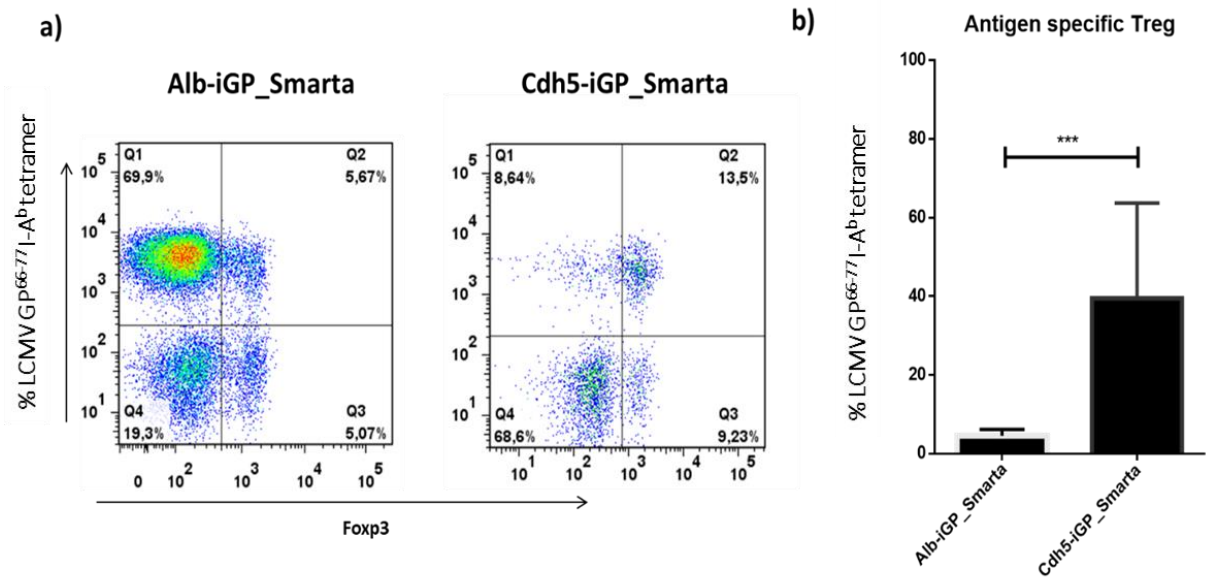


Figure 24. a) Dot plot showing the frequency of antigen specific Treg in the spleen of Alb-iGP_Smarta and Cdh5-iGP_Smarta mice. b) Quantification of splenic antigen specific Treg in Alb-iGP_Smarta (mean=4.55%; SD=1.61;) and in Cdh5-iGP_Smarta mice (mean=39.5%; SD=24.25). N= 8-10 mice per group.

### 3.7.2 Thymus-derived Treg (tTreg) versus peripheral derived Treg (pTreg)

Thymically generated Treg have been shown to be more stable then peripherally induced pTreg. It was possible that the predominance of less stable pTreg in the Treg pool of Alb-iGP_Smarta mice might have accounted for the loss of Treg in the severe phase of autoimmune inflammation. Indeed, the number of Treg in the thymus of Alb-iGP_Smarta mice was neglible (figure 2), indicating that the majority of the Treg found in the periphery were induced from non-Treg. tTreg can be distinguished from pTreg by the surface markers Neuropilin-1 and Helios. To investigate whether there were differences in frequency of tTreg or pTreg in Alb-iGP_Smarta and Cdh5-iGP_Smarta mice, thymocytes and splenocytes were isolated and Helios and Neuropilin-1 expression was analyzed by flow cytometry. Cdh5-iGP_Smarta mice had significantly higher numbers of Helios and Neuropilin-1 expressing Treg in the thymus (mean=73.6; SD=7.07; p=0.0159; figure 25) as well as in the periphery (mean=92.9; SD=3.4; p=0.0159; figure 25) compared to thymus (mean=10.47; SD=2.42) and spleen (mean=28.48%; SD=13.06) of Alb-iGP_Smarta. These data suggest that the majority of Treg in Alb-iGP_Smarta mice were probably induced in the periphery. Taken together, the significant differences in frequency and composition of antigen-specific Treg between Cdh5-iGP_Smarta mice and Alb-iGP_Smarta mice may be one explanation for the sustained tolerance in the former and the exacerbation of autoimmune disease in the latter.

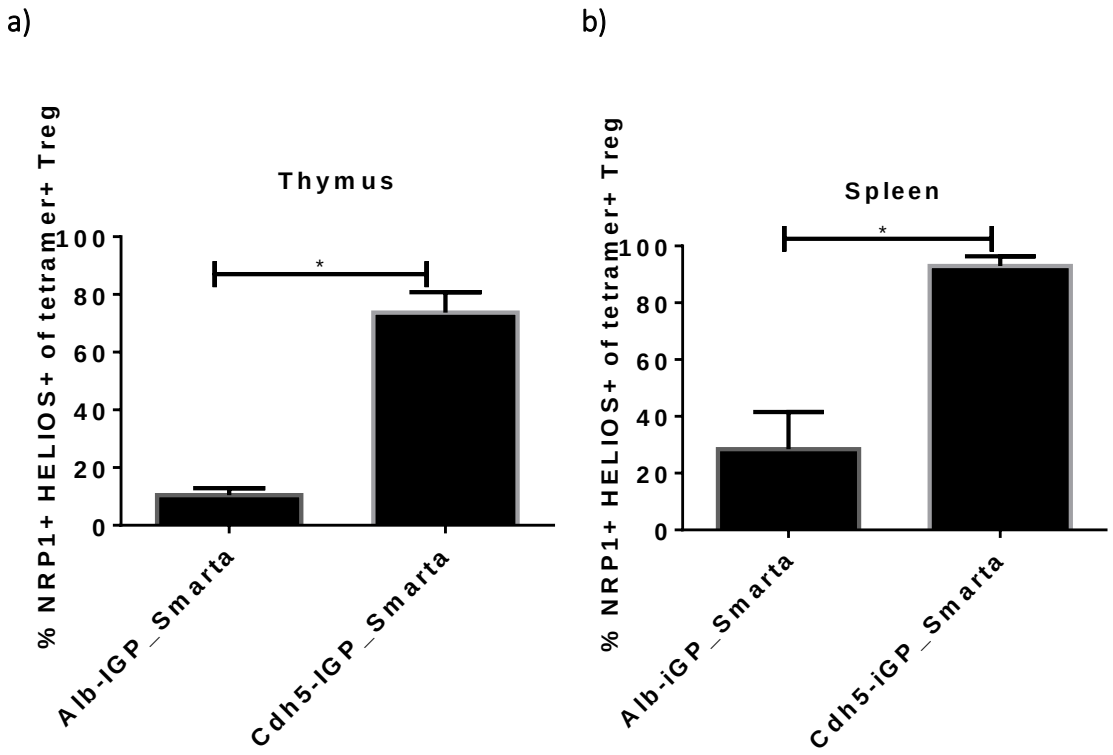


Figure 25. a) Helios and Neuropilin-1 expression on thymic Treg of Alb-iGP_Smarta mice (mean=10.47; SD=2.42) compared to Cdh5-iGP_Smarta mice (mean=73.6; SD=7.07). b) Helios and Neuropilin-1 expression on splenic Treg of Alb-iGP_Smarta mice (mean=28.48%; SD=13.06) compared to Cdh5-iGP_Smarta mice (mean=92.9; SD=3.4). N=4-5 mice per group.

### 3.7.3 Mean fluorescence intensity (MFI) of FOXP3

The intrahepatic and splenic Foxp3+ Treg were analyzed in the early disease stage. In the liver, the expression of Foxp3 was selectively reduced in GP61-80 specific Treg (Figure 26), as indicated by the significantly decreased mean fluorescence intensity (MFI) of Foxp3 in comparison to the Foxp3 MFI of non-specific Treg (686.8 vs. 1086, $p<0.0001$). In the spleen, the expression of Foxp3 was selectively reduced in GP61-80 specific Treg was found (568 vs. 835; $p=0.0015$, figure 26). Note that reduced Foxp3 expression is linked to Treg instability and reduced Treg function (59, 60).

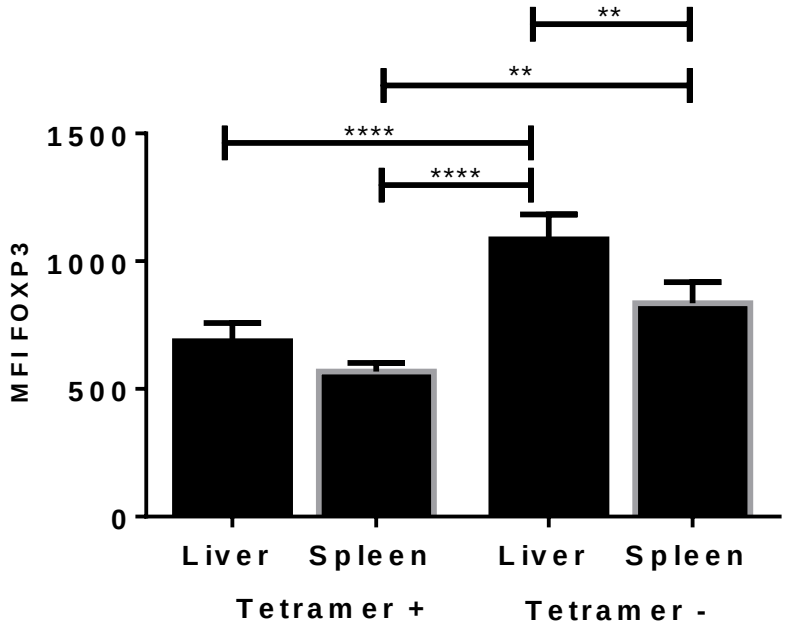


Figure 26. FOXP3 MFI of GP66-77 specific Treg and non-specific Treg in the spleen (568 vs. 835) and liver (mean=686.8 vs. 1086) of Alb-iGP_Smarta mice. N=4 mice per group.

### 3.7.4 In vivo short-term Treg enrichment

In some disease context such as experimental autoimmune encephalomyelitis and experimental type 1 diabetes, selective enrichment of Tregg using IL-2/IL-2Ab complex was protective (60,61). We tested whether such Treg enrichment may protect Alb-iGP_Smarta mice from disease development. Therefore, Alb-iGP_Smarta mice were treated for three consecutive days with IL-2/IL-2Ab complex, which should promote Treg function and survival due to their high expression of the IL2Rα, or with PBS as control, to assess the expansion of Treg and disease development. Treg failed to expand in the spleen of IL2/IL-2Ab complex treated Alb-iGP_Smarta mice (mean=7.69 vs 2.03; SD=1.74 vs. 3.93; p=0.62; figure 27) but were significantly enriched in the liver (mean=11.83 vs 5.6; SD= 1.60 vs.1.6, p=0.0286, figure 27).

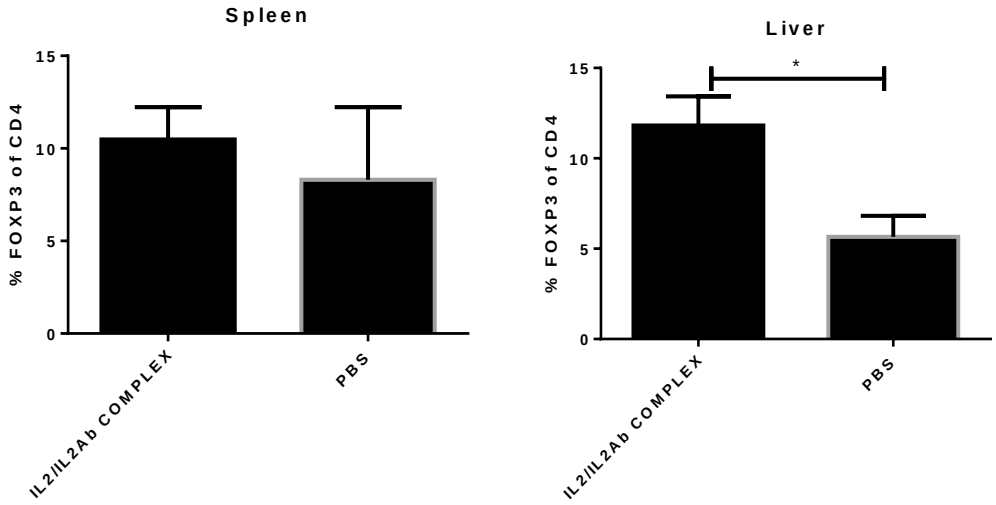


Figure 27. Splenic and hepatic Treg frequency 7 days after anti IL-2/IL-2Ab complex treatment for three subsequent days. Treg failed to expand in the spleen (mean=7.69 vs 2.03; SD=1.74 vs. 3.93) but were significantly enriched in the liver as compared to PBS treated controls (mean=11.83 vs 5.6; SD= 1.60 vs.1.6). N=4 mice per group.

Antigen-specific Treg were also enriched in the liver (mean=10.31 vs. 5.3; SD=2.49 vs. 2.72, SD=2.49, p=0.0286, figure 28).

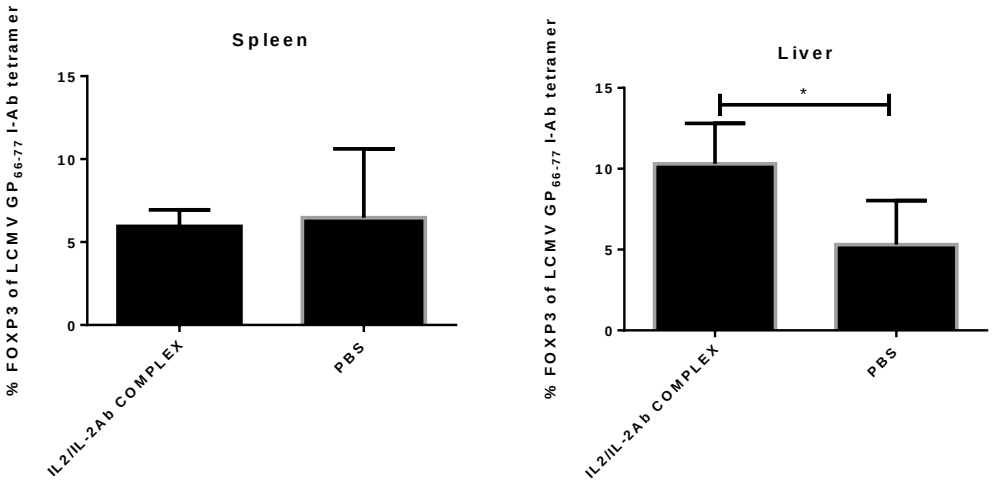


Figure 28. Splenic and hepatic antigen-specific Treg frequency. Treg failed to expand in the spleen but were significantly enriched in the liver. N=4 mice per group.

Notably, treatment with IL-2/IL-2Ab not only increased the expression of CD25 on Treg but also on effector T cells (figure 29). These data indicated that IL-2/IL-2Ab complex treatment increased the frequency of Treg but also activated effector T cells.

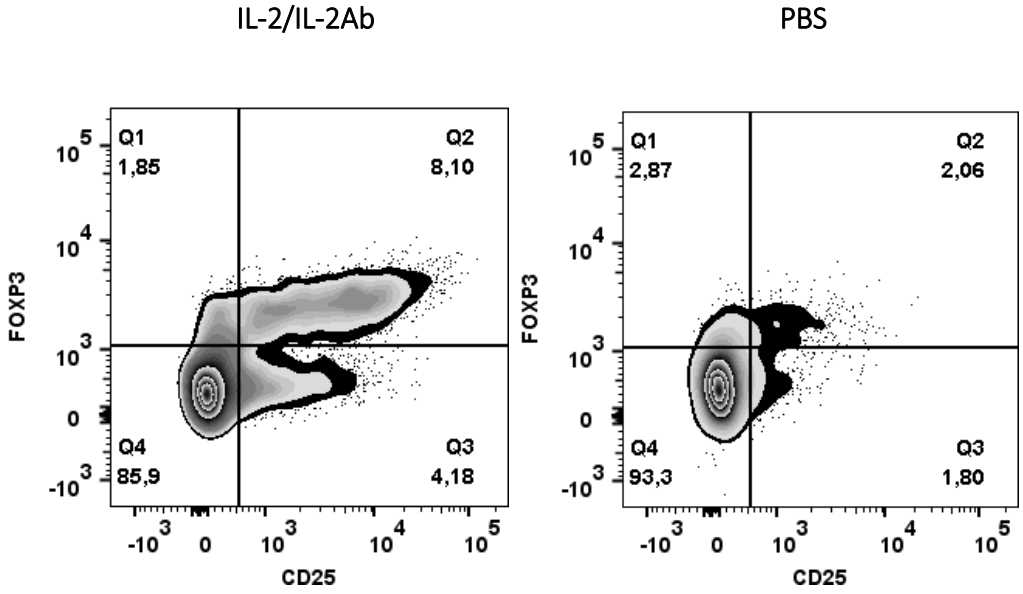


Figure 29. Representative dot plot showing CD25 expression on Treg and on effector T cells in the livers of Alb-iGP_Smarta mice on day 7 after IL-2/IL-2Ab (left) or PBS (right) treatment for 3 consecutive days.

### 3.7.5 In vivo long-term Treg enrichment

Short-term Treg expansion was achieved in the liver of Alb-iGP_Smarta mice in the early preclinical phase (8 weeks). Therefore, we hypothesized that long-term Treg enrichment might be protective or at least delay the clinical disease onset in Alb-iGP_Smarta mice. In order to assess the protective function of Treg enrichment, IL-2/IL-2Ab complex or PBS was administered weekly on three consecutive days for 24 weeks, and disease development was monitored. The experiment was started at 8 weeks of age, in an early disease stage. All the treated groups and the PBS control group were looking healthy at the beginning of the experiment. As shown in Figure 4, normally, Alb-iGP_Smarta mice start to show clinical manifestation at 20 weeks of age. Mice of the IL-2/IL-2Ab treated group showed clinical manifestations already after 16 weeks upon beginning of treatment. On the contrary, none of the PBS treated mice showed clinical manifestations at this early time point. At week 25, the experiment was terminated because two out of the four remaining mice in the treated group were moribund (p=0.0072, figure 30).

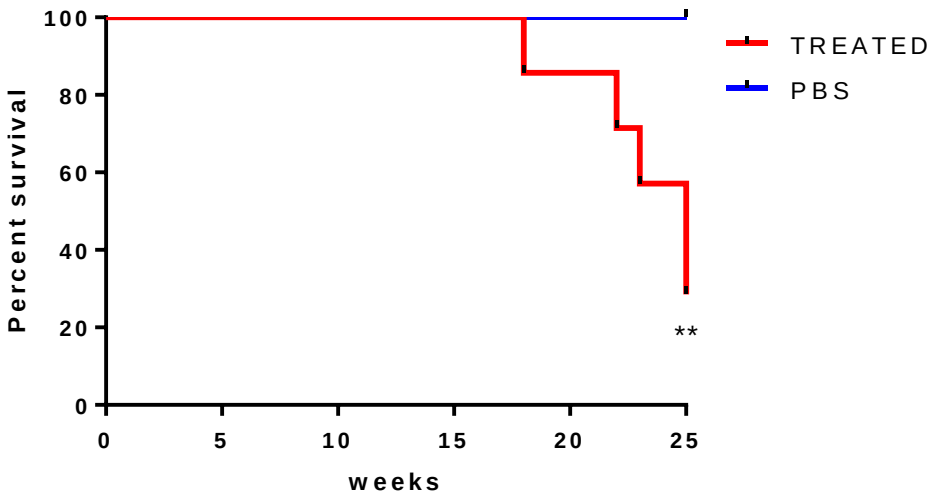


Figure 30. Survival curve showing IL-2/IL-2Ab treated compared with PBS treated Alb_iGP_Smarta mice. N=7 mice per group.

Liver histology of the treated mice showed bigger infiltrates compared to the PBS-treated group (figure 31).

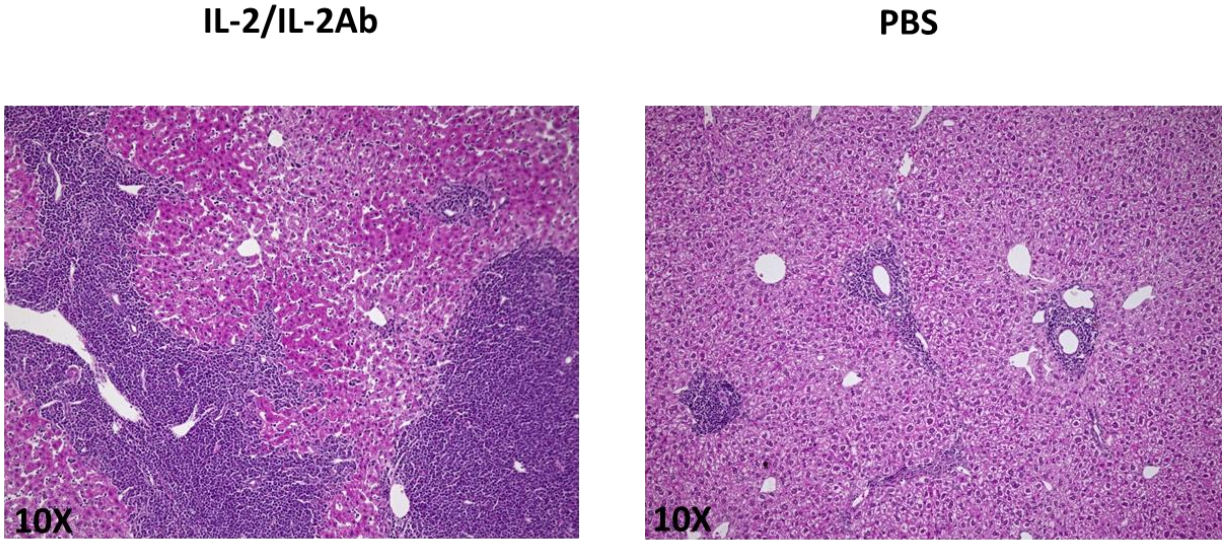


Figure 31. Representative H/E staining of IL-2/IL-2Ab treated mice compared to PBS controls.

Taken together these data show that Treg expansion via IL-2/IL-2Ab treatment did not protect Alb-iGP_Smarta mice from disease development, it seemed to even have side effects by accidential activation of pathogenic effector T cells, which also respond to the IL-2.

### 3.7.6 IL-12 expression

The failure of enriched Treg to suppress disease development in Alb-iGP_Smarta mice may be exlapined by defective IL-12 signalling as it was shown before (46). Therefore, the expression of IL-12a IL-12b, IL12rb1 and IL-12rb2 was investigated in the liver of late stage Alb-iGP_Smarta mice. IL-12a was significantly upregulated in the liver of late stage Alb-iGP_Smarta mice compared to Alb-iGP control mice (mean=9.023 vs. 1; SD=6.39 vs. 0.64; p=0.0063; figure 32). IL-12b was also upregulated in the liver of Alb-iGP_Smarta mice compared with Alb-iGP controls (mean =13.09 vs. 1; SD=10.02 vs. 0.48; p=0.0078). The receptor of IL12, IL12rb1 was upregulated in the liver of Alb iGP_Smarta comped to control mice (mean=24.4 vs. 1; SD=13.64 vs. 0.65; p=0.0006) as well as IL12rb2 (mean=59.57 vs. 1; SD=6.39 vs. 0.64; p=0.0044).

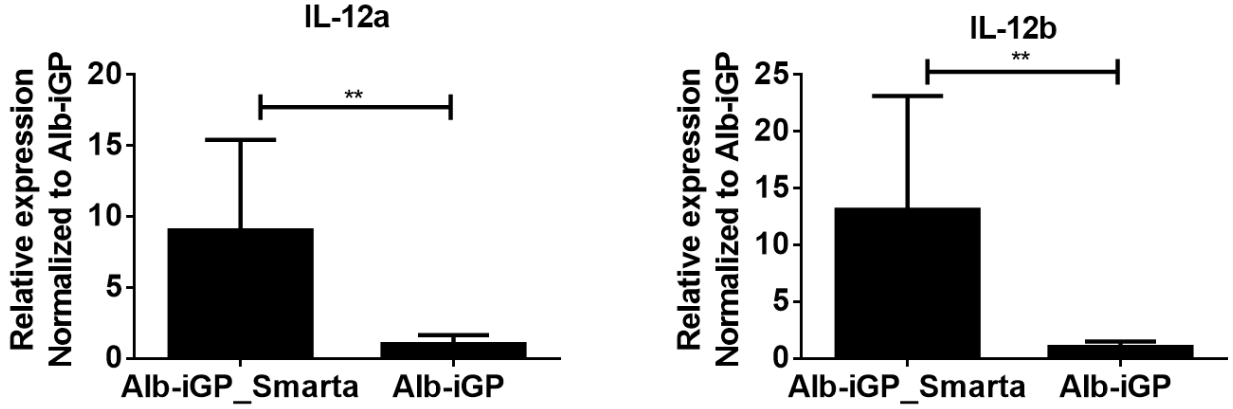


Figure 32. Hepatic IL12a (mean=9.023 vs. 1; SD=6.39 vs. 0.64) and IL12b (mean =13.09 vs. 1; SD=10.02 vs. 0.48) expression in late stage Alb-iGP_Smarta mice compared to Alb-iGP controls. N=7 mice per goup.

The receptor of IL12, IL12rb1 was upregulated in the liver of Alb iGP_Smarta comped to control mice (mean=24.4 vs. 1; SD=13.64 vs. 0.65; p=0.0006) as well as IL12rb2 (mean=59.57 vs. 1; SD=6.39 vs. 0.64; p=0.0044; figure 33).

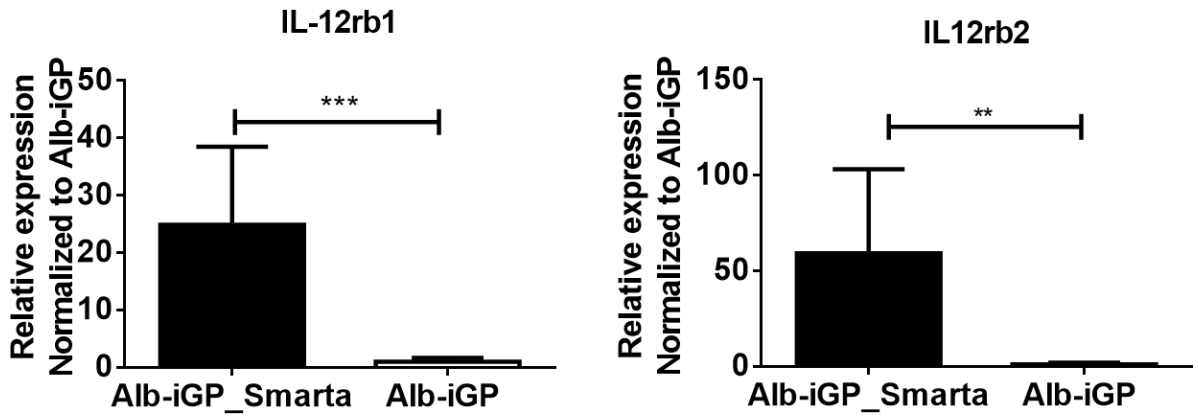


Figure 33. Hepatic IL12rb1 (mean=24.4 vs. 1; SD=13.64 vs. 0.65) and IL12rb2 (mean=59.57 vs. 1; SD=6.39 vs. 0.64) expression in the late stage Alb-iGP_Smarta compared to control mice. N=7 mice per group.

### 3.7.7 Cytokine production by Treg

Although Treg are normally associated with the production of anti-inflammatory molecules such as IL-10 and TGF-β, they may also acquire a T helper-like phenotype that is associated with the production of inflammatory cytokines and the loss of their suppressive capacity (72,73). We therefore tested cytokine production by Treg in Alb-iGP_Smarta and Alb-iGP or Smarta control mice. Liver NPCs and splenocytes were stained for TNF, IFN-γ, IL-17 and FOXP3. Treg of all the transgenic mouse strains produced comparable low levels of TNF and IFN-γ in the spleen as well as in the liver, suggesting that production of these cytokines by Treg may not be relevant in disease pathogenesis (figure 34).

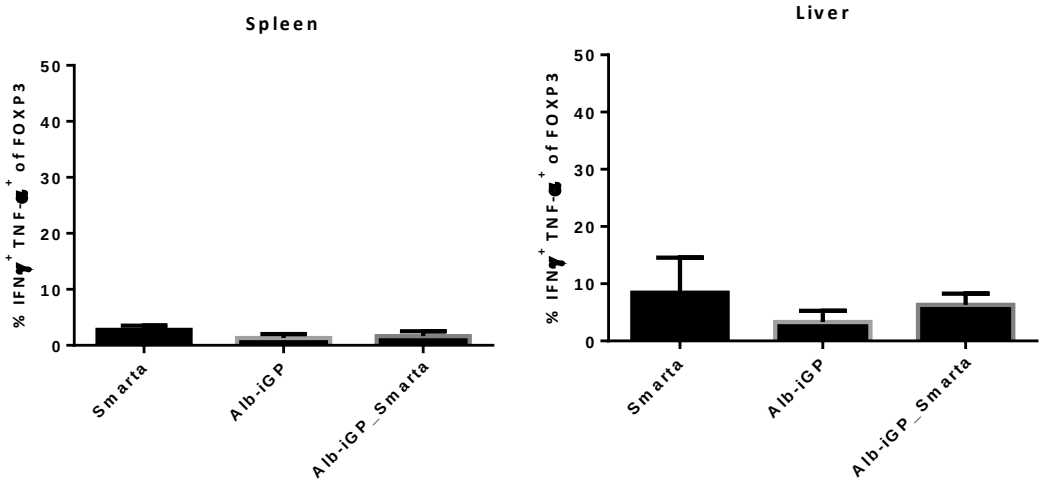


Figure 34. Frequency of IFN-γ and TNF-α producing Treg in spleen and liver of Smarta, Alb-iGP and Alb-iGP_Smarta mice. N= 3 to 4 mice per group.

To assess the actual inflammatory cytokine expression in the autoantigen-specific Treg, TNF-α and IFN-γ production was evaluated in $GP_{66-77}$ specific Treg. As shown for bulk Treg, also antigen-specific Treg produced low amounts of TNF and IFN-γ in the spleen (mean=0.84; SD=0.49; figure 35) and in the liver (mean=2.68; SD=1.82; figure 35) of Alb-iGP_Smarta mice as compared to Smarta controls.

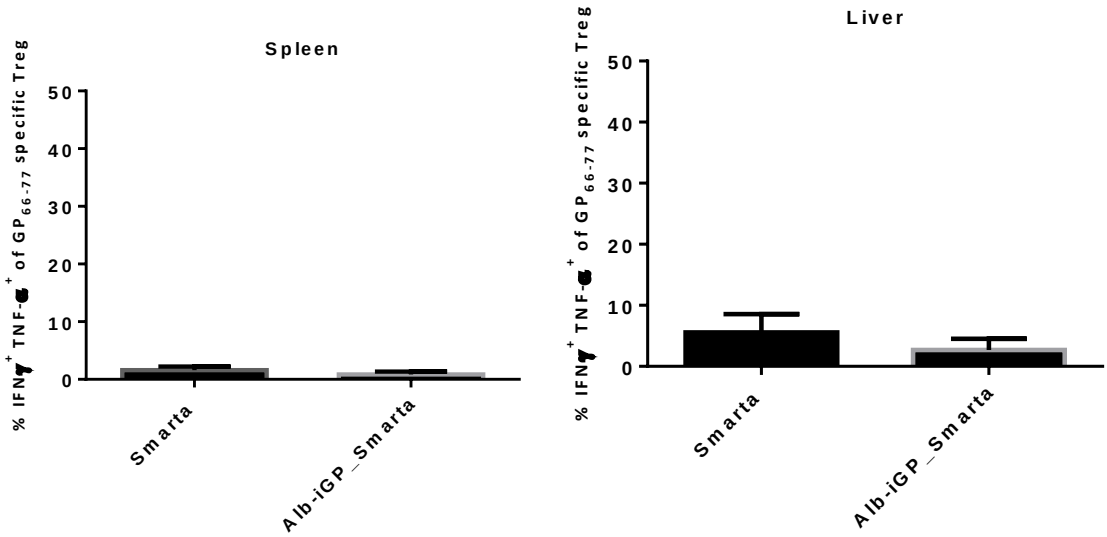


Figure 35. Frequency of IFN-γ and TNF-α producing $GP_{66-77}$ specific Treg in spleen and liver of Smarta and Alb-iGP_Smarta mice. N= 3 to 4 mice per group.

The levels of IL-17 produced by bulk Treg in the liver and in the spleen were comparable between all the lines (Figure 36).

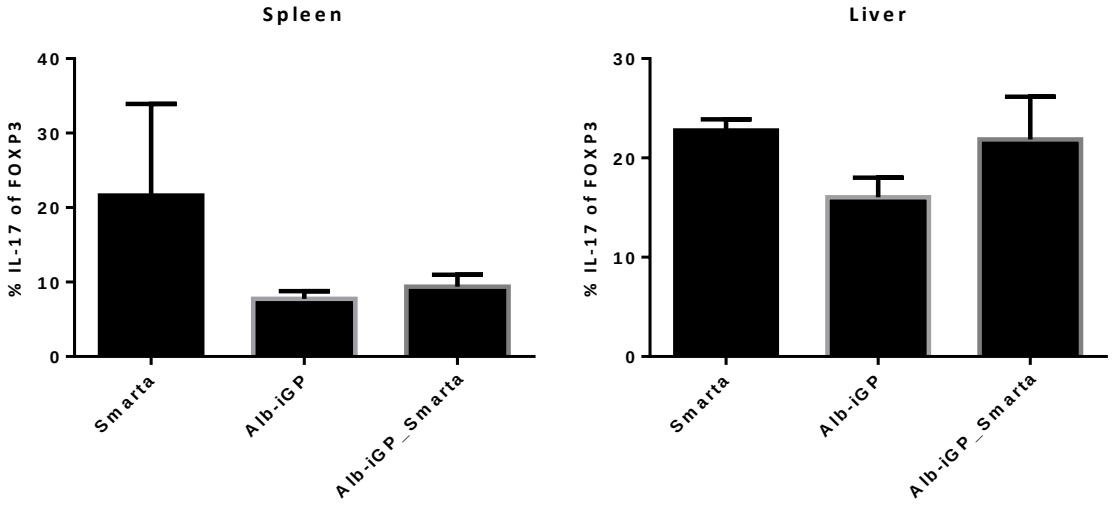


Figure 36. Frequency of IL-17 producing Treg in spleen and liver of Smarta, Alb-iGP and Alb-iGP_Smarta mice. N= 3 to 4 mice per group.

Differences in the production of IL-17 between tetramer positive (GP66-77 specific) and tetramer negative (non GP66-77 specific) Treg were evaluated in Alb-iGP_Smarta mice. Surprisingly, antigen-specific Treg produced higher amounts of IL-17 compared to tetramer negative Treg in the spleen of Alb-iGP_Smarta (mean=6.06; SD=2.95; vs. mean= 16.88; SD=11.28; p=0.1143; figure 37). In the liver, the difference was even more pronounced (mean=15.25; SD=4.37; vs mean= 27.65; SD= 3.54; p=0.0286; figure 37). Taken together, although bulk Treg seemed to have a similar cytokine profile in Alb-iGP_Smarta and control mice, the autoreactive Treg in Alb-iGP_Smarta mice selectively acquired a T helper 17-like phenotype that might counteract their regulatory function.

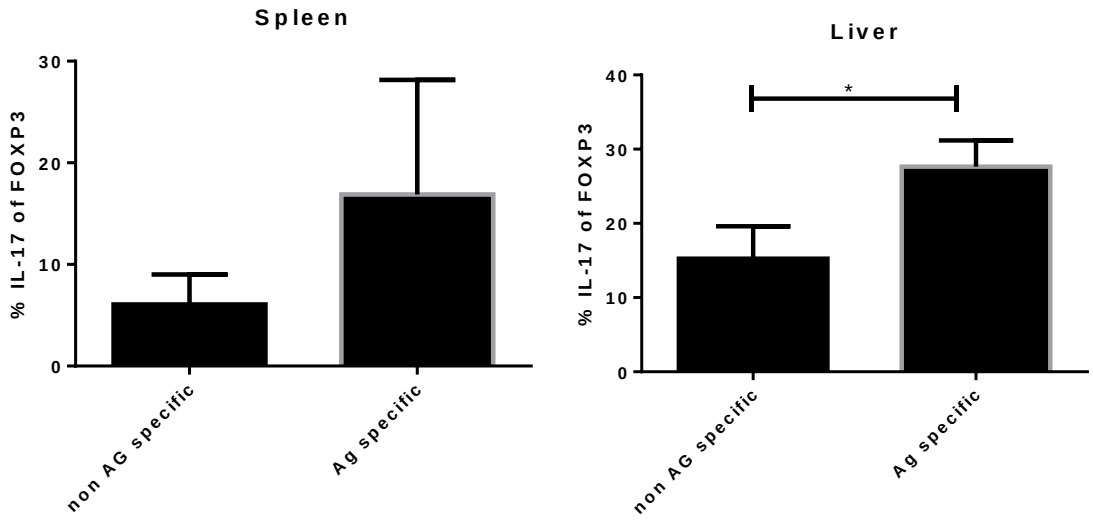


Figure 37. Production of IL-17 by non-antigen specific vs antigen specific Treg in the spleen (mean=6.06; SD=2.95; vs. mean= 16.88; SD=11.28) and liver (mean=15.25; SD=4.37; vs mean= 27.65; SD= 3.54) of Alb-iGP_Smarta mice. N=4 mice per group.

### 3.8 Inflammatory monocytes

In order to further define which cell types may contribute to the activation and expansion of autoreactive effector CD4 T cells, 8 weeks old asymptomatic Alb-iGP_Smarta and Alb-iGP control mice were stained for inflammatory monocytes in the spleen and in the liver. Higher frequency of inflammatory monocytes was found in Alb-iGP_Smarta compared with Alb-iGP control mice in the spleen (mean=0.15 vs. 0.5; SD=0.017 vs.0.15; p=0.0159; figure 38) but not in the liver as in the liver (mean=1.3; SD=0.42; p=0.19). These data suggest that inflammatory monocytes may not be relevant for the pathogenic activation of autoreactive CD4 T cells in the early disease phase.

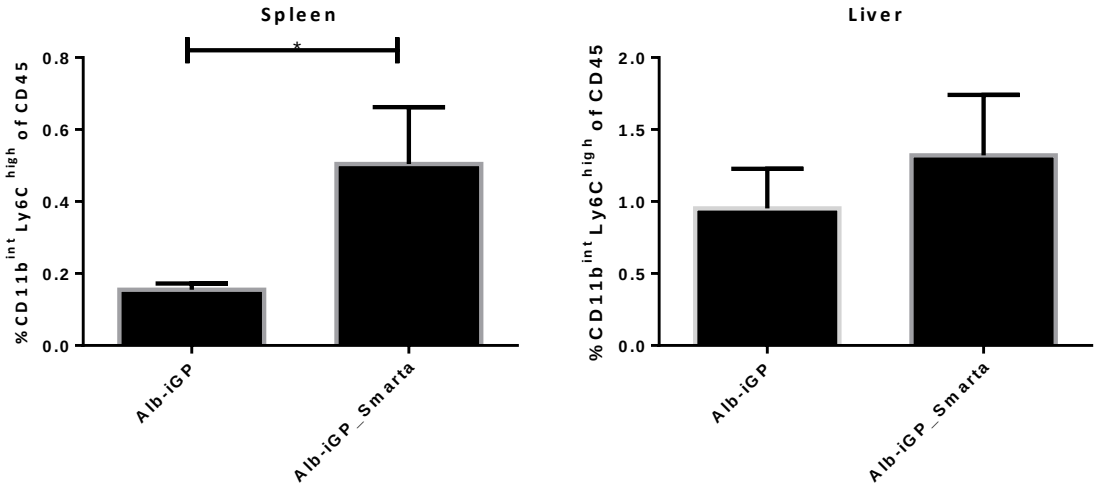


Figure 38. Frequency of inflammatory monocytes in the spleen (mean=0.50; SD=0.15) and liver (mean=1.3; SD=0.42; p=0.19) of Alb-iGP_Smarta and in the spleen (mean=0.15; SD=0.017) and liver (mean= 0.95; SD=0.42) of Alb-iGP cotrols. N=4-5 mice per group.

### 3.9 Macrophages

Splenocytes and hepatic NPCs of early stage Alb-iGP_Smarta and Alb-iGP control mice were isolated and stained for macrophages in the liver and spleen. No differences were found in the frequency of macrophages in Alb-iGP_Smarta compared with Alb-iGP control mice in the spleen (mean=2.88; SD=0.96; P=0.1111; figure 39) as well as in the liver (mean=1.5; SD=0.86; p=0.1667). These data suggest that macrophages may also not be relevant for the pathogenic activation of autoreactive CD4 T cells in the preclinical disease stage.

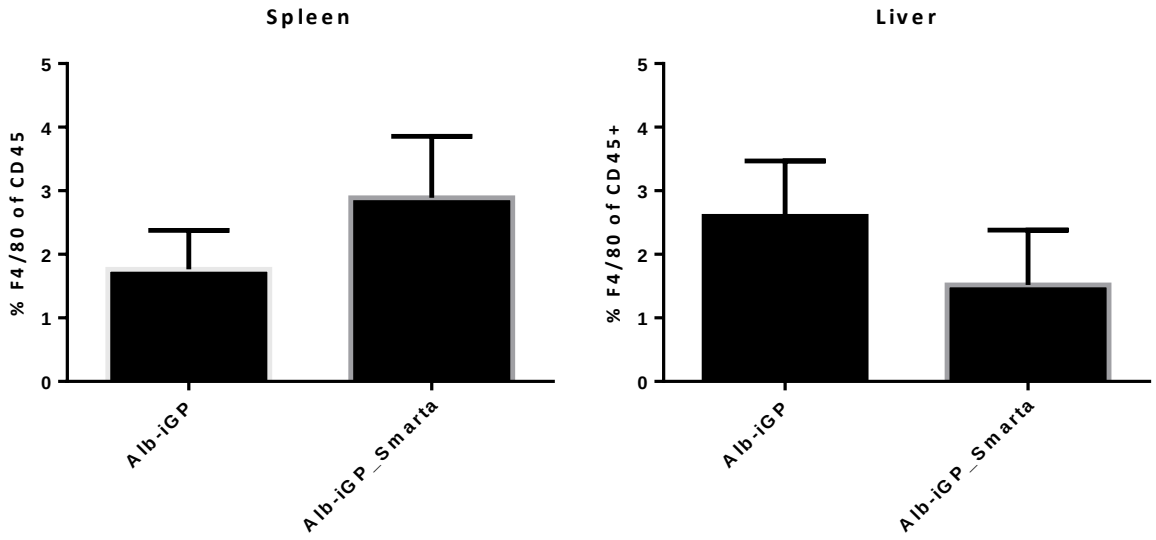


Figure 39. Frequency of macrophages in the spleen (mean=2.88; SD=0.96) and liver (mean=1.5; SD=0.86) of Alb-iGP and and Alb-iGP_Smarta do not differ. N=4-5 mice per group.

### 3.10 Dendritic cells are enriched in Alb-iGP_Smarta mice in the preclinical stage

Splenocytes and liver NPCs were isolated from early disease stage Alb-iGP_Smarta mice and Alb-iGP controls and stained by flow cytometry for the DC marker CD11c. In the spleen, Alb-iGP_Smarta mice showed higher frequencies of CD11c+ cells compared to Alb-iGP controls (mean=4.21; SD=1.48; p=0.0159; vs. mean=1.86; SD=0.13; figure 40). In the liver, CD11c+ cells further increased in Alb-iGP_Smarta mice (mean=15.94; SD=4.19; p=0.0159, figure 40), suggesting that DCs may be important drivers of autoreactive T cell activation already at the subclinical stage.

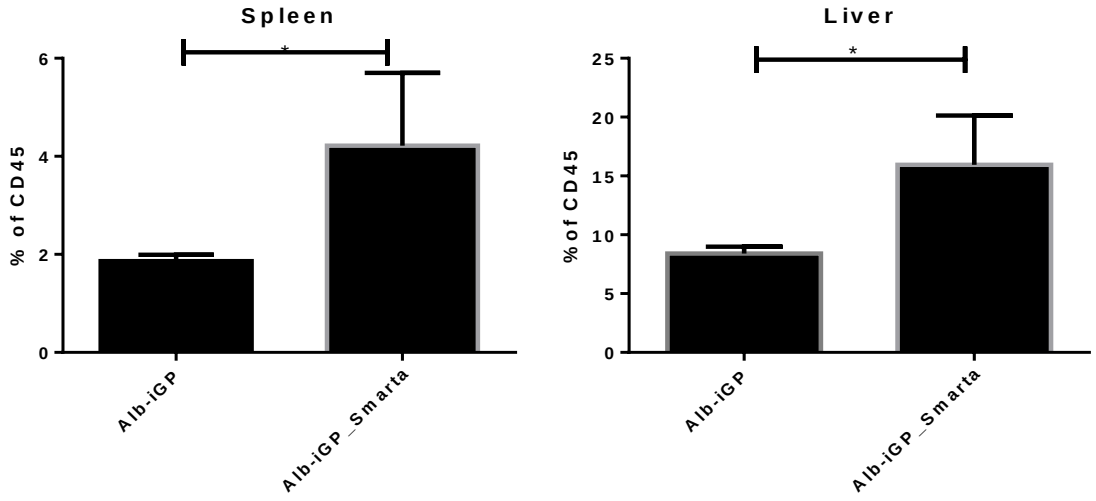


Figure 40. Frequency of CD11c+ cells in the spleen of Alb-iGP (mean=1.86; SD=0.13) compared to Alb-iGP_Smarta mice (mean=4.26; SD=1.48) and in the liver of Alb-iGP (mean=8.39; SD=0.58) and Alb-iGP_Smarta mice (mean=15.94; SD=4.19).

The high frequency of DCs was further confirmed by immunofluorescence staining on frozen liver sections. At an early disease stage, Alb-iGP_Smarta mice showed CD11c positive cells located within the ELTs as well as in the periportal tracts (figure 41). At 30 weeks of age upon clinical manifestation, the frequency of DCs had further increased. Interestingly, DCs are in close contact to CD4 T cells. These data indicate that DCs may be pathogenic drivers of autoreactive CD4 T cell activation.

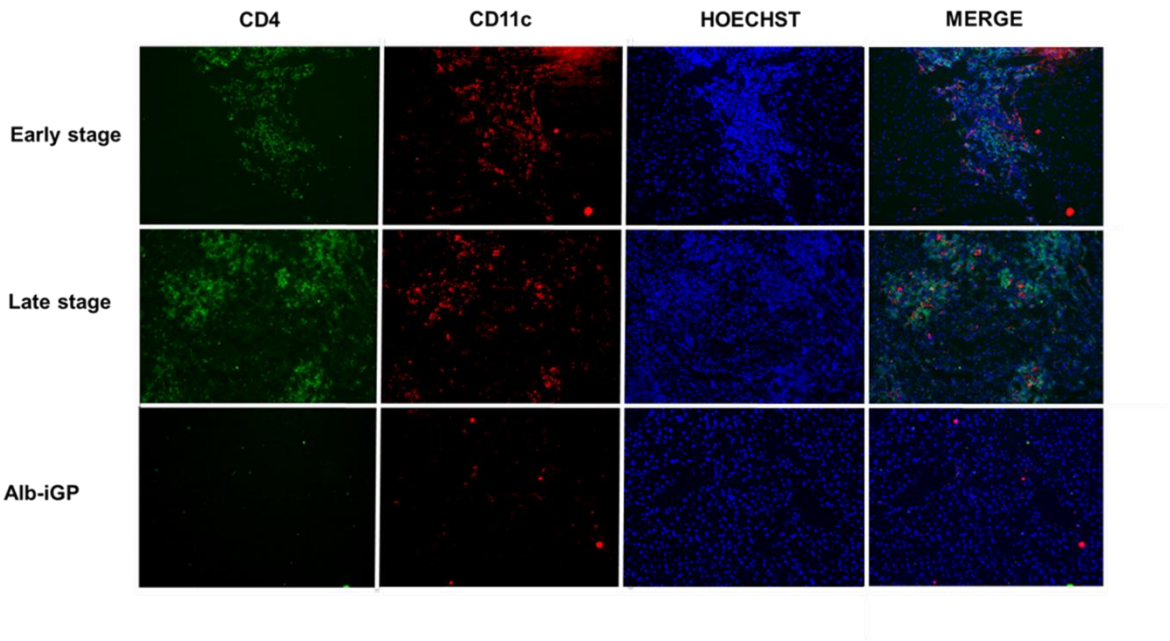


Figure 41. Representative immunofluorescence staining of Alb-iGP and Alb-iGP_Smarta mice. In green CD4 T cells and in red CD11c positive DCs are shown. Nuclei were counterstained in blue.

### 3.10.1 Phenotype of hepatic DCs

To identify which subset of DCs was most represented in Alb-iGP_Smarta mice, an immunofluorescence staining was performed in liver samples of mice with and without clinical manifestations. Different subsent of DCs with disptinct phnotype and function have benn descryibed. Plasmacytoid dendtritic cells (pDCs), which produces type 1 interferons, IL12 and IL-6 (63). Conventional dendritic cells type 1 (cDC1) cross-present antigens and activate Th1 response. Conventional dendritic cells type 2 (cDC2) induces Th2 and Th17 response (64). Liver sections were stained for CD11c, CD172a and MHCII to identify cDC2 and for CD11c, B220 and CD317 for pDCs. As seen in figure 42, the majority of DCs were also CD172a and MHC II positive indicating that they were cDC2. Interestingly, already at 8 weeks of age at an early disease stage, cDC2 numbers were elevated, indicating that they might be pathogenic drivers of CD4 T cells.

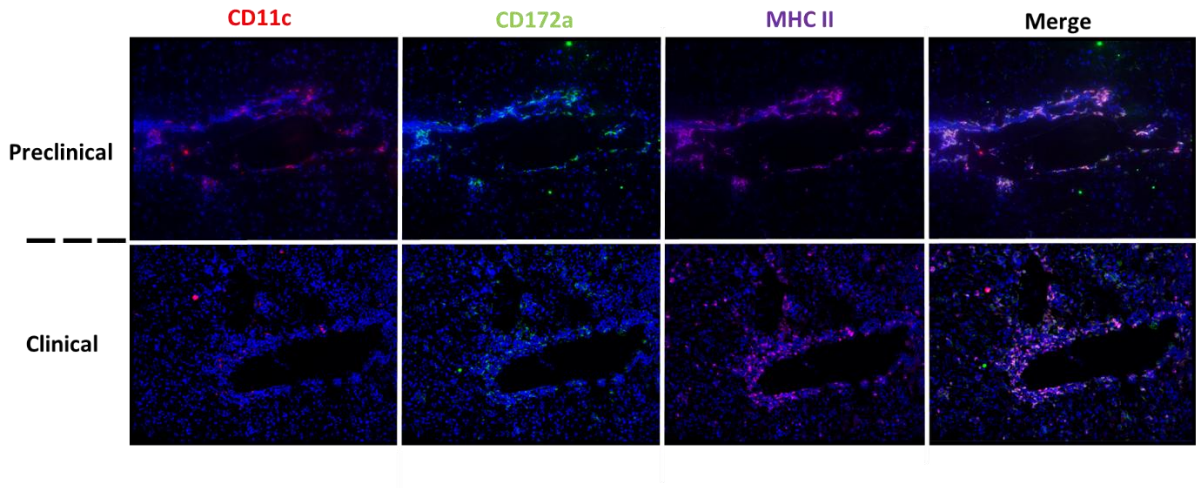


Figure 42. Representative immunofluorescence staining of Alb-iGP_Smarta mice before and after clinical disease manifestation. In red is shown CD11c, in green CD172a and MHCII in pink. Nuclei are counterstained in blue. All images were acquired at 10X magnification.

In contrast, few DCs were CD11c+, B220+ and CD317+ pDCs before and after appearance of any clinical manifestations (Figure 43).

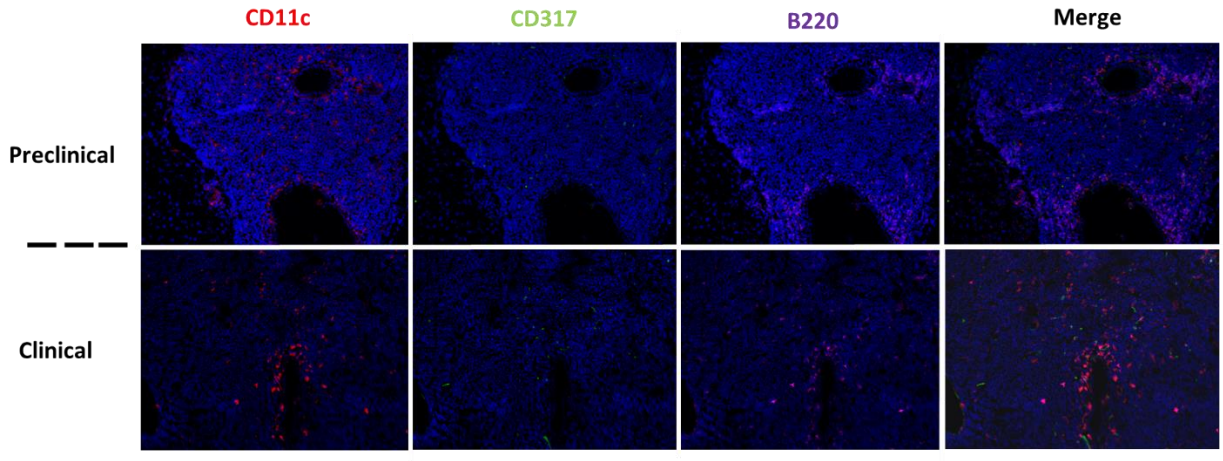


Figure 43. Representative immunofluorescence staining of Alb-iGP_Smarta mice before and after clinical disease manifestation. In red is shown CD11c, in green CD317 and B220 in pink. Nuclei are counterstained in blue. All images were acquired at 10X magnification.

### 3.10.2 DCs are enriched in human AIH

The presence of CD11c+ DCs in human AIH samples was evaluated by immunohistochemistry. An increase frequency of DCs was observed in AIH, similar to Alb-iGP_Smarta mice (figure 44).

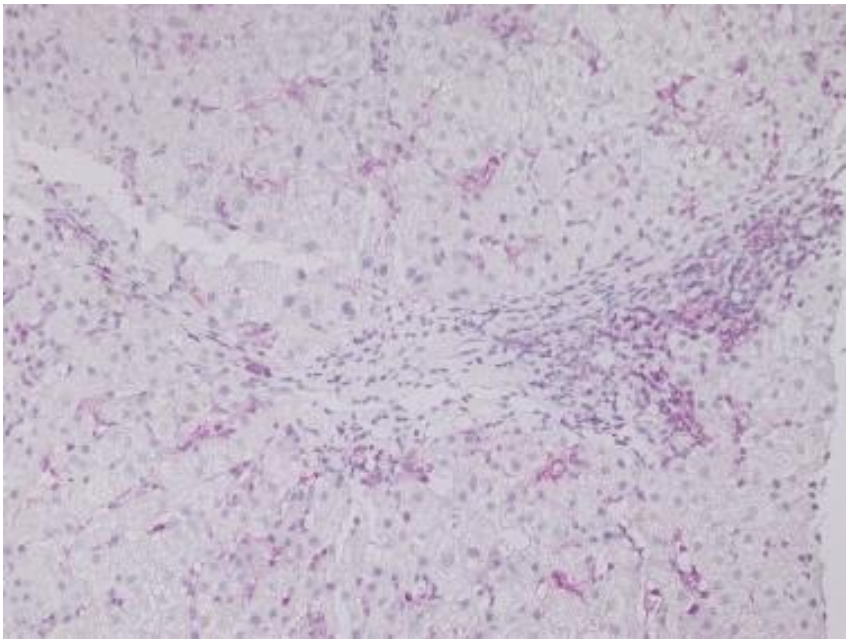

Figure 44. Representative immunohistochemical cd11c staining of a liver biopsy of AIH patient. 10X

### 3.10.3 Autoantigen-presentation by DCs is required for the activation of adoptively transferred autoreactive CD4 T cells

To directly address the hypothesis that in Alb-iGP_Smarta mice, the presentation of the hepatocytic autoantigen $GP_{61-80}$ to autoreactive CD4 T cells, adoptive transfer experiments were performed. Therefore, $10^6$ congenic CD4 CD25 $GP_{61-80}$-specific non-Treg from Smarta mice were transferred into Alb-iGP recipient mice that express the antigen by hepatocytes, into Itgax-iGP mice that express the antigen by DCs or into Alb/Itgax-iGP mice that express the antigen by hepatocytes and DCs. After seven days from the transfer, the spleen size, frequency of the transferred autoreactive T cells in spleen and liver, and liver inflammation were evaluated. Itgax-iGP and Alb/Itgax-iGP mice developed splenomegaly comparable to Alb-iGP_Smarta mice (figure 45; figure 10 showing splenomegaly in Alb-iGP_Smarta). In Alb-iGP mice, the spleen remained normal. Thus, autoreactive CD4 T cells expanded only in Itgax-iGP and Alb/Itgax-iGP mice (figure 46), indicating that efficient antigen presentation by DCs is necessary to drive the expansion of pathogenic autoreactive CD4 T cells.

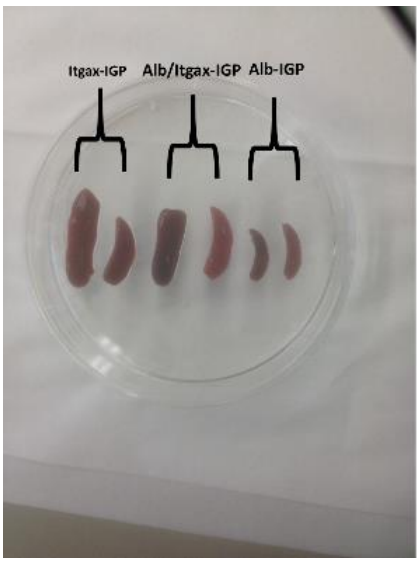


Figure 45. Representative image showing the size of the spleen of Itgax-iGP, Alb/Itgax-iGP and Alb-iGP mice after transfer of $10^6$ Smarta CD4 T cells (day 7).

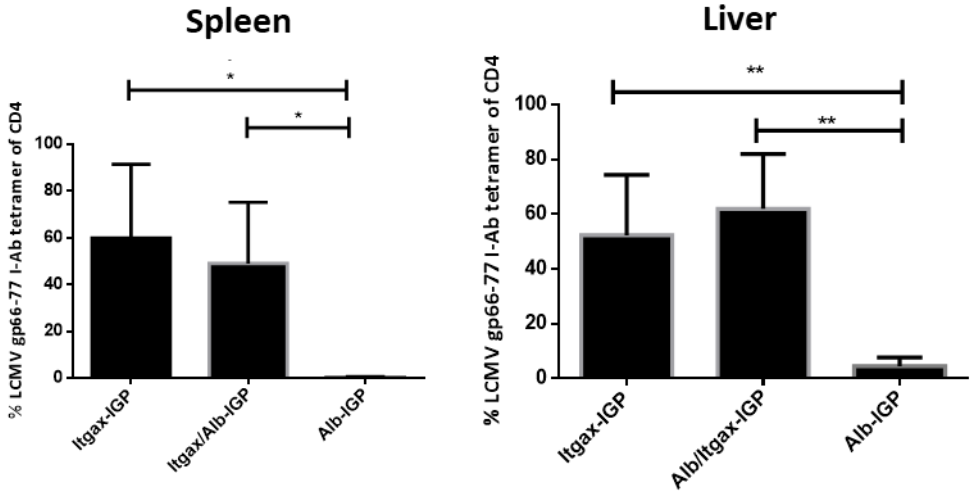


Figure 46. Frequency of autoreactive CD4 T cells in Itgax-iGP, Alb/Itgax-iGP and Alb-iGP mice after 7 days of transfer in the spleen and liver. N=4 mice per group.

Histologically, the liver of Itgax-iGP and Alb/ Itgax-iGP mice were comparable and showed periportal lymphocytic infiltration, whereas Alb-iGP control mice did not show any accumulation of infiltrating cells (figure 47)

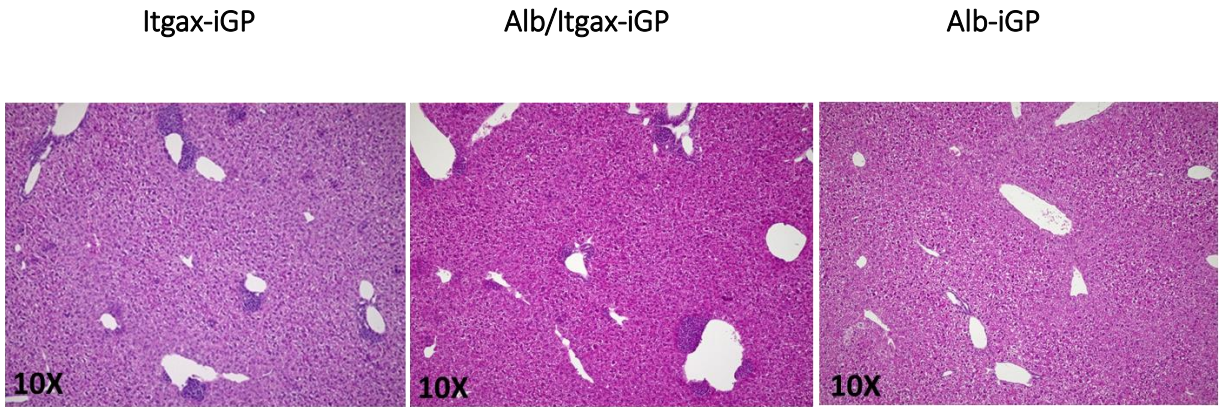


Figure 47. Representative H/E staining of Itgax-iGP, Alb/Itgax-iGP and Alb-iGP mice upon transfer of $10^6$ antigen-specific cells. Mice were opened 7 days after transfer. N=4 mice per group.

Taken together, these data show that transferred antigen-specific CD4 T cells massively expanded when the antigen was presented by DCs, leading to splenomegaly and hepatic lymphocyte infiltration that mirrored the phenotype observed in Alb-iGP_Smarta mice in the subclinical stage. Thus, autoantigen presentation by DC seems to be a decisive mechanism for the efficient activation of autoreactive cells that might explain the development of autoimmune liver disease over time in Alb-iGP_Smarta mice. Trensfer experiments suggests that DCs can activate antigen-specific cells. DCs are enriched in Alb-iGP_Smarta mice already at preclinical stage. We hypothesize that DCs in Alb-iGP_Smarta mice might capture the antigen from dying hepatocytes, thus leading to proliferation of autoreactive T cells.

# 4. DISCUSSION

The overall aim of this study was to understand the immunological mechanisms underlying the breach of hepatic tolerance and the exacerbation of AIH. We aimed to clarify the mechanisms that induce AIH, study the role of ignorant autoreactive T cells, the phenotype and function of autoreactive Treg, and the so far elusive role of ELTs in AIH development. To do that, we generated four different transgenic mice expressing the LCMV GP61-80 glycoprotein by different cell types (hepatocytes, DCs, endothelial cells and macrophages). Itgax-iGP_Smarta and Lyz2-iGP_Smarta mice express GP61-80 by DCs and macrophages respectively. Cdh5-iGP_Smarta by endothelial cells, and Alb-iGP_Smarta mice by hepatocytes. All mice strains mice also bear a transgenic TCR specific for GP61-80.

## 4.1 Tolerance mechanisms in thymus and periphery

We analyzed antigen-specific CD4 T cells in the thymus and spleen of Alb-iGP_Smarta, Cdh5-iGP_Smarta, Lyz2-iGP_Smarta and Itgax-iGP_Smarta mice to detect which tolerance mechanisms were active in the different strains in order to prevent autoimmunity. Itgax-iGP_Smarta and Lyz2-iGP_Smarta mice showed almost total deletion of single positive GP61-80 specific T cells in the thymus and in the periphery. Cdh5-iGP_Smarta mice displayed only partial deletion in the thymus but a considerable number of autoreactive CD4 T cells was deleted in the periphery. Autoreactive CD4 T cells were largely ignored in Alb-iGP_Smarta mice as no deletion occured in the thymus and only a small fraction of these cells were deleted in the spleen.

Treg were generated in the thymus of all the lines except Alb-iGP_Smarta and Smarta control mice, which showed detectable levels of Treg only in the periphery. These data are consistent with the previous finding that tolerance is established by different mechanisms, depending on the site of self-peptide expression (59). When the peptide is uniformly presented in the thymus by thymic epithelial cells, clonal deletion of autoreactive cells is the main mechanism of tolerance. On the contrary, ignorance is the mechanism that occurs in case the peptide is not presented in the thymus. When the peptide is expressed at an intermediate level in the thymus, only partial deletion accompanied by tTreg induction occurs (59). Our findings are in line with the published observations; suggesting that central deletion mechanisms are prominent in Itgax-iGP_Smarta and Lyz2-iGP_Smarta mice because the antigen is present at

high level in the thymus. Partial deletion and tTreg induction occured in Cdh5-iGP_Smarta mice, as previously observed for tissue-restricted antigens, that are only moderately present in the thymus (59). Autoreactive CD4 T cells were ignored in Alb-iGP_Smarta mice, suggesting that in these mice, thymic autoantigen presentation was completely absent. In light of these findings, it is not surprising that none of the monitored lines developed spontaneous autoimmune disease, except for Alb-iGP_Smarta mice. Indeed, Alb-iGP_Smarta mice developed AIH-like disease because of the lack of deletional tolerance in thymus and periphery, which enabled the proinflammatory activation of GP61-80 recognizing Smarta T cells. Of note, whereas in the study by Malhotra D. et al. (59) the behaviour of autoreactive T cells might have been influenced by immunization, we performed autoreactive T cell characterization in treatment-naïve mice. Moreover, peripheral deletion mechanisms had not been considered in the aforementioned study and clinical signs of autoimmunity had not been monitored.

### 4.2 Alb-iGP_Smarta mice as a new mouse model for AIH

Alb-iGP_Smarta mice were analyzed in detail because of their high frequency of autoreactive CD4 T cells in the thymus as well as in the spleen and liver. We also analyzed the phenotype of polyclonal and GP61-80 specific CD4 T cells in the spleen and liver. We observed that antigen-specific CD4 T cells had a $CD44^{high}CD62L^{low}$ effector/memory phenotype, explaining the finding that Alb-iGP_Smarta mice were prone to develop autoimmune disease. Accordingly, the frequency of naive CD4 T cells was reduced in Alb-iGP_Smarta mice compared to Smarta controls. These data strongly suggest that CD4 T cells were antigen-experienced in Alb-iGP_Smarta mice. In the future, it would be interesting to include CD69 and CD103 in the panel of T cell surface markers to assess the presence of tissue-resident memory CD4 T cells in the liver.

Starting at the age of 19 weeks, Alb-iGP_Smarta mice developed autoimmune liver disease with some features of human AIH. Already at an early disease stage (8 weeks), Alb-iGP_Smarta mice showed an elevated mHAI score, high levels of IgG in the sera and the presence of ANAs at relevant titers. At this early stage, transaminases were not elevated. In a later disease stage, clinical symptoms were evident, and the mice showed also portal inflammation with interphase hepatitis accompanied by elevated transaminase levels and a

further increase in the mHAI score. Similarly to human AIH, CD4 T cells were dominating the infiltrate (40). Thus, the new mouse model characterized in this study seems to be suitable to mimic human AIH. However, when the activation of autoreactive T cells exceeded a certain threshold, Alb-iGP_Smarta mice developed fulminant multi-organ inflammation which resulted in a mortality rate of 50% at the age of 30 weeks. Unlike other mouse models of AIH that develop transient liver inflammation (29-39), AÌH in Alb-iGP_Smarta mice was followed by proliferation of autoreactive CD4 T cells in multiple organs causing lymphadenopathy and hepatosplenomegaly. Interestingly, some AIH patients may also develop splenomegaly and/or hepatomegaly (65).

### 4.3 Role of ELTs in AIH development

ELTs are organized structures of T cells, B cells and antigen-presenting cells such as DCs. ELTs have been described in the target organ of several autoimmune diseases like salivary gland in Sjörgen syndrome (SS) and kidneys in systemic lupus erythematosus (48,49). Interestingly, not every patient shows the formation of ELTs in the target organ (48,49,66). The presence of ELTs in the target organ is associated with worse prognosis. For example, SS patients that develop ELTs are more likely to develop B-cell lymphomas (66). As mentioned above, ELTs work as germinal centers promoting affinity maturation of autoreactive B cells into plasma cells (48,49). Alb-iGP_Smarta mice showed formation of ELTs in the liver already at an early disease stage. With disease progression, ELTs disappeared as they merged with the hepatic infiltrate. However, B cells and DCs were still highly represented at an advanced disease stage even though dispersed into the larger periportal infiltrates of interphase hepatitis. In contrast, Itgax-iGP_Smarta, Lyz2-iGP_Smarta, Cdh5-iGP_Smarta mice as well as Smarta and Alb-iGP controls did not develop ELTs in the liver (data not shown). One might speculate that blocking the formation of these structures could protect Alb-iGP_Smarta mice from disease development or at least delay the clinical manifestation. As mentioned in the introduction, in patients with rheumatoid arthritis, anti TNF-α treatment was found to revert ELT formation, showing the importance of this cytokine in the maintenance of ELTs (66). We are planning to perform an anti-TNF-α treatment in Alb-iGP_Smarta mice and monitor ELT disaggregation as well as disease development. Moreover, as ELTs are composed mostly of segregated T and B cells, it is planned to perform B cell depletion experiments with anti-B220 and anti-CD19 to check ELT reversion and disease development. We hypothesize that these transient structures

that boost the immune response may be present in human AIH as well. Unfortunately, AIH patients are normally diagnosed at an advanced disease stage, when these structures are also absent in mice. Importantly, AIH patients at an advance disease stage, have an increased amount of B cells (23) and DCs (figure 44), like in Alb-iGP_Smarta mice.

### 4.4 Effector immune response in Alb-iGP_Smarta mice

We could detect an increased co-production of TNF-α and IFN-γ by CD4 T cells in the liver of Alb-iGP_Smarta mice. This is an interesting similarity to human AIH, because in a recent study of our department, it was found that TNF-α/IFN-γ producing Th1 cells are expanded in AIH patients (manuscript under revision). Importantly, anti TNF-α treatment was shown to be effective in difficult-to treat AIH patients, highlighting the importance of this cytokine in disease perpetuation (67). The production of IL-4 was also evaluated. Alb-iGP_Smarta mice did not produce high levels of IL-4, suggesting that Th2 cells may not be relevant in AIH disease progression. However, IL-17 production was also increased in Alb-iGP_Smarta mice, indicating that Th17 might be important in disease pathogenesis and progression. Interestingly, higher levels of IL-17 are also found in patients with AIH (68).

### 4.5 Regulatory T cells in Alb-iGP_Smarta mice

We compared Treg from the early and late disease stage in Alb-iGP_Smarta mice. Treg were present in a normal frequency as compared to Smarta controls in an early disease stage. However, in an advanced disease stage FOXP3+ Treg were not detectable in the spleen as well as in the liver anymore. *In vivo* ablation of FOXP3 causes systemic autoimmunity characterized by lymphoadenopathy and splenomegaly (69). In Alb-iGP_Smarta mice, it is not clear which mechanism drives the loss of FOXP3. It is possible that antigen-specific Treg are not enough in number to suppress the high frequency of autoreactive effector cells in the long run. Cdh5-iGP_Smarta mice showed much higher frequencies of antigen-specific Treg, which might explain why these mice were protected from the development of AIH. One other reason for the observed loss of Treg in sick Alb-iGP-Smarta mice might be their origin. tTreg originate in the thymus and pTreg are induced in the periphery. These cells differ in the methylation status of the Foxp3 Treg-specific demethylated region (TSDR) and in their stability (8-11). The continuous antigen exposure in the thymus makes tTreg more stable. This is because tTreg

also have a constantly demethylated TSDR. On the contrary, pTreg have a highly methylated TSDR region, thus rendering these cells less stable (70). In an ongoing experiment, we are currently analyzing this issue in autoantigen-specific and, as control, in polyclonal Tregs from Alb-iGP_Smarta mice. Notably, we found that antigen-specific Treg express low levels of Helios and Neuropilin-1 in the thymus and spleen of Alb-iGP_Smarta mice, suggesting that these cells are pTreg generated in the periphery. On the contrary, Treg from Cdh5-iGP_Smarta mice expressed high levels of Helios and Neuropilin-1 suggesting that they have more tTreg generated in the thymus. Therefore, the composition of the Treg pool in Alb-iGP_Smarta mice that is dominated by pTreg and that lacks tTreg might contribute to the loss of immune tolerance and the development of AIH in Alb-iGP_Smarta mice. The lower Treg stability was further confirmed by the observation that antigen-specific Treg had a decreased level of FOXP3 expression as indicated by a lower MFI as compared to non-specific Treg, which is indicative of lower stability (58,59).

Of note, Treg can lose the expression of Foxp3 and become “ExTreg” that produce INF-γ and IL-17 upon IL-2 depletion and strong TCR interaction with antigens and cytokines (71). This is an intriguing explanation for the loss of these cells. However, without fate mapping mice allowing to monitor the conversion of Tregs into effector cells, it will remain difficult to prove, whether such inflammatory T cell conversion might also happen in Alb-iGP_Smarta mice.

Normally, Treg produce suppressive cytokines such as IL-10, but under inflammatory conditions, they can also acquire T helper cell function and start to produce IFN-γ (Th1 like) or IL-17 (Th17 like) while maintaining FOXP3 expression. Such potentially pathogenic Treg are found in several autoimmune diseases such as psoriasis (72). In Alb-iGP_Smarta mice, we observed an increased frequency of GP61-80 specific Treg that produced high levels of IL-17. It is tempting to speculate that these Th17-like Tregs might have contributed to the disease pathogenesis. Indeed, it has been reported that the acquisition of Th17-like features may result in reduced suppressive potential of Treg under inflammatory conditions (73). However, it is not clear whether Th17-like Tregs are a stable cell type or whether they reflect an intermediate state in a conversion process (58,59).

Enrichment of Treg with the IL-2/IL-2ab complex was proven to be effective in treatment of experimental autoimmune encephalomyelitis and experimental type 1 diabetes (60,61) but not in a mouse model of PSC due to a defective IL-12 signaling which impaired the

suppressive capacity of the expanded Treg (62). We successfully enriched Treg with IL-2/IL-2ab complex in the liver of Alb-iGP_Smarta mice, but not in the spleen. However, the hepatic Treg expansion in Alb-iGP_Smarta mice was not as prominent as in the previously published data (62). Next, we observed that IL-2/IL-2ab complex also drives the expansion of $CD25^{high}FOXP^{neg}$ effector cells. This data indicates that although IL-2/IL-2ab complex seems to be a suitable method for expansion of Treg *in vivo*, as a side-effect, it concomitantly can induce an increase of potentially pathogenic CD4 effector T cells. In particular, in light of the currently ongoing clinical trials evaluating IL-2 treatment for Treg expansion in patients (74), our findings sound a note of caution. Along these lines, in a long-term Treg enrichment experiment using the IL-2/IL-2ab complex treatment Alb-iGP_Smarta mice were not rescued. On the contrary, the treatment seemed to accelerate disease development. This failure in suppression may be explained by a concomitant expansion of Tregs, but also of autoreactive effector T cells.

Another mechanism that seemed to be involved in Treg failure in Alb-iGP_Smarta mice is increased IL-12 signalling. According to the study showing IL-12 dependent hepatic Treg dysfunction in a mouse model of PSC (62), our data showed that the IL-12 receptor subunits IL-12rb1 and IL-12rb2 were upregulated in the livers of Alb-iGP_Smarta mice in the late disease stage. We also observed high expression levels of IL-12a and IL12b in the liver of Alb-iGP_Smarta mice in the late disease stage. Overall, these data suggest that Treg in Alb-iGP_Smarta mice may have an impaired suppressive capacity. However, further *in vitro* suppression assays will be required to confirm this hypothesis.

Taken together, these data indicate that Treg were present in the liver of Alb-iGP_Smarta mice, were mostly generated in the periphery, were less stable, could acquire a T helper-like phenotype and produce effector cytokines such as IL-17, and were not suppressive enough to prevent the expansion of autoreactive effector cells. When the disease was in a late stage, Treg were not detectable anymore, presumably due to the massive outgrowth by effector cells or their acquisition of pro-inflammatory features. Treg dysfunction in our AIH model seemed to occur selectively in autoantigen-specific Tregs, and as an adaptation to sustained moderate inflammatory conditions and ELT formation in the liver in the early disease stage. Thus, it is possible that the selectively reduced functionality of GP61-80-reactive Tregs was a consequence of their stimulation in portal ectopic lymphoid tissue.

### 4.6 Pathogenic drivers of autoreactive CD4 T cell activation

We investigated which cells may be the drivers of pathogenic activation of autoreactive CD4 T cells leading to AIH in Alb-iGP_Smarta mice. The number of inflammatory monocytes, macrophages and neutrophils did not differ between Alb-iGP_Smarta and control mice, at least not in the early stage, suggesting that these cells were not critically involved in disease pathogenesis. However, we observed an increased frequency of DCs in the liver of Alb-iGP_Smarta mice. DCs were also present within ELTs in an early disease stage suggesting that as professional antigen-presenting cells, they may drive the activation of autoreactive CD4 T cells. To assess the role of DCs in more detail, we had a look on different DC subtypes, including cDC1, cDC2 and pDC. cDC1 cross-present antigen and polarize CD4 T cells to a Th1 phenotype whereas cCD2 foster the differentiation into Th2 or Th17 cells (63,64). pDCs produce high amounts of type 1 interferons (63,64). Interestingly, we observed high frequencies of cDC2 in the liver of Alb-iGP_Smarta mice and few pDC. In the future, we will better characterize the different DC subsets in Alb-iGP_Smarta mice, not only phenotypically as shown in the current study, but also functionally. So far, few studies have analyzed the role of DCs in AIH pathogenesis, both in mice and patients. However, in addition to our mouse study, we have stained liver sections of some AIH patients and observed a very high frequency of CD11c+ DCs in the infiltrates. As in mice, we will also perform further studies with patient samples to characterize the different DCs subsets in human AIH as well.

Next, we performed adoptive transfer experiments to confirm the importance of DCs for autoreactive T cell activation and AIH pathogenesis. We found that transfer of antigen-specific Smarta cells into Itgax-iGP mice (expressing the antigen solely in DCs) led to proliferation of the autoreactive T cells in the spleen and in the liver. The liver showed high portal infiltration as shown by histology. We observed the same proliferation of autoreactive T cells and the same level of portal infiltration in Itgax/Alb-iGP mice (expressing the antigen in DCs and hepatocytes) after transfer of antigen-specific Smarta cells. Interstingly Alb-iGP mice did not develop portal infiltration and CD4 T cells proliferated less compared to Itgax/iGP and Itgax/Alb-iGP mice. This could be explained by the fact that in steady state hepatocytes do not express MHCII (75). However, during inflammatory conditions hepatocytes can upregulate MHCII and activate CD4 T cells (75). These data indicate that autoantigen presentation by DCs fosters the activation of autoreactive T cells in the liver. Taken together, these data show that

DCs are required for disease development and are the pathogenic drivers of autoreactive CD4 T cells in our model.

## 4.7 Future perspectives

### 4.7.1 Pre-clinical evaluation of new therapeutic options for AIH in Alb-iGP_Smarta mice

We will test different therapeutic approaches for the treatment of human AIH in Alb-iGP_Smarta mice, both in early disease stage and after clinical manifestation. The resulting data of these pre-clinical studies might lead to the development of new treatment strategies that on the long-term might be translated into clinical applications.

1) Regarding the finding that ELTs in the liver of Alb-iGP_Smarta mice might function as an inflammatory hub already in an early disease stage, we will try to prevent ELT formation or dissolve already existing ELTs by antibody-mediated depletion of B cells.

2) Based on the recent findings of our colleagues that TNF seems to be a major pathogenic mediator in human AIH and the presence of TNF-producing autoreactive T cells in Alb-iGP_Smarta mice, we will evaluate anti-TNF treatment in our newly established mouse model of AIH.

3) LSEC are liver-resident APCs which have an important role in inducing hepatic tolerance by suppressing effector CD4 T cells and by generating Treg (76,77). It was recently published that nanoparticle-based autoantigen delivery to liver sinusoidal endothelial cells (LSEC) enables the control of autoimmunity by inducing antigen-specific Treg (78). Making use of such nanoparticles, we want to selectively deliver GP61-80 peptide to LSEC of Alb-iGP_Smarta mice, in order to boost the production of antigen-specific Treg that might protect from development of severe clinical AIH. Even more importantly, we want to check if these nanoparticles have a therapeutic potential also in the late stage, in Alb-iGP_Smarta mice with clinical manifestation.

### 4.7.2 Antigen-presenting cells in AIH

In Alb-iGP_Smarta mice the autoantigen is solely expressed in hepatocytes. However, at least under homeostatic conditions, hepatocytes do not express significant amounts of MHC II (75).

Thus, neighbouring APCs, including DCs, B cells or LSECs have to be involved in the activation of the autoreactive T cells in Alb-iGP_Smarta mice.

In the present study, we could show that DCs and also B cells are present in the hepatic infiltrates of Alb-iGP_Smarta mice, suggesting that they might be involved in pathogenic autoantigen-presentation. Moreover, it is known that also LSEC can present antigens to CD4 T cells, however this normally leads to CD4 T cell tolerance (76,77).

In order to study the respective contributions of B cells or endothelial cells to the activation of autoreactive cells in the liver, we will breed CD19/Alb-iGP_Smarta mice and Cdh5/Alb-iGP_Smarta mice, in which the autoantigen is expressed concomitantly in hepatocytes and B cells or hepatocytes and endothelial cells. Moreover, in these mice we will evaluate whether antigen co-presentation by B cells or endothelial cells might lead to the maintenance of tolerance or the development of autoimmunity.

### 4.7.3 Treg stability and function in Alb-iGP_Smarta mice

To further study stability and function of the Treg in Alb-iGP_Smarta mice, we are breeding the FOXP3-GFP reporter mice into the Alb-iGP_Smarta and Cdh5-iGP_Smarta mouse strains. This will allow us to sort highly pure GFP-expressing Foxp3 positive Tregs. For the moment, we rely on the rather unspecific surface markers CD4 and CD25. The highly pure Tregs will then be obtained from the liver, separated in autoantigen specific versus non-specific Tregs and further characterized in terms of stability by methylation analysis of the Treg-Specific Demethylated Region (TSDR) which stabilizes FOXP3 expression and in terms of function in *in vitro* suppression assays.

## 5. SUMMARY

The overall aim of this study was to understand the immunological mechanisms underlying the breach of hepatic tolerance and the exacerbation of AIH. In this study we described a new mouse model of spontaneous CD4 T cell-driven AIH, which allowed us to elucidate several potential key factors in AIH pathogenesis. First, we demonstrated that the lack of deletional tolerance due to antigen ignorance of GP61-80-reactive CD4 T cells enabled the recognition of their cognate antigen in hepatocytes (Alb-iGP_Smarta mice) and spontaneous development of typical AIH-like disease features. Macrophages (Lyz2-iGP_Smarta mice) and dendritic cell (Itgax-iGP_Smarta mice) expression of the LCMV GP61-80 antigen lead to deletional tolerance of autoreactive CD4 T cells in the thymus. Endothelial (Cdh5-iGP_Smarta mice) expression of the antigen led to partial deletion of autoreactive CD4 T cell in the thymus and in the spleen. These mice showed few effector CD4 T cells but generated high frequencies of antigen-specific Treg. According to their respective pool of autoreactive T cells, except Alb-iGP_Smarta mice, all other strains were protected from autoimmune disease development.

Next, we clarified the mechanisms that induce AIH in Alb-iGP_Smarta mice. In particular, we found that AIH was driven by maturation of previously ignorant autoreactive CD4 effector T cells towards IFN and TNF co-producers as well as IL-17 producers. Moreover, the activation of the GP61-80-reactive CD4 T cells seemed to occur in ectopic lymphoid tissue, which transiently formed within hepatic portal fields of Alb-iGP_Smarta mice.

Subsequently, we analyzed the frequency and the phenotype of Treg. We found that the majority of Treg in Alb-iGP_Smarta mice were pTreg, that are less stable then tTreg. Interestingly, GP61-80 specific Treg showed lower Foxp3 expression than non-specific Treg. Low expression of Foxp3 is associated with Treg instability and reduced function. GP61-80 specific Treg produced also higher levels of IL-17 compared to non-specific Treg which is also an indicator of decreased stability and loss of suppressive function. With disease progression, Treg completely disappeard, probably because they were outgrown by effector cells. Moreover, *in vivo* Treg enrichment failed to rescue Alb-iGP_Smarta because of a defective IL-12 signaling and because, concomitant with Treg expansion, it also induced proliferation of effector cells. These data suggest that Treg (in particular GP61-80 specific Treg) were less stable, acquired a Thelper-like phenotype, and failed to suppress autoreactive effector cells.

Finally, we found that DCs seemed to be the major pathogenic drivers of autoreactive CD4 T cell activation in Alb-iGP_Smarta mice. DCs were enriched already at a preclinical stage, they were mostly cDC2 and their numbers further increased with disease development. An adoptive transfer experiment confirmed that presentation of hepatocytic antigen by DCs seems to be key to the activation of autoreactive T cells and the induction of autoimmune liver inflammation.

To sum up, in our new autoantigen-driven mouse model of experimental AIH, disease was initiated by previously ignorant autoreactive GP61-80 T cells that became activated in the periphery, and matured towards inflammatory effector cells. Moreover, autoreactive Treg failed to control such inflammatory effector cells, because of their selective plasticity and instability. The maturation of effector cells and dedifferentiation of Treg seemed to originate in the liver within ELTs.

Das übergeordnete Ziel dieser Studie war es, die immunologischen Mechanismen zu verstehen, die dem Bruch der Lebertoleranz und der Pathogenese der AIH zugrunde liegen. In dieser Studie haben wir ein neues Mausmodell für spontane CD4-T-Zellen-gesteuerte AIH beschrieben, mit dem wir mehrere mögliche Schlüsselfaktoren für die AIH-Pathogenese aufklären konnten. Zunächst zeigten wir, dass aufgrund von Antigen-Ignoranz von GP61-80-reaktiven CD4-T-Zellen ein Mangel an immunologischer Toleranz durch klonale Deletion entsteht. Dies ermöglichte den GP61-80-reaktiven CD4-T-Zellen die Erkennung des Antigens in Hepatozyten (Alb-iGP_Smarta-Mäuse) und die spontane Entwicklung typischer AIH-ähnlicher Krankheitsmerkmale. Die Expression des LCMV GP61-80-Antigens durch Makrophagen (Lyz2-iGP_Smarta-Mäuse) und dendritische Zellen (Itgax-iGP_Smarta-Mäuse) führte zu der klonalen Deletion autoreaktiver CD4-T-Zellen im Thymus. Die endotheliale (Cdh5-iGP_Smarta-Mäuse) Expression des Antigens führte zu einer partiellen Deletion der autoreaktiven CD4-T-Zelle im Thymus und in der Milz. Diese Mäuse zeigten wenige Effektor-CD4-T-Zellen, erzeugten jedoch hohe Frequenzen von Antigen-spezifischem Treg. Gemäß ihrem jeweiligen Pool autoreaktiver T-Zellen, mit Ausnahme von Alb-iGP_Smarta-Mäusen, waren alle anderen Stämme vor der Entwicklung einer Autoimmunkrankheit geschützt.

Das übergeordnete Ziel dieser Studie war es, die immunologischen Mechanismen zu verstehen, die dem Bruch der Lebertoleranz in der Pathogenese der autoimmunen Hepatitis (AIH) zugrunde liegen. In dieser Studie haben wir ein neues Mausmodell einer spontanen,

CD4 T-Zell-vermittelten AIH beschrieben, mit dem wir mehrere mögliche Schlüsselfaktoren für die AIH-Pathogenese aufklären konnten. Zunächst zeigten wir, dass eine unzureichende klonale Deletion autoreaktiver CD4 T-Zellen aufgrund von Antigen-Ignoranz im Thymus zu einer Persistenz autoreaktiver Zellen in der Peripherie führte und die Erkennung des Autoantigens in Hepatozyten ermöglichte, was zur spontanen Entwicklung typischer Krankheitsmerkmale der AIH führte. Wenn das Autoantigen hingegen nicht durch Hepatozyten, sondern durch Makrophagen oder dendritische Zellen exprimiert wurde, fand eine weitgehende klonale Deletion der autoreaktiven CD4-T-Zellen im Thymus statt, was die Entstehung einer Autoimmunerkrankung verhinderte. Bei endothelialer Expression des Autoantigens fand lediglich eine partielle Deletion autoreaktiver CD4 T-Zellen im Thymus statt, jedoch bestand der überwiegende Teil der reifen autoreaktiven T Zellen aus Foxp3+ regulatorischen T Zellen (Treg), und nur ein kleinerer Teil aus Effektor-CD4-T-Zellen. Auch diese Tiere entwickelten keine Autoimmunerkrankung, erzeugten jedoch hohe Frequenzen von Antigen-spezifischen Treg. Demnach konnte hier Antigen-Ignoranz im Thymus als ein entscheidender Faktor für die Entwicklung einer Autoimmunkrankheit in der Leber identifiziert werden.

Als nächstes haben wir die Immunmechanismen näher untersucht, die zur Krankheitsauslösung in Mäusen mit AIH führten. Wir fanden, dass die Auslösung der AIH durch die Reifung der zuvor ignoranten autoreaktiven CD4 Effektor T-Zellen zu IFN- und TNF-Koproduzenten, sowie zu IL-17-Produzenten ermöglicht wurde. Darüber hinaus schien die Aktivierung der autoreaktiven CD4 T-Zellen in ektopischem lymphoiden Gewebe zu erfolgen, welches sich vorübergehend in Portalfeldern der Tiere mit konditionaler Autoantigen-Expression in Hepatozyten bildete.

Weiterhin analysierten wir die Häufigkeit und den Phänotyp von Treg im AIH Modell. Wir entdeckten, dass die Mehrheit der Treg in Alb-iGP_Smarta-Mäusen in der Peripherie induziert waren und eine geringere Stabilität aufwiesen als im Thymus generierte Treg. Interessanterweise zeigten autoreaktive Treg eine geringere Foxp3-Expression als nicht-spezifische Treg, was mit einer Instabilität und verminderte Funktion von Treg verbunden ist. Autoreaktive Treg produzierten auch größere Mengen an IL-17 als nicht-spezifische Treg, was ebenfalls ein Indikator für verminderte Stabilität und den Verlust der immunsupprimierenden Funktion ist. Mit fortschreitender Krankheit verschwanden die Treg vollständig,

möglicherweise aufgrund eines Überwachsens durch Effektor T-Zellen. Darüber hinaus konnte eine in vivo-Treg-Anreicherung in Mäusen mit AIH durch therapeutische Gabe von IL-2 den Krankheitsausbruch nicht verhindern, sondern induzierte gleichzeitig mit der Treg-Expansion auch eine Expansion von Effektorzellen. Die beoabachtete Treg Instabilität bei AIH könnte durch IL-12-Signale in der Leber verursacht worden sein. Diese Daten legen nahe, dass insbesondere die Autoantigen-spezifischen Tregs weniger stabil waren, einen T-Helferzell-ähnlichen Phänotyp erwarben und autoreaktive Effektorzellen nicht mehr unterdrückten.

Schließlich fanden wir heraus, dass dendritische Zellen (DC) die maßgeblichen pathogenen Treiber der autoreaktiven CD4-T-Zellaktivierung zu sein schienen. DCs, insbesondere vom cDC2 Subtyp, expandierten in der Leber bereits in einem präklinischen Stadium, und ihre Anzahl nahm mit der Krankheitsentwicklung weiter zu. Ein adoptives Zelltransferexperiment bestätigte, dass die Präsentation von Hepatozyten-Autoantigen durch DCs der Schlüssel zur Aktivierung autoreaktiver T-Zellen und zur Induktion einer autoimmunen Leberentzündung zu sein scheint.

Zusammenfassend konnte in einem neuen, spontanen CD4 T-Zell-getriebenen Mausmodell der AIH die Krankheit durch zuvor ignorante autoreaktive CD4 T-Zellen ausgelöst werden, wobei diese in der Peripherie aktiviert wurden und zu entzündlichen Effektorzellen reiften. Darüber hinaus konnten autoreaktive Tregs solche entzündlichen Effektorzellen aufgrund ihrer selektiven Plastizität und Instabilität nicht kontrollieren. Sowohl die Reifung der Effektorzellen als auch die Dedifferenzierung der Treg schien in der Leber innerhalb ektopischen lymphatischen Gewebes stattzufinden.

## 6. REFERNCES

1. Sprent J., Kishimoto H. The thymus and central tolerance. Philos Trans R Soc Lond B Biol Sci. 2001 May 29; 356(1409): 609–616.

2. Sakaguchi S1, Yamaguchi T, Nomura T, Ono M. Regulatory T cells and immune tolerance. Cell. 2008 May 30;133(5):775-87.

3. Xing Y. and K. A. Hogquist. T-Cell Tolerance: Central and Peripheral. Cold Spring Harb Perspect Biol. 2012 Jun; 4(6): a006957

4. Jonuleit H., Schmitt E. The Regulatory T Cell Family: Distinct Subsets and their Interrelations. J Immunol Dec, 2003, 171 (12) 6323-6327;

5. Fontenot J. D., Gavin M. A., Rudensky A. Y. 2003. Foxp3 programs the development and function of CD4+CD25+ regulatory T cells. Nat. Immunol, 2003 Apr;4(4):330-6

6. Shevach EM. Mechanisms of foxp3+ T regulatory cell-mediated suppression. Immunity. 2009 May;30(5):636-45.

7. Akkaya B., Oya Y., Akkaya M., Al Souz J., Holstein AH., Kamenyeva O., Kabat J., Matsumura R., Dorward DW., Glass DD., Shevach EM. Regulatory T cells mediate specific suppression by depleting peptide-MHC class II from dendritic cells. Nat Immunol. 2019 Feb;20(2):218-231.

8. Lin X., Chen M., Liu Y., Guo Z., He X., Brand D., Zheng SG. Advances in distinguishing natural from induced Foxp3(+) regulatory T cells. Int J Clin Exp Pathol. 2013;6(2):116-23.

9.Thornton A. M., Korty P. E., Tran D. Q., Wohlfert E. A., Murray P. E., Belkaid Y, Shevach EM. Expression of Helios, an Ikaros transcription factor family member, differentiates thymic-derived from peripherally induced Foxp3+ T regulatory cells. J. Immunol. 184, 3433–344110.

10. Bruder D., Probst-Kepper M., Westendorf AM., Geffers R., Beissert S., Loser K., von Boehmer H., Buer J., Hansen W. Neuropilin-1: a surface marker of regulatory T cells. Eur J Immunol. 2004;34:623–630.

11. Xiaohong Lin, Maogen Chen, Ya Liu, Zhiyong Guo, Xiaoshun He, David Brand, Song Guo Zheng. Advances in distinguishing natural from induced Foxp3. Int J Clin Exp Pathol. 2013; 6(2): 116–123.

12. Sakaguchi S., Sakaguchi N., Asano M., Itoh M., Toda M: Immunologic self-tolerance maintained byactivated T cells expressing IL-2 receptor alpha-chains (CD25). Breakdown of a single mecha-nism of self-tolerance causes various autoimmune diseases. J Immunol 1995;155:1151–1164.

13. Haribhai D., Lin W., Edwards B., Ziegelbauer J., Salzman NH., Carlson MR., Li SH., Simpson PM., Chatila TA., Williams CB. A central role for induced regulatory T cells in tolerance induction in experimental colitis. J Immunol. 2009 Mar 15;182(6):3461-8.

14. Carambia A., Herkel J. CD4 T cells in hepatic immune tolerance. J Autoimmun. 2010 Feb;34(1):23-8.

15. Muratori L., Longhi MS. The interplay between regulatory and effector T cells in autoimmune hepatitis: Implications for innovative treatment strategies. J Autoimmun. 2013 Oct;46:74-80.

16. Szabo, S. J., S. T. Kim, G. L. Costa, X. Zhang, C. G. Fathman, and L. H. Glimcher. A novel transcription factor, T-bet, directs Th1 lineage commitment. Cell 100: 655–669

17. C.N. Ting, M.C. Olson, K.P. Barton, J.M. Leiden. Transcription factor GATA-3 is required for development of the T-cell lineage. Nature, 384 (1996), pp. 474-478

18. Ivanov II., McKenzie BS., Zhou L., Tadokoro CE., Lepelley A., Lafaille JJ., Cua DJ., Littman DR. The orphan nuclear receptor RORgammat directs the differentiation program of proinflammatory IL-17+ T helper cells. Cell. 2006 Sep 22;126(6):1121-33.

19. Calne RY., Sells RA., Pena JR., Davis DR., Millard PR., Herbertson BM., Binns RM., Davies DA. Induction of immunological tolerance by porcine liver allografts. Nature. 1969 Aug 2;223(5205):472-6.

20. Washinton MK. Autoimmune liver disease: overlap and outliers. Mod Pathol. 2007 Feb;20 Suppl 1:S15-30.

21. Cusick MF. Libbey JE. Fujinami RS. Molecular mimicry as a mechanism of autoimmune disease.

22. Rojas M., Restrepo-Jiménez P., Monsalve DM., Pacheco Y., Acosta-Ampudia Y., Ramírez-Santana C., Leung PSC., Ansari AA., Gershwin ME., Anaya JM. Molecular mimicry and autoimmunity. J Autoimmun. 2018 Dec;95:100-123

23. Krawitt EL. Autoimmune hepatitis. N Engl J Med 2006;354:54-66.

24. Sebode M., Hartl J., Vergani D., Lohse A.W. Autoimmune hepatitis: From current knowledge and clinical practice to future research agenda. Liver Int. 2018 Jan;38(1):15-22.

25. European Association for the Study of the Liver. EASL Clinical Practice Guidelines: Autoimmune hepatitis. J Hepatol. 2015 Oct;63(4):971-1004.

26. Lohse AW, Mieli-Vergani G. Autoimmune hepatitis. J Hepatol. 2011 Jul;55(1):171-82

27. Donaldson P.T., Doherty D.G., Hayllar K.M., McFarlane I.G., Johnson P.J., Williams. R. Susceptibility to autoimmune chronic active hepatitis: human leukocyte antigens DR4 and A1–B8-DR3 are independent risk factors. Hepatology, 13 (1991), pp. 701-706

28. Teufel A., Wörns M., Weinmann A., Centner C., Piendl A., Lohse A.W., et al. Genetic association of autoimmune hepatitis and human leucocyte antigen in German patients. World J Gastroenterol., 12 (2006), pp. 5513-5516

29. Yüksel M., Laukens D., Heindryckx F., Van Vlierberghe H., Geerts A., Susan Wong F., Wen L., Colle I. Hepatitis mouse models: from acute-to-chronic autoimmune hepatitis. Int J Exp Pathol. 2014 Oct;95(5):309-20.

30. Kuriki J., Murakami H., Kakumu S., Sakamoto N., Yokochi T., Nakashima I., Kato N. Experimental autoimmune hepatitis in mice after immunization with syngeneic liver proteins together with the polysaccharide of Klebsiella pneumoniae. Gastroenterology. 1983 Mar;84(3):596-603.

31. Tiegs G., Hentschel J., Wendel A. A T cell-dependent experimental liver injury in mice inducible by concanavalin A. J Clin Invest. 1992 Jul;90(1):196-203.

32. Limmer A., Sacher T., Alferink J., Kretschmar M., Schönrich G., Nichterlein T., Arnold B., Hämmerling GJ. Failure to induce organ-specific autoimmunity by breaking of tolerance: importance of the microenvironment. Eur J Immunol. 1998 Aug;28(8):2395-406.

33. Derkow K., Loddenkemper C., Mintern J., Kruse N., Klugewitz K., Berg T., Wiedenmann B., Ploegh HL., Schott E. Differential priming of CD8 and CD4 T-cells in animal models of autoimmune hepatitis and cholangitis. Hepatology. 2007 Oct;46(4):1155-65.

34. Zierden M., Kühnen E., Odenthal M., Dienes HP. Effects and regulation of autoreactive CD8+ T cells in a transgenic mouse model of autoimmune hepatitis. Gastroenterology. 2010 Sep;139(3):975-86

35. Gorham J.D., Lin J.T., Sung J.L., Rudner L.A. & French M.A.) Genetic regulation of autoimmune disease: BALB/c background TGF-beta 1-deficient mice develop necroinflammatory IFN-gamma-dependent hepatitis. J. Immunol. 2001. 166, 6413–6422.

36. Lapierre P., Djilali-Saiah I., Vitozzi S. & Alvarez F. A murine model of type 2 autoimmune hepatitis: xenoimmunization with human antigens. Hepatology 39, 2004; 1066–1074.

37. Holdener M., Hintermann E., Bayer M., Rhode A., Rodrigo E., Hintereder G., Johnson EF., Gonzalez FJ., Pfeilschifter J., Manns MP., Herrath Mv., Christen U. Breaking tolerance to the natural human liver autoantigen cytochrome P450 2D6 by virus infection. J Exp Med. 2008 Jun 9;205(6):1409-22.

38. Gil-Farina I., Di Scala M., Salido E., López-Franco E., Rodríguez-García E., Blasi M., Merino J., Aldabe R., Prieto J., Gonzalez-Aseguinolaza G. Transient Expression of Transgenic IL-12 in Mouse Liver Triggers Unremitting Inflammation Mimicking Human Autoimmune Hepatitis. J Immunol. 2016;197:2145-56.

39. Bonito AJ, Aloman C, Fiel MI, Danzl NM, Cha S, Weinstein EG, Jeong S, Choi Y, Walsh MC, Alexandropoulos K. Medullary thymic epithelial cell depletion leads to autoimmune hepatitis. J Clin Invest 2013;123:3510-24.

40. Senaldi G., Portmann B., Mowat AP., Mieli-Vergani G., Vergani D. Immunohistochemical features of the portal tract mononuclear cell infiltrate in chronic aggressive hepatitis. Arch Dis Child. 1992 Dec;67(12):1447-53.

41. Muratori L., Longhi MS. The interplay between regulatory and effector T cells in autoimmune hepatitis: Implications for innovative treatment strategies. J Autoimmun. 2013 Oct;46:74-80.

42. Weiler-Normann C, Schramm C, Quaas A, Wiegard C, Glaubke C, Pannicke N, Möller S, Lohse AW. Infliximab as a rescue treatment in difficult-to-treat autoimmune hepatitis. J Hepatol. 2013 Mar;58(3):529-34

43. Peiseler M., Sebode M., Franke B., Wortmann F., Schwinge D., Quaas A., Baron U., Olek S., Wiegard C., Lohse AW., Weiler-Normann C., Schramm C., Herkel J. FOXP3+ regulatory T cells in autoimmune hepatitis are fully functional and not reduced in frequency. J Hepatol. 2012 Jul;57(1):125-32.

44. Webb GJ., Hirschfield GM., Krawitt EL., Gershwin ME. Cellular and Molecular Mechanisms of Autoimmune Hepatitis.Annu Rev Pathol. 2018 Jan 24;13:247-292.

45. Jeffery HC, Jeffery LE, Lutz P, Corrigan M, Webb GJ, et al. 2017. Low dose interleukin-2 promotes STAT5 phosphorylation, Treg survival and CTLA-4 dependent function in autoimmune liver diseases. Clin. Exp. Immunol. 188:394–411.

46. Schwinge D., von Haxthausen F., Quaas A., Carambia A., Otto B., Glaser F., Höh B., Thiele N., Schoknecht T., Huber S., Steffens N., Lohse AW., Herkel J., Schramm C. Dysfunction of hepatic regulatory T cells in experimental sclerosing cholangitis is related to IL-12 signaling. J Hepatol. 2017 Apr;66(4):798-805.

47. Corsiero E., Nerviani A., Bombardieri M., Pitzalis C. Ectopic Lymphoid Structures: Powerhouse of Autoimmunity. Front Immunol. 2016 Oct 17;7:430.

48. Pitzalis C., Jones GW., Bombardieri M., Jones SA. Ectopic lymphoid-like structures in infection, cancer and autoimmunity. Nat Rev Immunol. 2014 Jul;14(7):447-62

49. Jones GW, Jones SA. Ectopic lymphoid follicles: inducible centres for generating antigen-specific immune responses within tissues. Immunology. 2016 Feb;147(2):141-51.

50. Canete JD., Celis R., Moll C., Izquierdo E., Marsal S., Sanmarti R., et al. Clinical significance of synovial lymphoid neogenesis and its reversal after anti-tumour necrosis factor alpha therapy in rheumatoid arthritis. Ann Rheum Dis (2009) 68:751–6.10.1136/ard.2008.089284

51. Pikarsky E., Heikenwalder M. Focal and Local: Ectopic Lymphoid Structures and Aggregates of Myeloid and Other Immune Cells in Liver. Gastroenterology. 2016 Nov;151(5):780-783.

52. Finkin S., Yuan D., Stein I., Taniguchi K., Weber A., Unger K., Browning J., Goossens N., Nakagawa S., Gunasekaran G., Schwartz ME., Kobayashi M., Kumada H., Berger M., Pappo O., Rajewsky K., Hoshida Y., Karin M., Heikenwalder M., Ben-Neriah Y., Pikarsky E1. Ectopic lymphoid structures function as microniches for tumor progenitor cells in hepatocellular carcinoma. Nat Immunol. 2015 Dec;16(12):1235-44.

53. Frommer F., Heinen TJ., Wunderlich FT., Yogev N., Buch T., Roers A., Bettelli E., Müller W., Anderton SM., Waisman A. Tolerance without clonal expansion: self-antigen-expressing B cells program self-reactive T cells for future deletion. J Immunol 2008;181:5748-59.

54. Köntgen F., Süss G., Stewart C., Steinmetz M., Bluethmann H. Targeted disruption of the MHC class II Aa gene in C57BL/6 mice. Int Immunol 1993;5:957-64

55. Ishak K, Baptista A, Bianchi L, et al. Histological grading and staging of chronic hepatitis. J Hepatol 1995;22:696-9.

56. Soriano P. Generalized lacZ expression with the ROSA26 Cre reporter strain. Nat Genet 1999; 21: 70-71.

57. Oxenius A, Bachmann MF, Zinkernagel RM, et. al. Virus-specific MHC-class II-restricted TCR-transgenic mice: effects on humoral and cellular immune responses after viral infection. Eur J Immunol 1998; 28: 390-400.

58. Qiu R, Zhou L, Ma Y, et. al. Regulatory T Cell Plasticity and Stability and Autoimmune Diseases. Clin Rev Allergy Immunol 2018 Nov 17. doi: 10.1007/s12016-018-8721-0.

59. Sakaguchi S, Vignali DA, Rudensky AY, et. al. The plasticity and stability of regulatory T cells. Nat Rev Immunol 2013; 13: 461-467.

60. Webster KE., Walters S., Kohler R.E., Mrkvan T., Boyman O., Surh CD., Grey ST., Sprent J. In vivo expansion of T reg cells with IL-2-mAb complexes: induction of resistance to EAE and long-term acceptance of islet allografts without immunosuppression. J Exp Med. 2009 Apr 13;206(4):751-60.

61.Grinberg-Bleyer Y.., Baeyens A, You S., Elhage R., Fourcade G., Gregoire S., Cagnard N., Carpentier W., Tang Q., Bluestone J., Chatenoud L., Klatzmann D., Salomon BL., Piaggio E. IL-2 reverses established type 1 diabetes in NOD mice by a local effect on pancreatic regulatory T cells. J Exp Med. 2010 Aug 30;207(9):1871-8.

62. Schwinge D., von Haxthausen F., Quaas A., Carambia A., Otto B., Glaser F., Höh B., Thiele N., Schoknecht T., Huber S., Steffens N., Lohse AW., Herkel J., Schramm C. Dysfunction of hepatic regulatory T cells in experimental sclerosing cholangitis is related to IL-12 signaling. J Hepatol. 2017 Apr;66(4):798-805.

63. Schlitzer A, Ginhoux F. Organization of the mouse and human DC network. Curr Opin Immunol. 2014 Feb;26:90-9.

64. Schlitzer A., Sivakamasundari V., Chen J., Sumatoh HR., Schreuder J., Lum J., Malleret B., Zhang S., Larbi A., Zolezzi F., Renia L., Poidinger M., Naik S., Newell EW., Robson P., Ginhoux F. Identification of cDC1- and cDC2-committed DC progenitors reveals early lineage priming at the common DC progenitor stage in the bone marrow. Nat Immunol. 2015 Jul;16(7):718-28. doi: 10.1038/ni.3200. Epub 2015 Jun 8.

65. Ye H. Oo, Stefan G. Hubscher, David H. Adams. Autoimmune hepatitis: new paradigms in the pathogenesis, diagnosis, and management. Hepatol Int. 2010 Jun; 4(2): 475–493.

66. Corsiero E., Nerviani A., Bombardieri M., Pitzalis C. Ectopic Lymphoid Structures: Powerhouse of Autoimmunity. Front Immunol. 2016 Oct 17;7:430.

67. Weiler-Normann C, Schramm C, Quaas A, Wiegard C, Glaubke C, Pannicke N, Möller S, Lohse AW. Infliximab as a rescue treatment in difficult-to-treat autoimmune hepatitis. J Hepatol. 2013 Mar;58(3):529-34.

68. Zhao L, Tang Y, You Z, Wang Q, Liang S, Han X, Qiu D, Wei J, Liu Y, Shen L, Chen X, Peng Y, Li Z, Ma X. Interleukin-17 contributes to the pathogenesis of autoimmune hepatitis through inducing hepatic interleukin-6 expression. PLoS One. 2011 Apr 19;6(4):e18909. doi: 10.1371/journal.pone.0018909.

69. Kim JM, Rasmussen JP, Rudensky AY. Regulatory T cells prevent catastrophic autoimmunity throughout the lifespan of mice. Nat Immunol. 2007 Feb;8(2):191-7.

70. Dhamne C, Chung Y, Alousi AM, Cooper LJ, Tran DQ. Peripheral and thymic foxp3(+) regulatory T cells in search of origin, distinction, and function. Front Immunol. 2013 Aug 27;4:253.

71. Joller N, Kuchroo VK. Good guys gone bad: exTreg cells promote autoimmune arthritis. Nat Med. 2014 Jan;20(1):15-7.

72. Min Kyung Jung, Jeong-Eun Kwak, Eui-Cheol Shin. IL-17A-Producing Foxp3+ Regulatory T Cells and Human Diseases. Immune Netw. 2017 Oct; 17(5): 276–286.

73. Beriou G, Costantino CM, Ashley CW, et. al. IL-17-producing human peripheral regulatory T cells retain suppressive function. Blood 2009; 113: 4240-4249.

74. Rosenzwajg M, Lorenzon R, Cacoub P, Pham HP, Pitoiset F, El Soufi K, RIbet C, Bernard C, Aractingi S, Banneville B, Beaugerie L, Berenbaum F, Champey J, Chazouilleres O, Corpechot C, Fautrel B, Mekinian A, Regnier E, Saadoun D, Salem JE, Sellam J, Seksik P, Daguenel-Nguyen A, Doppler V, Mariau J, Vicaut E, Klatzmann D. Immunological and clinical effects of low-dose interleukin-2 across 11 autoimmune diseases in a single, open clinical trial. Ann Rheum Dis. 2019 Feb;78(2):209-217. doi: 10.1136/annrheumdis-2018-214229.

75. Herkel J1, Jagemann B, Wiegard C, Lazaro JF, Lueth S, Kanzler S, Blessing M, Schmitt E, Lohse AW. MHC class II-expressing hepatocytes function as antigen-presenting cells and activate specific CD4 T lymphocyutes. Hepatology. 2003 May;37(5):1079-85.

76. P.A. Knolle, E. Schmitt, S. Jin, T. Germann, R. Duchmann, S. Hegenbarth, et al. Induction of cytokine production in naive CD4[+] T cells by antigen-presenting murine liver sinusoidal endothelial cells but failure to induce differentiation toward Th1 cells. Gastroenterology, 116 (1999), pp. 1428-1440

77. Carambia A, Freund B, Schwinge D, Heine M, Laschtowitz A, Huber S, Wraith DC, Korn T, Schramm C, Lohse AW, Heeren J, Herkel J. TGF-β-dependent induction of $CD4^+CD25^+Foxp3^+$ Tregs by liver sinusoidal endothelial cells. J Hepatol. 2014 Sep;61(3):594-9.

78. Carambia A, Freund B, Schwinge D, Bruns OT, Salmen SC, Ittrich H, Reimer R, Heine M, Huber S, Waurisch C, Eychmüller A, Wraith DC, Korn T, Nielsen P, Weller H, Schramm C, Lüth S, Lohse AW, Heeren J, Herkel J. Nanoparticle-based autoantigen delivery to Treg-inducing liver sinusoidal endothelial cells enables control of autoimmunity in mice. J Hepatol. 2015 Jun;62(6):1349-56.

## 7. ABBREVIATIONS

| | |
|---|---|
| AIH | Autoimmune Hepatitis |
| Ab | Antibody |
| AF488 | Alexa Fluor 488 |
| ALT | Alanine transaminase |
| ANA | Antinuclear antibodies |
| APC | Antigen presenting cell |
| APC | Allophycocyanin |
| BCL6 | B-cell lymphoma 6 |
| BSA | Bovine serum albumin |
| CD | Cluster of differentiation |
| ConA | Concavalin A |
| DC | Dendritic cell |
| DMSO | Dimethylsulfoxide |
| DNA | Desossriribonucleic acid |
| EDTA | Ethylenediaminetetraacetic acid |
| ELISA | Enzyme-linked immunosorbent assay |
| FCS | Fetal calf serum |
| FITC | Fluorescein isothiocyanate |
| FOXP3 | Forhead Box Protein 3 |
| HBV | Hepatitis B Virus |
| HCC | Hepatocellular carcinoma |
| HCV | Hepatitis C Virus |
| HLA | Human Leukocyte Antigen |
| i.p. | Intraperitoneal |
| i.v. | Intravenous |
| IFN | Interferon |
| Ig | Immunoglobulin |
| IL | Interleukin |
| IPEX-Syndrome | Immunodysregulation polyendocrinopathy enteropathy X-linked Syndrom |
| LCMV | Lymphocytic choriomeningitis |
| M | Molar |
| MACS | Magnet Activated Cell Sorting |
| mg | Milligram |
| MHC | Major Histocompatibility Complex |
| min | Minute |
| ml | Milliliter |
| mRNA | Messenger Ribonucleic Acid |
| Nrp-1 | Neuropilin-1 |
| nTreg | Natural regulatory T cell |
| Ova | Ovalbumin |
| pTreg | Peripherally induced Treg |
| PBC | Primary biliary cholangitis |

| | |
|---|---|
| PBS | Phosphate-buffered saline |
| PCR | Polymerase chain reaction |
| PE | Phycoerythrin |
| PFA | Paraformaldehyd |
| PSC | Primary Sclerosing Colangitis |
| RA | Rheumatoid Arthritis |
| rpm | Rotation per minute |
| RORC | RAR-related orphan receptor C |
| RT | Room temperature |
| sec | Second |
| TBX21 | T-box transcription factor |
| TCR | T cell receptor |
| TGF | Transforming growth factor |
| tTreg | Thymic derived Treg |
| Th | T helper |
| TNF | Tumor necrosis factor |
| Treg | Regulatory T cell |
| WT | Wild type |

## 8. CONFERENCE PARTICIPATIONS

-Selected as oral presenter at 46th Annual Meeting of the German Society for Immunology, Hamburg 2016.

Ignorance of hepatic autoantigen in thymus and periphery favours the development of autoimmune liver disease.

Max Preti, Ansgar W. Lohse, Antonella Carambia, Johannes Herkel

-Selected as oral presenter at German society for the study of the liver (GASL) congress, Essen 2017.

Ignorance of hepatic autoantigen in thymus and periphery enables the development of autoimmune liver disease.

Max Preti, Ansgar W. Lohse, Antonella Carambia, Johannes Herkel

-Selected as oral presenter at European Association for the study of the liver (EASL) congress, Amsterdam 2017.

Ignorance of liver autoantigens by CD4 T cells elicits autoimmune liver disease in mice.

Max Preti, Ansgar W. Lohse, Antonella Carambia, Johannes Herkel.

-Poster presentation at German society for the study of the liver (GASL), Hamburg 2018.

Experimentally induced autoimmune hepatitis is initiated by formation of ectopic lymphoid tissue in the liver

Max Preti, Anna-Lena Müller, Daria Krzikalla, Dorothee Schwinge, Ansgar W. Lohse, Christoph Schramm, Antonella Carambia, Johannes Herkel.

-Poster presentation at European Association for the study of the liver (EASL) congress, Paris 2018.

Experimental autoimmune hepatitis in mice is associated with formation of ectopic lymphoid tissue in the liver

Max Preti, Anna-Lena Müller, Daria Krzikalla, Dorothee Schwinge, Ansgar W. Lohse, Christoph Schramm, Antonella Carambia, Johannes Herkel.

## 9. PUBLICATIONS

-Kozik JH., Trautmann T., Carambia A., Preti M., Lütgehetmann M., Krech T., Wiegard C., Heeren J., Herkel J. Attenuated viral hepatitis in Trem1-/- mice is associated with reduced inflammatory activity of neutrophils. Sci Rep. 2016 Jun, 22;6:28556

- Glaser F., John C., Engel B., Höh B, Weidemann S., Dieckhoff J., Stein S., Becker N., Casar C., Amrei Schuran F., Wieschendorf B., Preti M., Jessen F., Franke A., Carambia A., Lohse AW., Ittrich H., Herkel J., Heeren J., Schramm C., Schwinge D. Liver infiltrating T cells regulate bile acid metabolism in experimental cholangitis.J Hepatol. 2019 Jun 14. pii: S0168-8278(19)30347-2.

- Preti M., Schlott L., Lübbering D., Krzikalla D., Müller AL., Schakat M., Weidemann S., Lohse AW., Schwinge D., Schramm C., Weiler-Normann C, Carambia A., Herkel J. Insufficient deletion of autoreactive CD4 T cells and plasticity of Tregs drive spontaneous autoimmune hepatitis in mice. Manuscript submitted.

## 10. AKNOWLEDGMENTS

Ringrazio il mio papa, la mia mamma e mio fratello che attraverso innumerevoli sacrifici hanno fatto sì che io finissi questa straordinaria esperienza. Vi voglio bene. In particolare dedico la tesi a mio papa che putroppo non e piu con noi, ma sarebbe orgoglioso

Rignrazio i miei amici Baldo, Caru, Gibbo, Karim, e Tia che sono sempre stati al mio fianco

I thank my girlfriend Marie for all the love of these years.

I want to thank Professor Johannes Herkel for supervise my PhD and for being a great mentor

I want to thank Dr. Antonella Carambia for the really great help and supervision of my PhD

I thank every colleague of I clinical medicine department

I thank Prof. Ansgar Lohse

## 11. EIDESSTATTLICHE VERSICHERUNG

Hiermit erkläre ich an Eides statt, dass ich die vorliegende Dissertationsschrift selbst verfasst und keine anderen als die angegebenen Quellen und Hilfsmittel benutzt habe.

Hamburg, den Unterschrift